Abstract

CORNELIUS, CARRIE ELIZABETH. Atmospheric Plasma Characterization and Mechanisms of Substrate Surface Modification. (Under the direction of Mohamed A. Bourham and Marian G. McCord).

The purpose of this research has been to characterize the parameters of an Atmospheric Plasma Device used for surface modifications and functionalization of textile materials. Device parameters are determined in absence and presence of a substrate to quantify the optimal operational conditions. Neutral gas temperature profiles were determined for a variety of gas mixtures including 100% helium and helium with 1 or 2% reactive gases, such as oxygen and carbontetrafluoride. A plasma model was developed to solve for other plasma parameters including the electron-neutral collision frequency and the electron number density. Wool substrates were treated with various gas mixtures for a range of exposure durations and the effects of plasma treatment on weight, surface-functionality, and strength were assessed. Assessment methods include percent weight change calculations, energy dispersive X-ray spectroscopy (EDS), and tensile testing. In addition, cellulosic paper was exposed to 1% oxygen plasma to determine the feasibility of permanently grafting the anti-microbial agent HTCC (quaternized ammonium chitosan). The success of the bond was tested using Fourier transform infrared spectroscopy (FTIR), scanning electron microscopy (SEM), colorimetry, and percent weight change, and the permanency of the bond was tested though soxhlet extraction.

Atmospheric Plasma Characterization and Mechanisms of Substrate Surface Modification

By

Carrie Elizabeth Cornelius

A thesis submitted to the Graduate Faculty of
North Carolina State University
In partial fulfillment of the requirements for the Degree of
Master of Science

Nuclear Engineering

Raleigh
2006

Approved by:

_____
O.E. Hankins

_____
M.A. Bourham
(Chair of Advisory Committee)

_____
M.G. McCord
(Co-Chair of Advisory Committee
and Minor Representative)

Biography

Carrie Elizabeth Cornelius was born on the 8th of October 1983. She was raised in Raleigh, North Carolina and attended Swift Creek Elementary, Carnage Middle School, and Enloe Highschool. She went to College at North Carolina State University and obtained two undergraduate degrees, a B.A. in Art & Design and a B.S. in Textile Technology. After a semester research project working with atmospheric plasma, she applied and was accepted into graduate school in the Department of Nuclear Engineering at NC State University.

Acknowledgements

First and foremost, I would like to acknowledge and thank Dr. Bourham. I will never understand when he began believing an art and textile major could be a nuclear engineer, but without his support and unwavering faith I would never have even attempted much less finished this degree. I will never be able to thank him properly or sufficiently for all the precious time he gave me, for his infinite patience and wisdom, and for the strength and possibility he has instilled in me. Without a shadow of a doubt, what I have achieved I owe to him.

On that note, I would also like to give a special thank you to my sister Johanna, for introducing me to Dr. Bourham, and for helping me through the transition between departments and subject matters. Thanks for always being there for me.

Next I would like to acknowledge Dr. McCord for all her effort and support. I would like to thank her for her guidance, her time, and for her dedication to my project and lab space. Her endless enthusiasm to try new things and to seek out new answers will continue to inspire me.

Also, a special thanks to Lori Downen and Laura Bruschi, undergraduates in the Department of Nuclear Engineering for their help this past summer. Thank you both for treating samples, run gas trials, and typing up models. I hope I will see you both as fellow graduate students in a couple of years.

Lastly, I would like to mention Elijah Martin. Thank you for taking the time to come to my lab with all your equipment and run the optical spectroscopy tests. I also appreciate your patience in explaining the data, the limitations, the techniques, and for helping me to understand the spectra and its meanings.

Table of Contents

List of Figures vi
List of Tables ix
1. Introduction 1
1.1 Introduction to Plasma 1
1.2.1 Introduction 4
1.2.2 Direct Current DC 'Glow' Discharges 5
1.2.3 Oscillatory Discharges 8
1.2.3.1 Homogeneous Model 9
1.2.3.2 Inductively Coupled Discharges 11
1.2.3.3 Capacitive Coupling 12
1.2 Atmospheric Plasma and Substrate Modifications 13
2. Experimental 15
2.1 Atmospheric Pressure Plasma Facility 15
2.2 Operational Parameter 19
2.2.1 Data, Display, Storage, and Analysis with LABVIEW 20
2.3.1 Obtainable Data 23
2.3.2 Data Acquisition Method 23
2.3.2.1 DAQ Boards 23
2.3.2.2 Triggering 24
2.3.2.3 Voltage and Current Acquisition 25
2.3.2.3.1 One Loop Iteration Data 26
2.3.2.3.2 RMS Voltage and Current 26
2.3.2.3.3 Absolute Voltage or Current 26
2.3.2.4 Gas Flow Regulation 26
2.3.2.5 Gas Temperature Measurements 27
2.4 Goal and Extent of Research 27
3. Characterization of Plasma Parameters 29
3.1 Plasma Impedance 29
3.2 Plasma Gas Thermal Energy 33
3.2.1 Introduction 33
3.2.2 Experimental 35
3.2.3 Ambient Gas Temperature Data 37
3.3 Plasma Models 47
3.3.1 Electron Number Density 47
3.3.2 Electron Neutral Collision Frequency 50
3.3.2 Solid Sphere Collision Model 51
3.3.2.2 Maxwellian Velocity Distribution Function 52
3.3.2.3 Ideal gas Law 53
3.3.3 Electron Number Density Model 54
3.3.4 Electron Number Density Model Data 55
3.4 Optical Emission Spectroscopy 60
3.4.1 Introduction 60
3.4.2 Experimental 64
3.4.3 Optical Emission Data 64

4. Plasma Interaction with Substrates 69
4.1 Plasma Modification of Substrates 69
4.1.1 Etching 70
4.1.2 Redeposition and Backscattering 72
4.1.3 Radical Formation 73
4.1.4 Chain Scission and Cross-linking 74
Bond Type 75
4.1.5 Plasma Deposition/Polymerization 75
4.1.6 Hydrophilicity and Oleophilicity 76
4.2 Substrate Characterization 77
4.2.1 Wool 77
4.2.2 Cellulosic Paper 81
4.2.3 Chitosan 83
4.3 Characterization Methods 86
4.3.1 Weight Change 86
4.3.2 Scanning Electron Microscopy (SEM) 87
4.3.3 Energy Dispersive X-ray Spectroscopy (EDS) 87
4.3.4 Tensile Testing 88
4.3.5 Contact Angle and Absorption Time 90
4.3.6 Fourier Transform Infrared Spectroscopy 90
4.1.7 Colorimetry 91
4.4 Wool Research 92
4.4.1 Experimental 92
4.4.2 Plasma Characterization 93
4.4.3 Temperature Characterization 93
4.4.2.2 Electron Number Density Characterization 101
4.4.2.3 Weight Change 109
4.4.2.4 Contact Angle and Absorption Time 113
4.4.2.5 Energy Dispersive X-ray Spectroscopy 117
4.4.2.6 Tensile Testing 118
4.5 Cellulosic Paper Research 123
4.5.1 Experimental 123
4.5.1.1 Weight Change 124
4.5.1.2 Scanning Electron Microscopy (SEM) 126
4.5.1.3 Colormetric Testing 128
4.5.1.4 Fourier Transform Infrared Spectroscopy 129
Possible Functional Groups 132
4.5.1.5 Proposed Chemical Grafting Reaction 134
5. Conclusions and Future Work 137
5.1 Conclusions 137
5.2 Recommendations for Future Work 140
References 141

List of Figures

Figure 1: Voltage-Current Characteristics of a DC Glow Discharge [2] 4
Figure 2: Illustration of the DC 'Glow' Discharge Features [3] 7
Figure 3: Plasma Sheaths 10
Figure 4: Inner and Outer Plasma Chamber 16
Figure 5: Inner Plasma Chamber and Optional Cell 17
Figure 6: Schematic circuit diagram of the atmospheric plasma DBD device 17
Figure 7: A picture of the atmospheric plasma device showing the inner and outer chambers, and fabric rolling system 18
Figure 8: Front Panel and Block Diagram of LabVIEW System 21
Figure 9: Hysteresis and Triggering Diagram 25
Figure 10: Amplitude of Voltage and Current 31
Figure 11: Diagram of Thermocouple Positions 36
Figure 12: Test cell temperature distribution, 100% Helium plasma after 5 seconds operation 37
Figure 13: Test cell temperature distribution, 100% Helium plasma after 15 minutes operation 38
Figure 14: Temperature distribution, 99% Helium+1% O2 plasma after 5 seconds operation 39
Figure 15: Temperature distribution, 99% Helium+1% O2 plasma after 15 minutes operation 39
Figure 16: Temperature distribution, 98% Helium + 2% Oxygen after 5 seconds operation 40
Figure 17: Temperature distribution, 98% Helium + 2% Oxygen after 15 minutes operation 41
Figure 18: Temperature distribution, 99% Helium + 1% CF4 after 5 seconds operation 42
Figure 19: Temperature distribution, 99% Helium + 1% CF4 after 15 minutes operation 42
Figure 20: Temperature distribution, 98% Helium + 2% CF4 after 5 seconds operation 43
Figure 21: Temperature distribution, 98% Helium + 2% CF4 after 15 minutes operation 44
Figure 22: Temperature distribution, 98% Helium +1% O2 + 1% CF4 after 5 seconds operation 45
Figure 23: Temperature distribution, 98% Helium + 1% O2 + 1% CF4 after 15 minutes operation 45
Figure 24: Single capacitor model equivalent plasma and insulators 48
Figure 25: Triple capacitor model representing plasma and insulators' capacitances 48
Figure 26: Complex inductor, resistor, and capacitor plasma model 48
Figure 27: Illustration of the solid sphere collision model 52
Figure 28: Maxwellian velocity distribution function 53
Figure 29: Density distribution for 1% CF4 at 5 seconds 56
Figure 30: Density distribution for 1% CF4 at 5 minutes 57
Figure 31: Density distribution for 1% CF4 at 15 minutes 57
Figure 32: Density distribution for 2% CF4 at 5 seconds 58
Figure 33: Density distribution for 2% CF4 at 5 minutes 59
Figure 34: Density distribution for 2% CF4 at 15 minutes 59
Figure 35: Spectra for a 100% helium discharge 65
Figure 36: Spectra of a 99% He + 1% Oxygen discharge 65

Figure 37: Spectra of 98%He + 2% Oxygen discharge 66
Figure 38: Spectra of 99% He + 1% CF4 discharge 67
Figure 39: Spectra of 98% He + 2% CF4 discharge 67
Figure 40: Spectra of 98% He + 1% Oxygen + 1% CF4 discharge 68
Figure 41: Illustration of basic plasma etching processes 70
Figure 42: Wool fiber cross-section 78
Figure 43: Structure of a wool fiber [23] 79
Figure 44: Chemical structure of wool [24] 80
Figure 45: Basic chemical structure of cellulose (a) and with its derivatives (b) [26] 82
Figure 46: Processing of shellfish waste into chitin and deacetylation into chitosan [29] 84
Figure 47: Deacetylation of chitin to produce chitosan [29] 85
Figure 48: Chemical Structure of synthesized HTCC 86
Figure 49: Example of EDS Spectra taken for cotton fabric 88
Figure 50: Tensile testing of cotton and wool 89
Figure 51: Contact angle for hydrophilic (left) and hydrophobic (right) surfaces 90
Figure 52: Temperature change for a 100% helium discharge with and without wool substrate for 300 seconds duration 95
Figure 53: Temperature change for a 99% helium + 1% O2 discharge with and without wool substrate for 300 seconds duration 96
Figure 54: Temperature change for a 98% helium + 2% O2 discharge with and without wool substrate for 300 seconds duration 97
Figure 55: Temperature change for a 99% helium + 1% CF4 discharge with and without wool substrate for 300 seconds duration 98
Figure 56: Temperature change for a 98% helium + 2% CF4 discharge with and without wool substrate for 300 seconds duration 99
Figure 57: Temperature change for a 98% helium + 1% O2 + 2% CF4 discharge with and without wool substrate for 300 seconds duration 100
Figure 58: Temperature change with wool substrate in the plasma for all gas mixtures 101
Figure 59: Change in electron number density for a 100% helium discharge with and without wool sample 103
Figure 60: Change in electron number density for a 99% helium + 1% oxygen discharge with and without wool sample 104
Figure 61: Change in electron number density for a 98% helium + 2% oxygen discharge with and without wool sample 105
Figure 62: Change in electron number density for a 99% helium + 1% CF4 discharge with and without wool sample 106
Figure 63: Change in electron number density for a 98% helium + 2% CF4 discharge with and without wool sample 107
Figure 64: Change in electron number density for 98% helium + 1% O2 + 1% CF4 discharge with and without wool sample 108
Figure 65: Change in electron number density for all plasma gases with a wool sample 109
Figure 66: Change in weight of a wool substrate exposed to various plasmas 113
Figure 67: Absorption of wool fabric exposed to plasma 116
Figure 68: Contact angle of wool fabric exposed to plasma 116
Figure 69: Fluorine content on wool samples exposed to plasma with percentage of CF_4 .. 118
Figure 70: Peak Load of wool substrates for all plasma gas mixtures 120

Figure 71: Energy at the Peak Load of wool substrates for all gas mixtures..... 121
Figure 72: Elongation at the Peak Load of wool substrates for all plasma gas mixtures 122
Figure 73: Add-on of HTCC after one washing 125
Figure 74: Weight change after soxhlet extraction 126
Figure 75: SEM photographs of cellulosic samples, control, HTCC sprayed and 2-minutes exposed to plasma with HTCC spray..... 127
Figure 76: Colormetric testing of cellulosic paper samples grafted with HTCC 129
Figure 77: FTIR of HTCC grafted cellulosic paper from 3000-1800nm..... 131
Figure 78: FTIR of HTCC grafted cellulosic paper from 1500-900nm..... 131
Figure 79: FTIR of HTCC from 3600nm to 800nm 133
Figure 80: Proposed chemical grafting reaction for HTCC and cellulosic paper..... 136

List of Tables

Table 1: Gas Constants A and B and their E/P Range 6
Table 2: Flow Rates of Gases into the Plasma Chamber 20
Table 3: Melting Point and Glass Transition of selected Substrates [9,10] 34
Table 4: Experimental Gas Mixtures 36
Table 5: Common processes in helium, oxygen and carbontetrafluoride plasmas [11] 61
Table 6: Examples of chain scission and cross-linking 74
Table 7: Dissociation Energy of Typical Bonds 75
Table 8: Some of the important properties of wool [9,10,25] 81
Table 9: Wavenumber and associated functional groups 132

1. Introduction

1.1 Introduction to Plasma

The simplest description of plasma is a collection of ionized and unionized gas molecules. The degree of ionization may vary from complete ionization to only a small fractional ionization. For example, fusion plasmas and plasmas found in the cores of stars are completely ionized whereas most industrial plasmas are only partially ionized.

Plasma has often been called the fourth state of matter (solid⇒liquid⇒gas⇒plasma), because it forms when gas molecules achieve a kinetic energy beyond that of their ionization energy. At this energy, the most loosely bound electron can break free from the electron cloud surrounding the nucleus.

However, all gases contain some small degree of fractional ionization, and yet they are not classified as plasma. Thus the definition of plasma must be more refined. Francis Chen proposes three additional requirements to classify plasma [1]:

1) Quasi-neutrality

2) Collective Behavior

3) Motion controlled by Electromagnetic forces.

Quasi-neutrality is when an equal number of electrons and ions coexist. Plasma is normally formed when a neutral gas dissociates then ionizes, so it naturally contains an equal number of negative and positive particles. The implications of this quasi-neutrality can be summarized by the concept of Debye shielding. Due to the many charged particles within the plasma, it exhibits a characteristic behavior when exposed to point charges. A positive point charge placed within the plasma creates an electric field is immediately surrounded by

electrons. The electrons form a shield around the positive point charge and at a certain distance, the Debye length (λ_D), the bulk plasma no longer perceives the point charge. This is true of negative point charges as well, where ions can also form a sheath.

$$\lambda_D = \left(\frac{\varepsilon_0 K T_e}{n e^2} \right)^{\frac{1}{2}}$$

For Debye shielding to occur, it is essential that the length of the plasma be greater than the length of the Debye shield. If the length is not greater, then there will be no plasma to be shielded. The plasma profile will be that of a charge gradient.

The next necessary characteristic of plasma is collective behavior. Collective behavior means that plasma particles are influenced not only by their immediate surroundings, but also by regions a significant distance away. In a medium like air, waves travel only by collisions between one gas molecule and another. However, in plasma if a charge is displaced from its neutral location, it generates an electric field. This electric field disrupts the entire body of charged particles. Each one feels repulsions and attractions resulting in the general motion of all the particles. These moving charges can generate currents, magnetic fields, and influence the behavior of particles a significant distance away.

However, there must be a significant number of ionized particles within plasma for collective behavior to be exhibited. In addition, this number must be greater than the number needed to form a Debye shield. The number of particles in a Debye shield is:

$$N_D = \frac{4}{3} \pi \lambda_{De}^2 n_e$$

Thus, $N_D >>>> 1$ in order for plasma classification.

Lastly, plasma must have sufficient ionization. Every gas has some fractional

ionization, due to the effect of UV radiation, ionizing radiation from natural radioactivity, or the effect of an electric field caused by neighboring power lines, however this ionization is usually small enough to be considered negligible. The acceptable amount of ionization that allows for classification of an ionized gas mix as plasma is a combination of two factors, the collective behavior (the plasma oscillations), and the time between ionized particle and neutral gas collisions. With ω defined as the frequency of plasma oscillations, and τ as the time between ion/neutral collisions, then the value of $\omega\tau$ must be greater than or equal to 1 in order to classify an ionized gas as 'plasma.'

Plasmas exist throughout nature. They make up nearly 99% of the universe, and can be found in the vast empty spaces between planets and solar systems. Here on earth they also occur naturally and lightening is the most commonly observed example. The northern lights are also plasmas, with their brilliant variation in colors corresponding to different gases and energy levels.

In addition to naturally occurring sources, plasma is used in daily life. Many industries, such as the micro-chip industry use plasmas to create computer components. Welders use plasma arcs to bond metals, such as steel and restaurants and clubs use plasmas of different gases to create their advertisement signs. Even fluorescent lights, found overhead in most schools, businesses, and stores are nothing more than a form of room-temperature plasma.

1.2 Plasma Systems for Industrial Applications

1.2.1 Introduction

Industrial plasmas can be generated in a variety of ways, but they are generally divided into two groups, cold plasmas and hot plasmas. Temperature refers to the kinetic energy of the ionized particles rather than to the ambient temperature. This qualification is especially important when considering plasmas with small fractional ionization. Although the ambient temperature (gas molecules) may not be hot, ionized particles (generally the light, mobile electrons) may have very high kinetic energies.

Hot plasmas include arc discharges and plasma torches, such as those found in welding equipment and tandish heating in the metal industry. These discharges are characteristic of DC voltage systems in which the current has increased beyond the glow-to-arc transition and voltage has therefore significantly decreased. In addition, in these systems ions and electrons are often at equal temperatures, ie at local thermodynamic equilibrium.

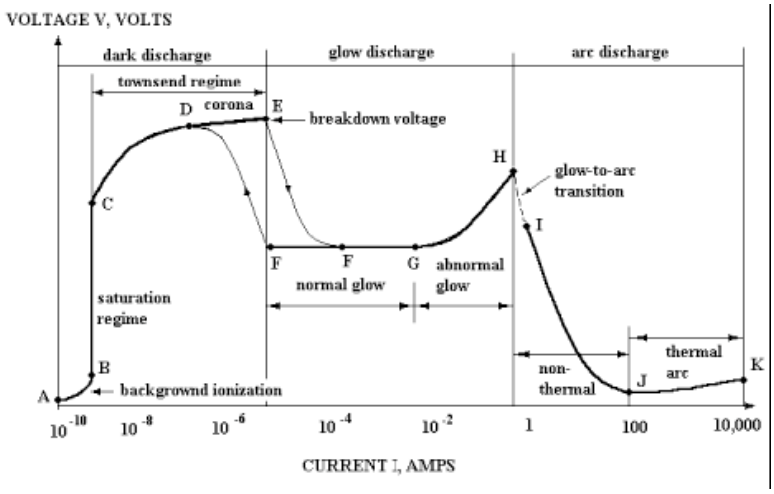

Figure 1: Voltage-Current Characteristics of a DC Glow Discharge [2]

Cold plasmas are generated when current remains relatively low in comparison to voltage. In this situation, the thermal energy of the ionized species remains lower than that of the hot plasmas and the ions and electrons often maintain different energies. Since the electrons are significantly lighter than the ions of most gases, the electrons will be able to carry significantly higher kinetic energies. Cold plasmas can be subdivided into oscillatory discharges which include capacitively coupled and inductively coupled discharges, and direct current or and 'glow' discharges. Microwave discharges are also cold plasmas, but can possess electrons at significantly higher thermal energies than the others.

1.2.2 Direct Current DC 'Glow' Discharges

Glow discharges are characterized by a direct current introduced into the discharge from an external power supply. They are generally composed of thin parallel electrodes with a large circular or square surface area. The voltage applied to each electrode is generally of the same magnitude and at opposite polarity, however systems may also be designed in which one electrode is connected to voltage and the other to ground. As a result, the positively charged electrode is often referred to as the anode and the negatively charged electrode the cathode. These designations refer to the particles attracted by each electrode rather than the charge placed on the electrode (hence anode refers to a positive electrode).

When creating a glow discharge, careful attention must be given to the initial or striking voltage. This voltage is needed to initiate the breakdown condition and the creation of the discharge. After the discharge is created, the self-sustaining condition can be met at a voltage significantly lower than the striking potential. The striking potential is a function of

pressure and electrode spacing. The equation of the breakdown voltage is given by:

$$V_b = \frac{Bpd}{\ln(Apd) - \ln\left[\ln\left(\frac{1}{1+\gamma_{se}}\right)\right]}$$

where V_b is the breakdown voltage, A and B are constants dependent on the gas type, and γ_{se} is the coefficient of secondary electron emission from the surface of the cathode. The constants A and B are only applicable for each gas within a range determined by the ratio of the electric field 'E' to the pressure 'P', and not applicable outside the specified E/P range. Table 1 list the constants A and B for several gases and the corresponding range of applicability.

Table 1: Gas Constants A and B and their E/P Range

Gas	A	B	E/P (Volt/Torr-cm)
Air	14.6	365	150 - 600
Argon	13.6	235	100 - 600
Helium	5	130	20 - 150
Carbon dioxide	20	466	500 - 1000
Hydrogen	5	130	150 - 400
Water vapor	12.9	289	150 - 1000

The DC glow discharge has distinctive features as shown in Figure 2.

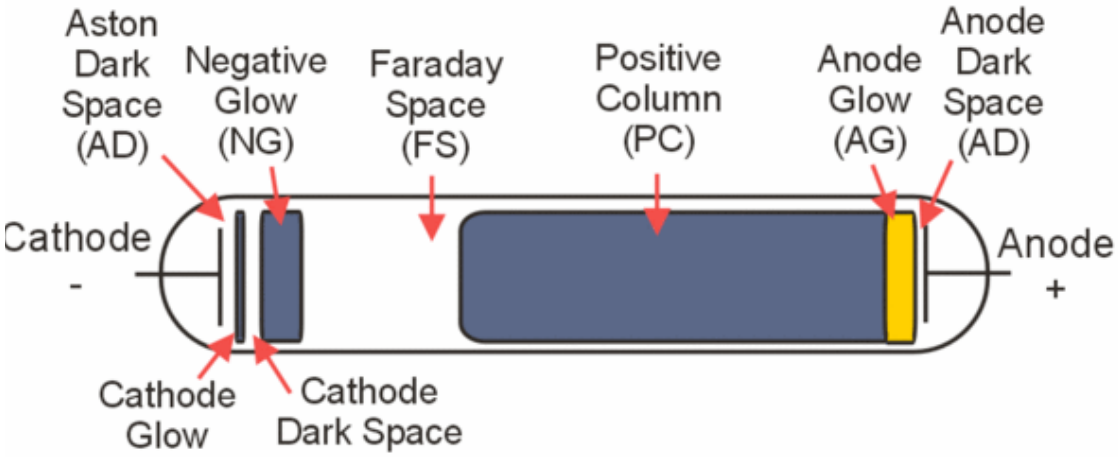

Figure 2: Illustration of the DC 'Glow' Discharge Features [3]

It is important to note that only within the positive column does conventionally defined "plasma" exist. Plasma, according to earlier definitions must meet three qualifications: quasi-neutrality, sufficient ionization, and collective behavior.

The most striking feature of direct current glow discharges is the creation of secondary electrons from the surface of the cathode. Ions are accelerated across the cathode fall and impact the cathode, inducing this secondary electron emission. Many industrial devices, such as those used in the microchip industry, make use of the ion impact to sputter atoms from the cathode and onto a substrate. Device configurations are optimized to increase the cathode sheath and therefore the acceleration potential of the ions. This

increases the kinetic energy of the ions that impact the cathode surface and increases the probability of sputtering.

1.2.3 Oscillatory Discharges

Oscillatory discharges utilize alternate current (AC) power supplies to generate a time-dependent 'oscillatory' electric field. Thus both voltage and current will alternate sinusoidally between positive and negative peaks. In addition, unlike the direct current discharges where ions and electrons are transferred directly between the electrodes, current is generated by a displacement rather than by conduction current.

An understanding of oscillatory discharge systems begins with an understanding of the homogenous model. This model was developed to explain experimentally observed phenomenon in a simplistic fashion. However, the model is an approximation and does not explain the imaginary portions associated with more realistic plasma calculations. More complex and accurate calculations of oscillatory plasma systems can be explained by the Child Law and the Inhomogeneous Model [4].

1.2.3.1 Homogeneous Model

a) Ions are only affected by time-averaged changes in the electric field. This is due to their large mass. For a RF discharge, the ions can essentially be considered stationary and uniformly distributed throughout the bulk plasma.
b) Electrons can respond instantaneously to changes in voltage. Again, this is due to their extremely light mass. As a result, they alone carry the current.
c) The population of electrons is zero, $n_e \sim 0$, within the sheaths. This is known as the ideal sheath. Ions are found in the sheath at equal populations as within the plasma bulk, $n_i \sim n_o$, where n_o is the quasi-neutral number density
d) Transverse variations of the plasma do not exist. Essentially, the plasma is considered uniform across the length of the discharge between the electrodes.
e) As described earlier, the ion density is uniform and constant both spatially and temporally.

For a plasma formation, as shown in Figure 3 (a), the separation between the plasma and the wall is determined by the sheath thickness. The ideal sheath, Figure 3 (b) is vacant from electrons and occupied by ions. The ion number density is the same everywhere and is equal to the quasi-neutral density in the plasma bulk. The inhomogeneous model, as shown in Figure 3(c), considers the actual sheath formation in which electrons are occupying the sheath with population less than that of ions, and in which the population of both electrons and ions decreases towards the wall. Any sheath is preceded by a pre-sheath in which electron and ion populations are the same (quasi-neutral) but less than that of the plasma bulk, as shown in Figure 3 (c). The potential is mostly across the sheath and exponentially

decays into the plasma region, such that the plasma potential is much less than that across the sheath, as shown in Figure 3 (d).

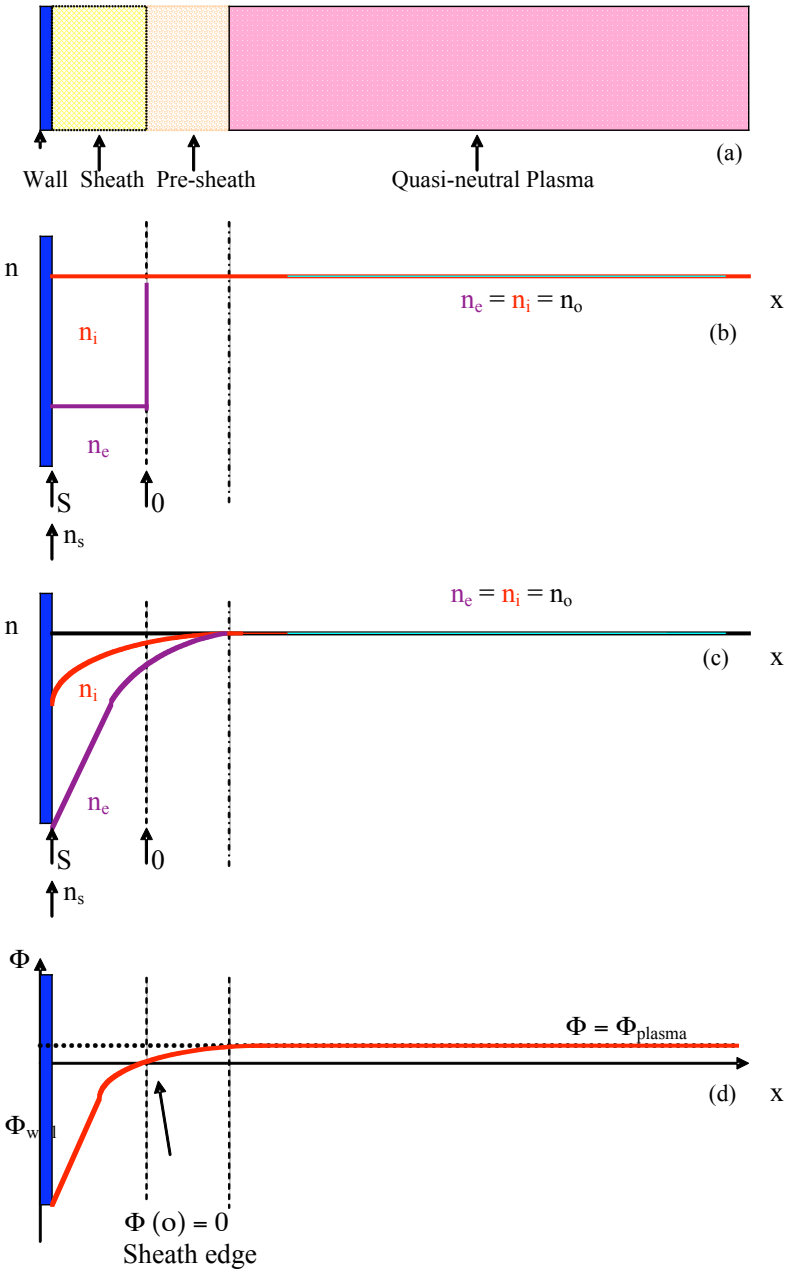

Figure 3: Plasma Sheaths

1.2.3.2 Inductively Coupled Discharges

Inductively coupled discharges operate with oscillatory power supplies at frequencies in the KHz or MHz range. The most common frequency of oscillation is 13.56 MHz, and this has been coined the "central industrial" frequency.

Inductively coupled plasmas do not have a direct connection between the electrodes and the power supply, and the coupling is achieved via an antenna or solenoid. This prevents degradation of the electrode by plasma currents, reduces contaminants and impurities from electrode sputtering, and transfers power through the skin layer (a thin layer near the plasma surface) to the electrons. The inductively coupled discharge can also be modeled using the homogenous model and thus the electrons are assumed to carry the current. As a result, the power is transferred to the electrons by Ohmic heating where the electrons collide with the electric field and are subsequently accelerated.

The power absorbed by the device will be a function of the skin depth and also of the number of turns, 'N'. Calculation of the skin depth differs for collisional and collisionless pressure regimes and the number of turns is a feature of the plasma system design. The fewer the turns, the greater the power absorbed by the plasma. Power must also be matched via a matching network to achieve the most effective forward power with the least reflected power. Ideally the forward power should be 100%, while reflected power should be 0%, but this is not always realistic. Compared to capacitively coupled systems, the inductively coupled system is more efficient in transferring power to the plasma.

1.2.3.3 Capacitive Coupling

Capacitively coupled discharges generally consist of two parallel electrodes that are directly attached to either an alternating power source for lower frequencies, or a RF power supply for MHz frequencies. The frequency of oscillation in the low range is within the radio frequency or audible range (AF). With sufficient power, a plasma bulk is generated between the electrodes and sheaths are formed between the plasma and the electrodes.

The oscillatory sheaths, unlike those found in the direct current system are not striated. They are uniform in composition and vary in thickness in direct relation to the frequency of the current and inversely with each other. However, due to an oscillation frequency greater than human eyes can perceive, the sheaths appear of constant and equal thickness. In addition to varying thickness, the sheaths also contain a very high potential and behave nonlinearly, generating second order harmonics. However, when they are averaged together, the voltage becomes linear.

The sheaths and the bulk plasma have different methods of heating as well. Since the homogenous model does not allow for electrons within the sheaths to carry the current, the sheath current is entirely collisionless (stochastic) and the sheaths carry a displacement current. In contrast, the bulk plasma is dominated by Ohmic or collisional heating. Additionally, the conduction current cannot be altogether ignored within the sheaths. Twice during every cycle one sheath will reach its maximum thickness while the other sheath falls approximately to zero. During this time the bulk plasma is slammed against an electrode and conduction current from plasma to electrode can occur.

Capacitively coupled discharges are used in a variety of substrate applications. The substrate is usually suspended in the bulk of the plasma, equidistant from both electrodes where both ions and electrons interact with it. The gas temperatures are low enough to prevent damage to the substrate while the high electron energies provide interactions that induce surface modifications.

1.2 Atmospheric Plasma and Substrate Modifications

Plasma systems have been used to modify substrates since their invention, especially vacuum plasmas, which have been used for sputter deposition, etching, and implantation techniques. The most famous and most successful application thus far has been within the microchip industry. Plasma allows for precise manufacturing ability at the micro and sub-micro levels necessary for the production of the tiny chips that are used in computers and electronic instrumentation. Other industries such as paper making, fabric and textiles, and the biomedical industry have shown interest and success in using plasma processes, but are yet to introduce plasma on a mass-production scale.

Interest in commercial use of plasma for product modification is due to the wide range of plasma applications. Plasma, as a surface interaction phenomena, can be applied to substrates to add coatings of a several micro-layer skin or can provide chemical modifications within a limited depth determined by the plasma energy, or more specifically, the ion energy. For ion implantation, plasma treatment is a uniform process, and all areas are equally treated. In addition, the surface modifications that can be produced (mostly a function of the working plasma gas) are numerous. Plasma has been used to sterilize, apply coatings (of all types), increase hydrophobicity or hydrophilicity, modify surface functional

groups for graft polymerization, cross-link to antimicrobial compounds or insect repelling agents, or modify the surface to kill insects.

However, despite the plethora of plasma possibilities, industrial scale plasma application has been rare with exception to the micro-chip industry. This stems from the limitations of the current vacuum plasma systems that require operation under vacuum and the need for continuous pump out of the reaction chamber. As a result, the vacuum plasma systems require vacuum pumps (even turbomolecular or ion pumps), lengthy pump down time, and restriction to batch treatment or large volume plasma chambers for continuous treatment. However, a plasma system capable of operating at atmospheric pressure was developed by Yokoyama et al in 1990 [5]. Feasibility of the atmospheric plasma hinges on three criteria:

1) The use of metastable helium as a seed gas

2) An oscillating electric field in the RF or audio range

3) Dielectric coating of the electrodes

When metastable helium is used as a seed gas, the duration of the Townsend discharge significantly increases. This delays the plasma transition to the arc regime and allows plasma treatment at lower temperatures non-damaging to substrates. Increases in the frequency of the plasma to RF change the plasma from a collection of individual point charges to a homogenous discharge plasma. Lastly, the dielectric barrier discharge helps in generating near-glow discharge conditions at lower operating voltages and allows for the displacement current $\bar{J}_{displacement} = \varepsilon_o \frac{\partial \bar{E}}{\partial t}$ to complete the electrical circuit of the discharge.

The ability to create an atmospheric pressure plasma system sparked new interest in industrial plasma applications and research is currently being conducted. Atmospheric

plasma has almost all the capabilities for surface activation and processes for surface functionalization [6]. Research still continues on the capabilities of these relatively new systems, which include, but are not limited to atmospheric pressure plasma liquid deposition devices, atmospheric pressure plasma jets, and atmospheric pressure powder injection systems.

2. Experimental

2.1 Atmospheric Pressure Plasma Facility

The facility used for the experiments in this research is an atmospheric plasma device located on Centennial Campus within the College of Textiles in Raleigh, NC. It is primarily used for surface modification and functionalization of textile materials, such as fabrics and films, and textile bio-materials. The facility was designed and constructed by a group of researchers from the Department of Nuclear Engineering, North Carolina State University.

The device is a dielectric barrier discharge (DBD), in which plasma is generated between two parallel planar electrodes and each electrode is embedded inside of a polycarbonate (Lexan) plate. Electrodes are located inside of a compartment that serves as the plasma chamber and further housed inside a large-volume chamber. The electrodes are made of 60x60 cm square copper plates imbedded inside of a 2cm thick Lexan. The gap between the electrodes is variable and can be extended from 0-25 cm. The input power to the electrodes is approximately 4.8kW, supplied by 2 direct current power supplies and the voltage is alternated by a type 4011 5MHz, BK Precision® Function Generator. The

function generator is tuned to operate in a frequency range of 5 to 10 KHz, thus supplying power to the plasma in the audio frequency range. Audio power amplifiers are used to amplify the power output to the desired operational level (4.8kW). Coupling between the power generator and the electrodes is via two transformers 180° out of phase.

The device is capable of batch treatment of films and fabric pieces using a test cell. Samples are placed on a nylon grid suspended in the middle of the test cell to ensure complete and uniform plasma exposure on all sides. The device is also capable of continuous operation using the roller feed system for large fabric rolls or continuous filaments and yarns. A schematic drawing of the device including the batch treatment inside the test cell and the roller system for continuous treatment of fabrics and yarns is shown in Figure 4 and 5.

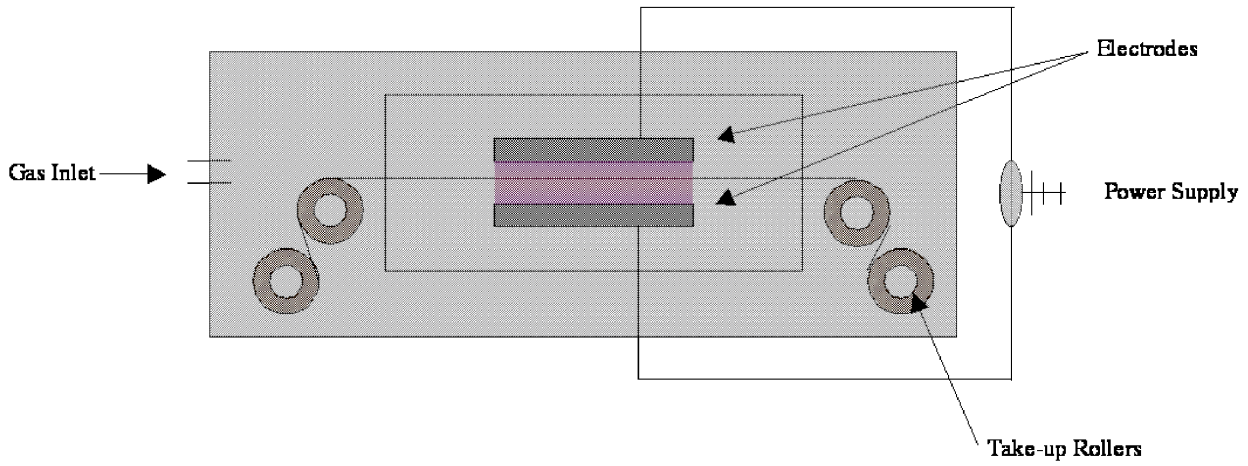

Figure 4: Inner and Outer Plasma Chamber

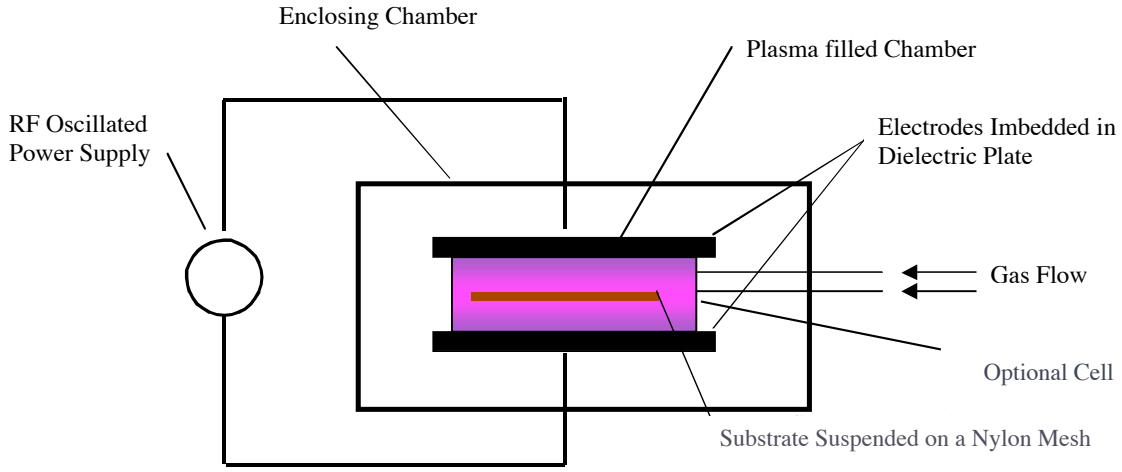

Figure 5: Inner Plasma Chamber and Optional Cell

Figure 6 shows a simplified circuit diagram of the device, in which C_T and R are coupling capacitors and resistors, and C represents the two electrodes in the capacitively coupled mode. The step-up transformers are at 180° out of phase, and "HVP" represents the locations of high voltage probes for voltage measurements. A picture of the device is shown in Figure 7, in which the fabric roller system for on-line continuous treatment of fabrics can be seen.

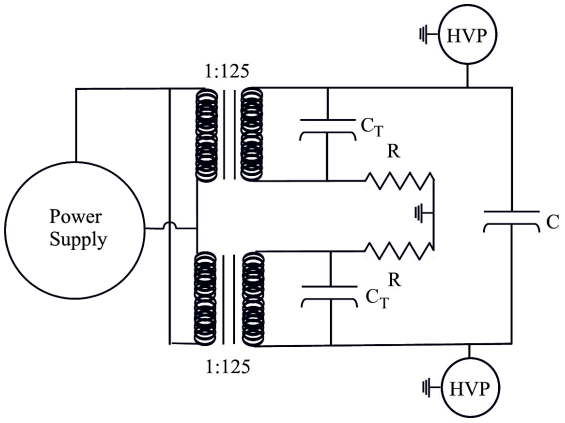

Figure 6: Schematic circuit diagram of the atmospheric plasma DBD device

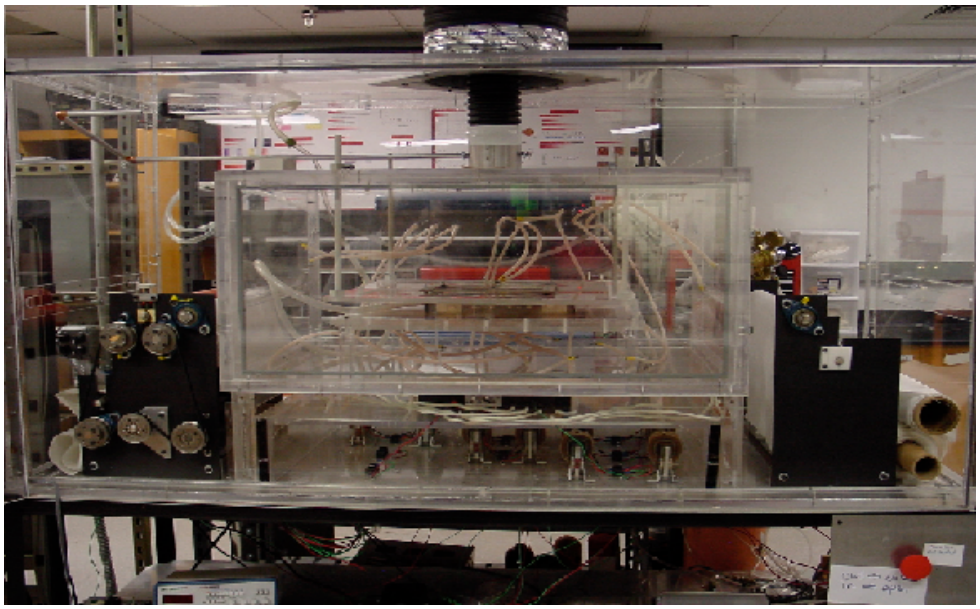

Figure 7: A picture of the atmospheric plasma device showing the inner and outer chambers, and fabric rolling system

To generate the plasma, the working gas (usually helium as the seed gas) is fed into the area between the electrodes at a specified flow rate. Other gases may be added with a determined percentage and are introduced to the chamber through a common gas feed line with helium. Typical gases to add in the flow stream are oxygen, carbontetrafluoride (CF_4), forming gas (90% nitrogen and 10% hydrogen), hexafluoropropylene (C_3F_6), and carbon dioxide (CO_2). These secondary gases are added in very small percentages, generally between 1-2 percent. All gases are regulated by MKS Mass-Flo Controllers (Model# 1478A14CR1BM), which are controlled by a MKS type 247 4-channel controller and readout unit. Gas, or gas mixes, can be fed directly into the gap between the electrodes or into a test cell inserted between the electrodes.

This cell can be used for batch treatments of various substrates or textile materials. It is made of Plexi-glass and consists of four walls, open on top and bottom with a nylon mesh in the center on which samples can be suspended. Use of the cell is perfect for experimenting on batches and for sample testing as it has a confined volume and reduces the amount of gas consumption

The internal chamber is housed inside another larger chamber, where the later incorporates a roller system for continuous processing of textile materials. These rollers are driven by a step motion with regulated speed to control the residence time in the plasma. Although continuous processing consumes more gases, the process is cost-effective compared to conventional wet chemical processes.

2.2 Operational Parameter

For the purposes of this research, the test cell was used to expose substrates to plasma. Due to the closed-volume geometry of the cell, no continuous processes were adopted. The operating frequency, plasma dimensions, gas flow rates, input power, and applied potential were all kept constant, and only substrate exposure time to plasma was varied. The operating frequency was kept at 5 KHz (±.001). Previous studies show little variation in treatment capabilities for atmospheric plasmas within the 5-10 KHz range, due to the fact that the essential plasma parameters (electron kinetic temperature and number density) do not change significantly as a function of the electric field frequency [7]. Use of the batch cell maintained a uniform treatment area of about 700 cm^3 with a fixed electrode gap of 3.0 cm.

Three different types of gas were used for the plasma experiments in this research, pure helium, helium with a percentage of oxygen, and helium with a percentage of carbontetrafluoride (CF_4). These three gases were combined to create six different gas mixes. Helium gas was used as the seed gas for all experiments and secondary gases were added either at 1 or 2% by mass. The gas mixtures are shown below in terms of mass fraction and volume fraction. Volume fraction is necessary for manual adjustment of the Mass Flo Controllers whereas mass fraction is necessary for calculations.

Table 2: Flow Rates of Gases into the Plasma Chamber

Gas Mixture (Mass Fraction)	Gas Mixture (Volume Fraction)
100% Helium	10L/min Helium
99% Helium + 1% Oxygen	10L/min Helium + .14L/min Oxygen
99% Helium + 1% Carbontetrafluoride	10L/min Helium + .34L/min CF_4
98% Helium +2% Oxygen	10L/min Helium + .29L/min Oxygen
98% Helium + 2% Carbontetrafluoride	10L/min Helium + .48L/min + CF_4
98% Helium + 1% CF_4 + 1% O_2	10L/min He + .34L/min CF_4 + .14L/min O_2

2.2.1 Data, Display, Storage, and Analysis with LABVIEW

Essential data includes the operating voltage, discharge current, operating frequency, gas flow rates, plasma gas temperature, electron kinetic temperature, and electron number density. Data that can be directly measured and stored are the voltage, current, frequency, gas flow rates, and plasma gas temperature. This data can be measured via probes, sensors,

and thermocouples. Kinetic temperature of electrons and the electron number density are quantities that must be determined by solving model equations. The atmospheric plasma device is interfaced to a data acquisition board (DAQ) via a connection board, and an IEEE interface card is installed on a PC to communicate with software from LABVIEW.

LABVIEW is a software package produced by national instruments intended to create an easy computer interface with measurement hardware. It allows for real-time presentation of the measurements being taken and also for analysis of those measurements.

Unlike other programming languages, LABVIEW uses pictures and icons rather than text windows to make programs. A schematic of the programming "code" (the block diagram) is shown below in conjunction with the user interface (front panel) created by the program. Each icon functions as a piece of code and can be easily modified or combined with other codes to create a complex program. LABVIEW comes complete with a collection of these iconic codes, so the need for traditional programming experience is greatly mitigated.

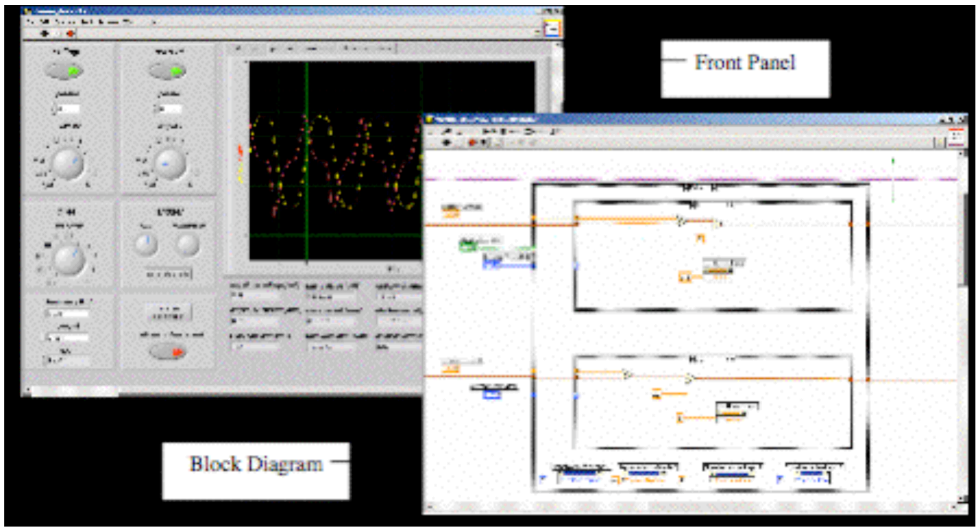

Figure 8: Front Panel and Block Diagram of LabVIEW System

As shown on the previous page, the front panel mimics the appearance of an oscilloscope, displaying voltage and current waveforms. The data can be manipulated by buttons similar to those found on a real oscilloscope with the use of a mouse. This characteristic of LABVIEW to mimic real devices is why it is called a Virtual Instrument or VI. Using a pre-programmed LABVIEW system is analogous to using a physical instrument, but prevents the need for an additional computer interface for the instrument. The LABVIEW also allows for mathematical solvers where the inputs to the solvers can be from real-time measured data and the output is the quantity of interest, such as electron number density or kinetic temperature and can be displayed on the front panel in real-time.

The LABVIEW system used on the Atmospheric Plasma Device is identical to the image shown above. The front panel mimics an oscilloscope, but includes additional information such as gas type, flow rate, and ambient temperature within the cell. The front panel information is updated every 200msec, making it practically real-time. This system was programmed by Thorsten Deichman, a graduate student from Asachen University, Germany and was completed during the summer of 2006 [8].

The LABVIEW system offers an essential innovation into the understanding of the behavior of atmospheric plasma in absence and in presence of a substrate inside of the test cell. Real-time monitoring allows the user to observe and detect changes in the operational parameters and plasma conditions as they occur. Data is viewed on the computer monitor and can be saved in data files for later use, analysis of variables, and to solve plasma models for indirect measurement of plasma parameters (such as the electron number density, electron kinetic temperature, and electron-neutral collision frequency).

2.3.1 Obtainable Data

The LABVIEW system has been programmed to record data in real-time and can automatically save and store data such as RMS current, absolute current, RMS voltage, absolute voltage, plasma gas temperature, gas flow rates, and it can calculate the impedance from voltage and current data. All data are automatically saved into a " .txt" file or an excel file as specified by the user.

There are two capabilities within LABVIEW for saving data. One method is controlled by the "save one loop iteration" button and will record all of the data for voltage, current, and time in one loop iteration (0.001 seconds, 125 data points). Information on flow rates, impedance, and electron number density solver is also obtained. Alternately, data can be collected using the "continuous data record" button. This button allows for monitoring of the voltage and current over an extended period (until the user ends the recoding process). The data collected includes RMS voltage and current, peak voltage and current, impedance, gas flow rates, and electron number density.

2.3.2 Data Acquisition Method

2.3.2.1 DAQ Boards

The measurement hardware of the system is connected to the LABVIEW data acquisition software by the use of two DAQ Boards.

The first DAQ board, a PCI-DAS1602/16 is manufactured by Omega Engineering and comes standard with a 16 bit resolution at a 200KHz sampling rate. In addition, it

contains two analogue output channels, analogue input channels (either a 16-channel single-ended or 8-channel differential), 16 digital input channels, and 16 digital output channels. It is used to monitor the temperature and gas flow rate of the system.

Additionally, another DAQ Board is used to sample the voltage and current. This DAQ Board produced by National Instruments, NI PCI-6221 M-series Multifunction data acquisition board, will be referred to as NI PCI-6221. Like the PCI-DAS1602/16 it has a 16 bit resolution, but it can sample at a higher rate of 250KHz. For this reason it is dedicated to the voltage and current, which need higher sampling rates. It features 16 single-ended analogue input channels, 2 analogue output channels, and 24 digital input/output channels.

2.3.2.2 Triggering

Software Triggering, also known as "conditional retrieval" is used to screen the data before it is introduced onto the front panel or into the spreadsheets. Triggering relies on the concept that certain specified conditions must be accepted before data display and solver processing. There are traditionally two conditions:

1) Data must be inside a window (defined by level and hysteresis) and

2) New data point values must be greater than the preceding value.

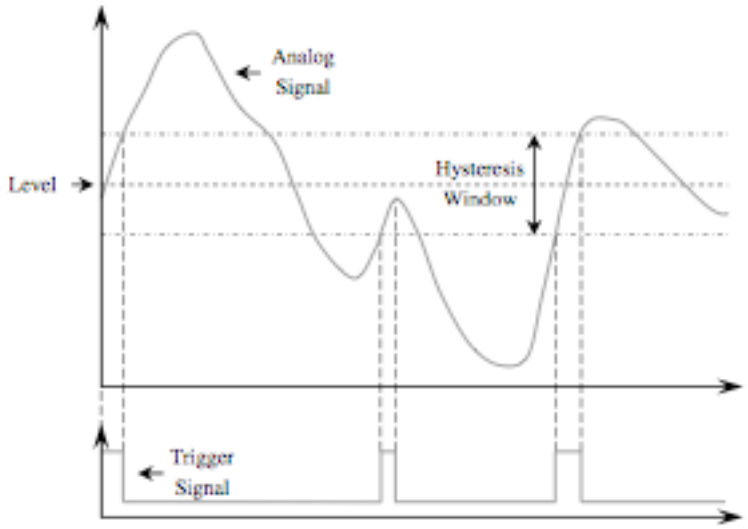

Figure 9: Hysteresis and Triggering Diagram

2.3.2.3 Voltage and Current Acquisition

A key component provided by the LABVIEW program is the ability to monitor discharge voltage and current in real-time. Voltage and current are essential for solving the plasma models to obtain key plasma parameters such as electron number density and electron kinetic temperature.

The hardware used to monitor voltage and current consist of a capacitively coupled, compensated high voltage probe and a Pearson current monitoring coil. The High Voltage probe is a Tektronizs P6051A with a 1mV: 1000V conversion and is attached to the NI PCI-6221 via input channel 1 (virtual channel address: dev1/ai1; physical channel: signal 33, ground 32). For measuring current there is a Pearson R Current Monitor with a 1mA:1mV converter attached to the same DAQ board via input channel 15 (virtual channel address: dev1/ai15; physical channel: signal 23, ground 2). The accuracy of the system is 1.5×10^{-4}

Volts and 6.1 x 10^{-6} Amperes.

2.3.2.3.1 One Loop Iteration Data

When activated, the one loop iteration button will record data on current, voltage and time for one loop iteration. 'One loop iteration' is defined as 0.001 seconds. During this time 125 data points will be collected. When plotted, this data can generate the sinusoidal oscillograms of voltage and current as displayed on the front panel.

2.3.2.3.2 RMS Voltage and Current

Root mean square (RMS) data represent the average value of RMS voltage and current over one cycle. Additionally, since data is collected using only one high voltage probe and one Pearson coil for both electrodes, the RMS values generated by LABVIEW are space averaged. The RMS values are calculated by LABVIEW using the following equation:

$$RMS_{cycle} = \sqrt{\frac{1}{numPo\,\mathrm{int}\,s}\sum_{i\in cycle}\left(waveform[i]\right)^2}$$

2.3.2.3.3 Absolute Voltage or Current

Absolute voltage or current represents the largest voltage swing during one cycle. If the magnitude of all points over the course of one cycle is obtained, the largest value will represent the peak voltage or current.

2.3.2.4 Gas Flow Regulation

The flow of gas into the plasma system is controlled by MKS Mass-Flo Controllers

(Model# 1478A14CR1BM) and the flow by volume is controlled by a MKS type 247 4-channel readout and control unit. The MKS 4-channel readout unit is connected to the LABVIEW software by PCI DAS1602/16 (virtual channel addresses: ai8 – ai11; physical channels: signal 3, 5, 7, 9, ground 18). This DAQ board is used for real time temperature monitoring by the flow controllers and the thermocouple. Thus the channel range is 0-1.25V and the accuracy of each data point is 1.9×10^{-4} L/min (where 1V equals 10 L/m). The data is displayed on the front panel in the corresponding real values.

2.3.2.5 Gas Temperature Measurements.

The ability to take real-time thermal measurements within the systems allows for characterization of the thermal spatial and temporal profiles in the presence or absence of a substrate. Temperature measurements are taken by an Omega Teflon coated thermo-couple moderated by a mV/ °F or a V/°C analog-to-digital converter. The data then enters PCI DAS 1602/16 (virtual channel address: ai7; physical channel: signal 16, ground 1), where it is processed by the LABVIEW system The temperature can be sampled at a rate of 5000Hz with an accuracy of ±0.019°F (channel range of 0-1.25V). LABVIEW records 1000 data points per while loop iteration. These data points are then averaged and displayed in the LABVIEW front panel every 200msec. They appear both numerically and quantitatively in the form of a thermometer icon.

2.4 Goal and Extent of Research

The goal of this work is to characterize the plasma produced in the Atmospheric Pressure Plasma device and to analyze the effects of plasma produced by this device on

several substrates.

Plasma characterization is essential for the understanding of plasma-substrate interaction. This device has been in use for several years, but the plasma parameters, including the electron density, electron temperature, and gas temperature have never been obtained and analyzed. The device has been used for treating fabrics with little attention to the types and variations of plasmas and their effects on the fabric.

This research focuses on obtaining the key plasma parameters for a variety of gas mixes. The electron number density and electron temperature are approximated using an electrical model as well as data from optical emission spectroscopy. Comparison between the data will help to benchmark the model as an accurate representation of the system and to further enhance the model for more generalized cases. Data for this model are obtained by using the LABVIEW software and the real time measurements of voltage, current, and plasma gas temperature.

In addition, gas temperature data are obtained to determine whether a temperature profile exists within the cell and to optimize the treatment of substrates. Data are obtained by varying the location of the thermocouple within the batch treatment cell to obtain the gas temperature spatial distribution.

Measurements and analysis in presence of substrates determines any changes occurring in the plasma parameters and how these changes may affect the substrates. The substrate chosen for this experiment is wool, a natural fiber. It is exposed to the same gas mixes for which the temperature profile and electron number density, were modeled. Comparisons between the changes in these values are obtained to gain insight on the processes at the plasma-substrate interface. These substrates are also subject to other tests

including weight change analysis, tensile testing, and EDS to determine if the plasma causes any changes in the substrates.

The ability of the plasma to create surface functional groups for chemical grafting was also studied. HTCC, an anti-microbial agent was grafted to cellulosic paper using oxygen plasma. The oxygen plasma functionalized the surface of the cellulose creating reactive groups onto which the HTCC could form permanent, covalent bonds. The success of the bond is examined using weight change analysis, SEM, colorimetry, and FTIR. A possible reaction mechanism is also developed.

3. Characterization of Plasma Parameters

3.1 Plasma Impedance

Plasma impedance is a function of the plasma dielectric constant, which in turn is a function of the plasma electron number density and the collision frequency. A capacitively coupled plasma (such as found in the atmospheric plasma device) can be modeled as a capacitor and a circuit model can be solved to obtain plasma parameters from measured discharge voltage and current.

A "one loop iteration" data can be obtained from LABVIEW for discharge voltage and current to ascertain the nature of the plasma. The sinusoidal behavior of the voltage and current and the phase angle determine the nature of the capacitive coupling and the plasma impedance. As seen from Figure 10, the voltage leads the current, confirming the predictions of a capacitive behavior. The voltage waveform is near-smooth sinusoidal, while the current has sharp rise and fall, indicating the fast breakdown condition. The phase angle appears to

be approximately 90 degrees, and thus the system behaves capacitively. The deviation of current and voltage from a pure sinusoidal form is a result of the series of breakdowns and plasma formations.

The admittance of the bulk plasma can be obtained from the amplitude of the current and voltage as:

$$Y_p = \frac{\tilde{I}_{RF}}{\tilde{V}_{RF}}$$

where $\tilde{I}_{RF}$ and $\tilde{V}_{RF}$ are the voltage and current amplitudes. The discharge current and voltage are both represented by a complex function in time:

$$I_{RF}(t) = R|\tilde{I}_{RF}e^{j\omega t}$$
$$V_P(t) = R|\tilde{V}_P e^{j\omega t}$$

Where $R|$ is the real value of voltage, $\tilde{V}_P e^{j\omega t}$ and the current, $\tilde{I}_{RF}e^{j\omega t}$.

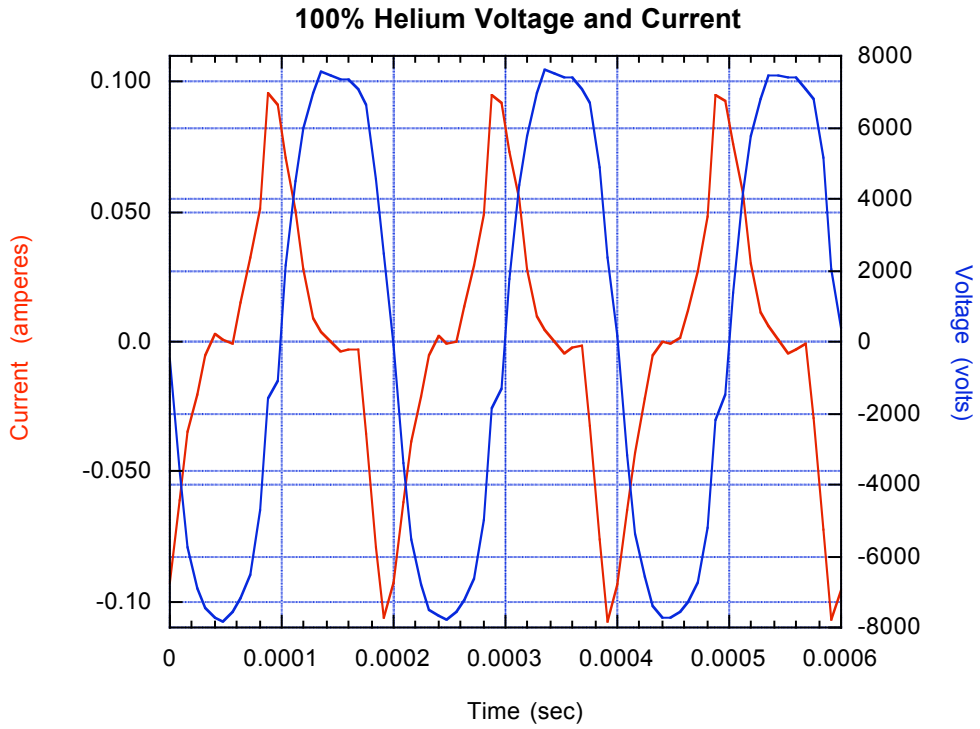

Figure 10: Amplitude of Voltage and Current

The plasma can be modeled as a capacitor in which the dielectric constant is determined by the plasma itself, and hence the plasma admittance is given by:

$$Y_p = \frac{j\omega\varepsilon_p A}{d}$$

$d = l - 2s = thickness\ \ of\ \ the\ \ plasma$

$s = thickness\ of\ the\ plasma\ sheath$

$A = Area\ \ of\ the\ \ electrode$

$\varepsilon_p = plasma\ \ p\text{ermittivity} = \varepsilon_0 k_p$

$\varepsilon_0 = permittivity\ of\ free\ space$

k_p = plasma dielectric constant

$j = \sqrt{-1}$

For simplicity, the thickness of the sheath will be neglected from the calculations of the plasma thickness, d. The plasma dielectric constant k_p is defined:

$$k_p = 1 - \frac{\omega_{pe}^2}{\omega(\omega - j\nu_{en})}$$

ω = *frequency of oscillating electric field*

ν_{en} = *electron – neutral collision frequency*

$$\omega_{pe} = \text{electron plasma freqency} = \left(\frac{ne^2}{\varepsilon_0 m_e}\right)^{\frac{1}{2}}$$

e = *unit charge*

n = *electron number density*(= *ions for quasineutral plasma*)

m_e = *electronmass*

ε_0 = *permittivity of free space*

$j = \sqrt{-1}$

Substituting ε_p in the plasma admittance equation and solving for the number density provides a means by which the electron number density can be obtained, hence:

$$Y_p = \frac{\tilde{I}_{RF}}{\tilde{V}_{RF}} = \frac{j\omega\varepsilon_p A}{d}$$

$$\frac{\tilde{I}_{RF}}{\tilde{V}_{RF}} = \frac{j\omega\varepsilon_0 A}{d}\left[\left[1 - \frac{\left(\frac{ne^2}{\varepsilon_0 m_e}\right)}{\omega(\omega - j\nu_{en})}\right]\right]$$

Since $\tilde{I}_{RF}$ and $\tilde{V}_{RF}$ are directly measured and stored by LABVIEW , it is possible to program the internal solver to display the number density in real time and store it in a

spreadsheet. Currently, only a single capacitor solver for electron number density is programmed into the LABVIEW system.

3.2 Plasma Gas Thermal Energy

3.2.1 Introduction

Plasma is a combination of ions, electrons, and neutral gas species. However, the ionization fraction for atmospheric pressure plasmas, as discussed earlier, is very small so the predominate species is the neutral gas. One essential characteristic of the neutral gas is its temperature, which can directly be measured (in degrees Celsius or Fahrenheit).

The neutral gas temperature within the plasma test cell is not expected to be constant and may change in both space and with time. As electrons gain kinetic energy, their collisions with the surrounding neutral gas causes an increase in the neutral gas temperature. This may also result in ionization of the gas molecules. In addition to electron-neutral collisions, the electrodes will get hotter due to the passage of conduction current through them, and thus transfer energy back to the gas in the form of conduction, convection, and radiation.

Measuring and monitoring the gas ambient temperature is very important for materials processing. All materials have transition points at which they change from solid to liquid and liquid to gas. If the ambient temperature approaches these thresholds, the material may change state within the plasma and become damaged. Certain materials, such as many synthetics and polymers, have a glass-transition temperature that is well below their melting

point, but irreparable damage to a fabric's structure, strength, and properties will occur if this temperature is reached. Measuring the temperature within the test cell allows for safe materials processing and control of the treatment. However, if ambient temperature is found to be too high, a cooling system can be incorporated in the electrodes. Furthermore, under some circumstances it may be desirable to have a hotter ambient temperature (still below glass transition), to induce the chemical reactions necessary for grafting compounds to a substrate.

The melting point, glass transition temperature, and point of irrevocable damage of several fiber materials are listed in Table 3.

Table 3: Melting Point and Glass Transition of selected Substrates [9,10]

Substrate	**Tg**	**Mp**	**Other Damage**
Acetate Paper)	190	260	---
Wool	---	---	140
Polyester	230	245	---
Rayon	---	---	150
Polyolefins	120	125-135	---

Grafting involves using plasma to create chemically reactive sites that can subsequently be reacted with, or grafted to a chemical compound. Generally this grafting is

accomplished post-plasma exposure, however a desired extension of this research is internal (one step) grafting, where chemical reactions will occur during plasma exposure. In order to induce a chemical reaction, the correct temperature must also be achieved and maintained. Thus, the ambient temperature must be known to ascertain whether a reaction will or will not occur, and whether the gas should be pre-heated before entering the chamber.

This internal grafting or "dry" chemistry would prove more cost effective and environmentally safe, since large amounts of solvent would be unnecessary, and would reduce the exposure of humans to chemicals.

The data obtained by measuring and monitoring the ambient temperature within the plasma test cell also helps in modeling the plasma itself. The plasma model for electron number density includes a solver for the electron-neutral collision frequency, which is a function of the neutral gas temperature.

3.2.2 Experimental

The ambient temperature was obtained for several spatial locations and for the gas mixes used in this research. These gas mixes are shown in Table 4 and the measuring locations are shown in Figure 11.

Table 4: Experimental Gas Mixtures

100% Helium
99% Helium 1% Carbontetrafluoride
98% Helium 2% Carbontetrafluoride
99% Helium 1% Oxygen
98% Helium 2% Oxygen
98% Helium 1% Carbontetrafluoride 1% Oxygen

A Teflon-coated thermocouple is inserted into the test cell with the thermocouple's tip at the pre-determined location. Due to the symmetrical geometry, data were only collected from one side of the test cell.

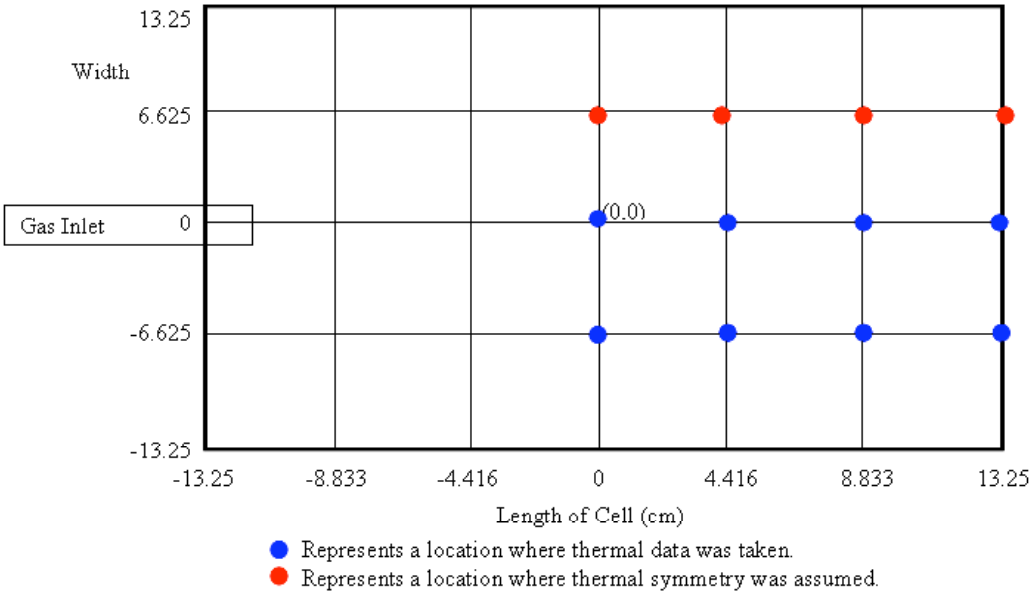

Figure 11: Diagram of Thermocouple Positions

3.2.3 Ambient Gas Temperature Data

Figures 12 through 13 show the temperature distribution inside the test cell. Figure 12 shows the temperature distribution for a pure helium discharge after 5 seconds of operation. As seen from the figure, the temperature distribution is near uniform, however, the center is cooler than the boundaries due to the attachment to the electrodes. Figure 13 shows how the temperature distribution changed after 15 minutes (pure helium discharge), in which it is clear that the temperature rises to about 50°C and remains slightly cooler in the center.

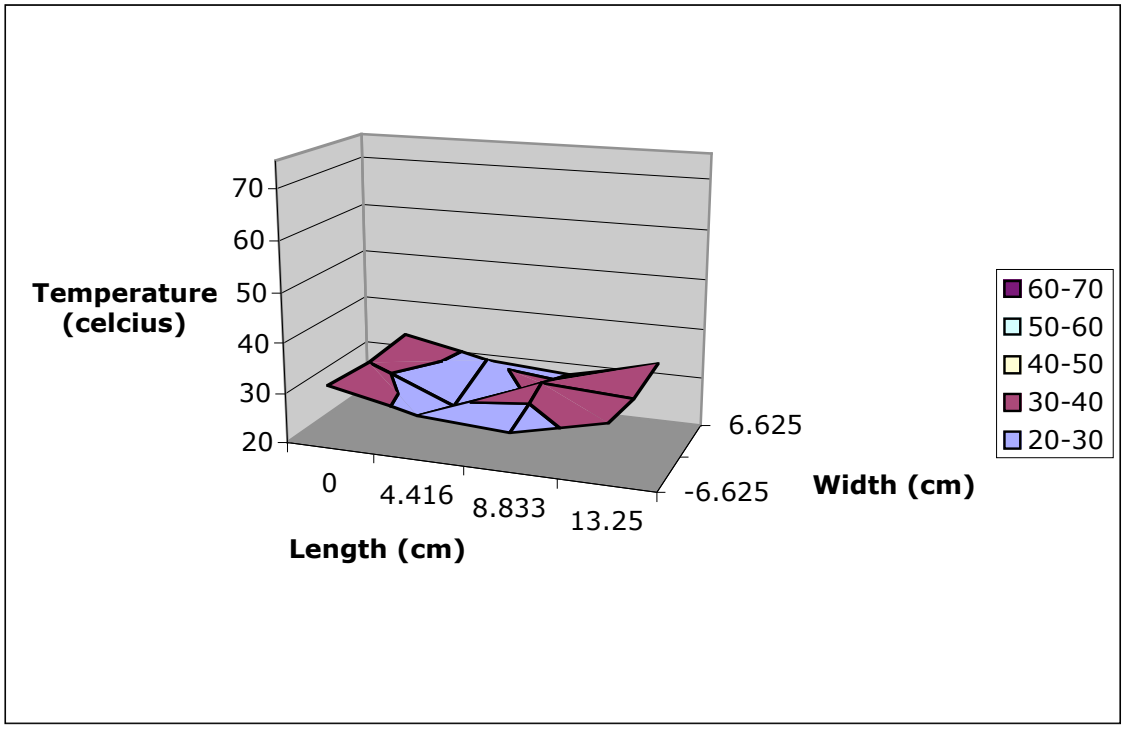

Figure 12: Test cell temperature distribution, 100% Helium plasma after 5 seconds operation

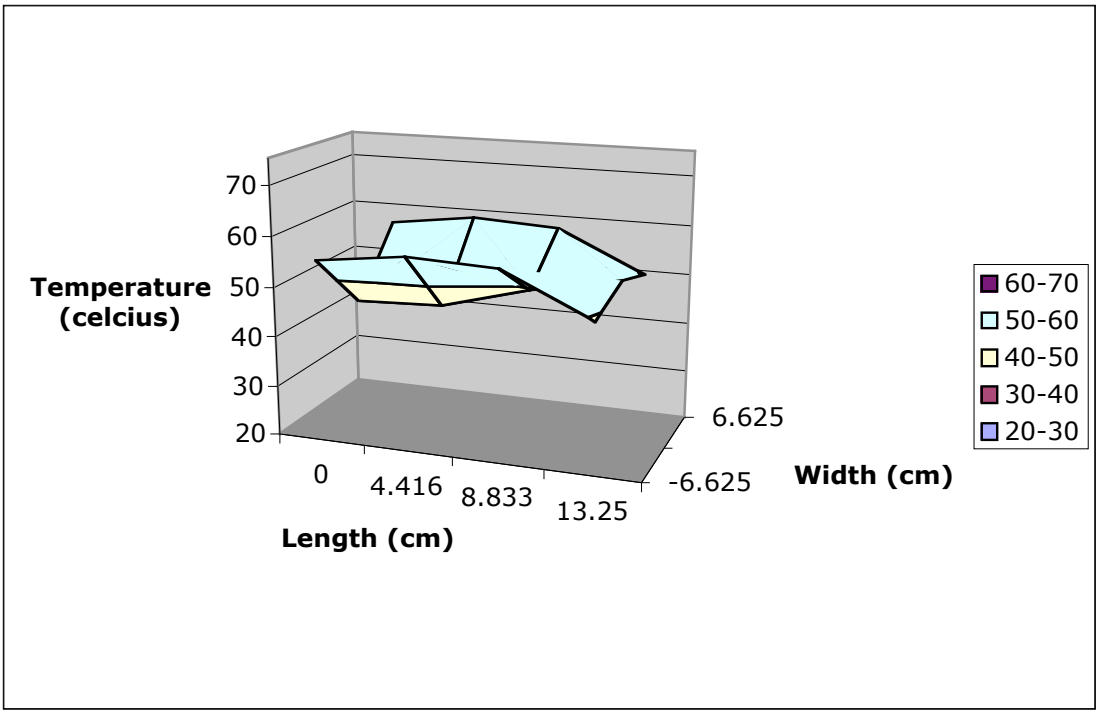

Figure 13: Test cell temperature distribution, 100% Helium plasma after 15 minutes operation

When adding 1% oxygen to the helium plasma, the temperature after 5 seconds appears uniform and close to 40°C with a slight gradient as seen in Figure 14. Monitoring the temperature rise up to 15 minutes shows an increase to the range of 50-60°C with end gradient effects as shown in Figure 15.

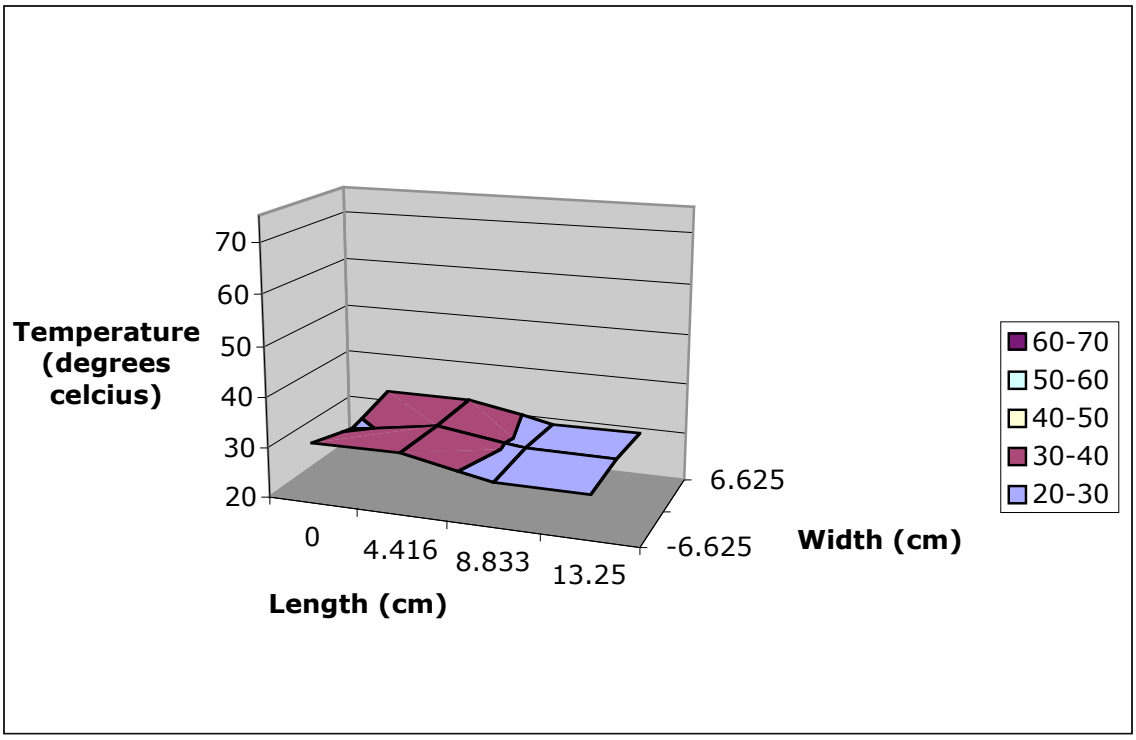

Figure 14: Temperature distribution, 99% Helium+1% O2 plasma after 5 seconds operation

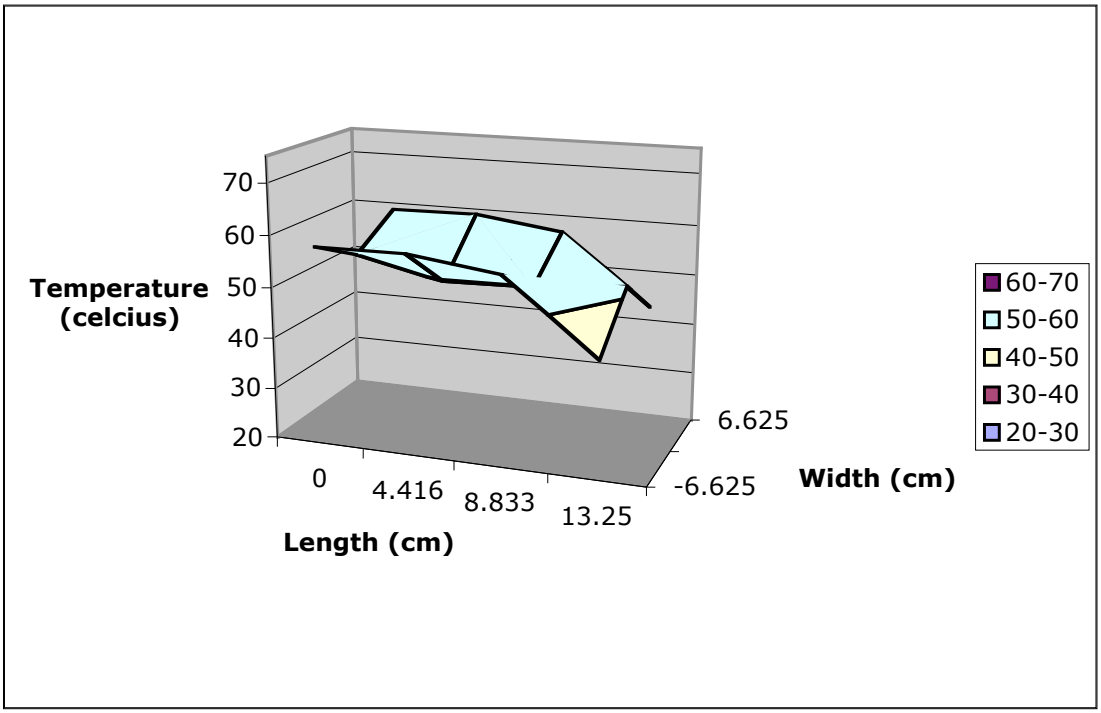

Figure 15: Temperature distribution, 99% Helium+1% O2 plasma after 15 minutes operation

Further increase in oxygen content to 2% allows for the temperature to be almost uniform with much less gradient, but maintained at close to 30-40°C for a 5 second operation (Figure 16) and maintained uniform with an increased operation time of 15 minutes (Figure 17), however the distribution has a slight gradient in the middle.

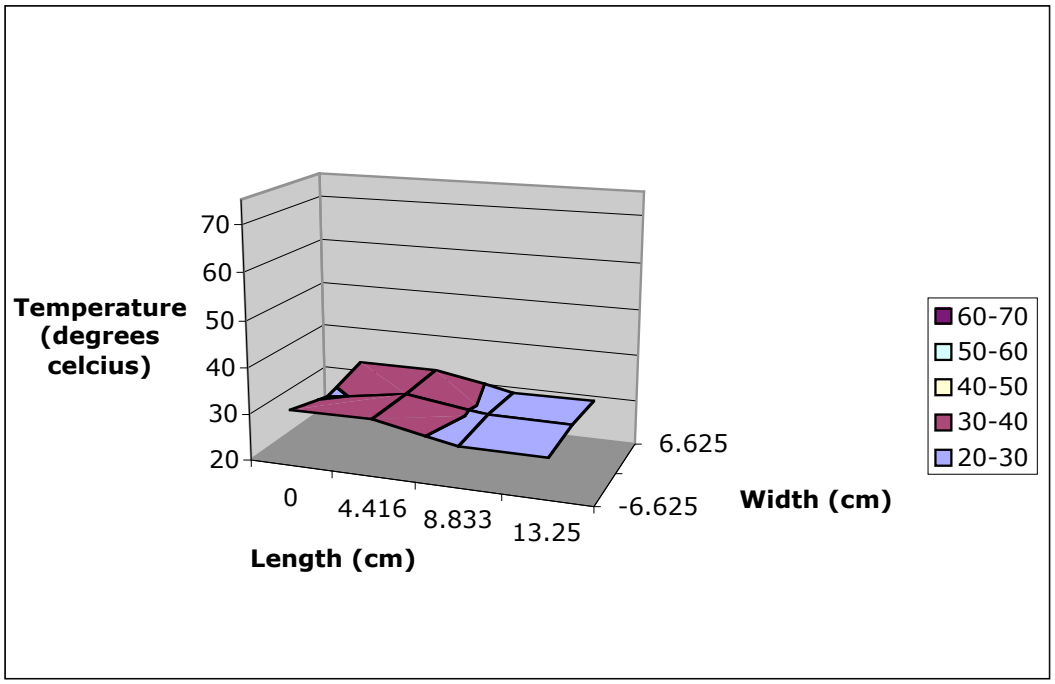

Figure 16: Temperature distribution, 98% Helium + 2% Oxygen after 5 seconds operation

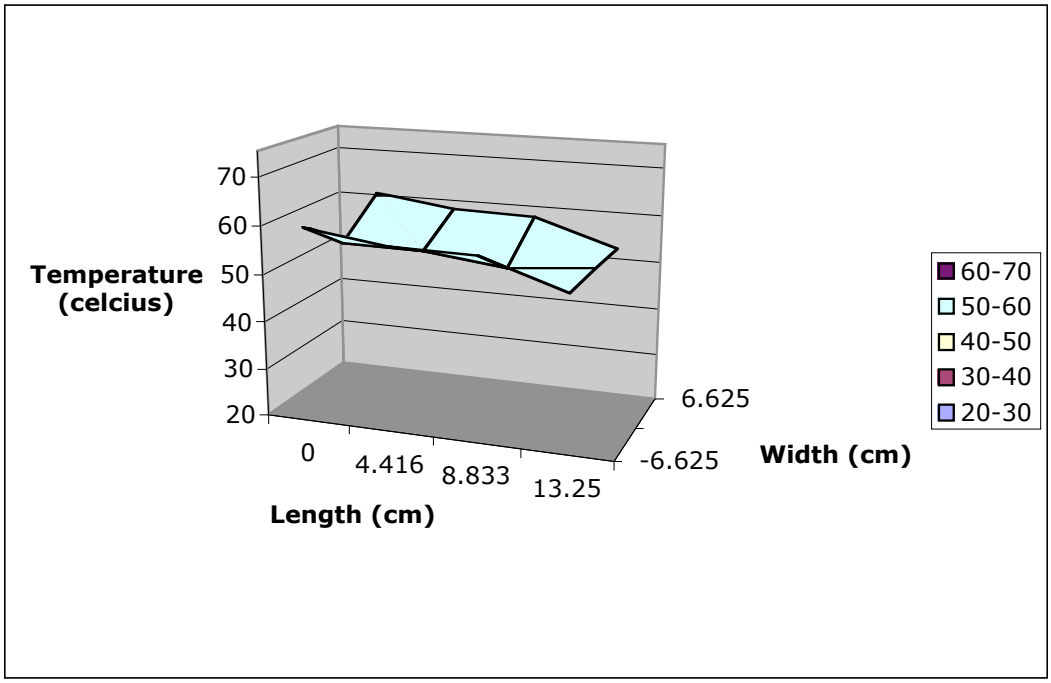

Figure 17: Temperature distribution, 98% Helium + 2% Oxygen after 15 minutes operation

Figures 18 and 19 show the distribution when using a 1% carbontetrafluoride (CF_4) for 5 seconds and 15 minutes of operation. Similar trends were observed for the shorter operation time of 5 sec, however a stronger gradient takes place for longer operation times (15 minutes).

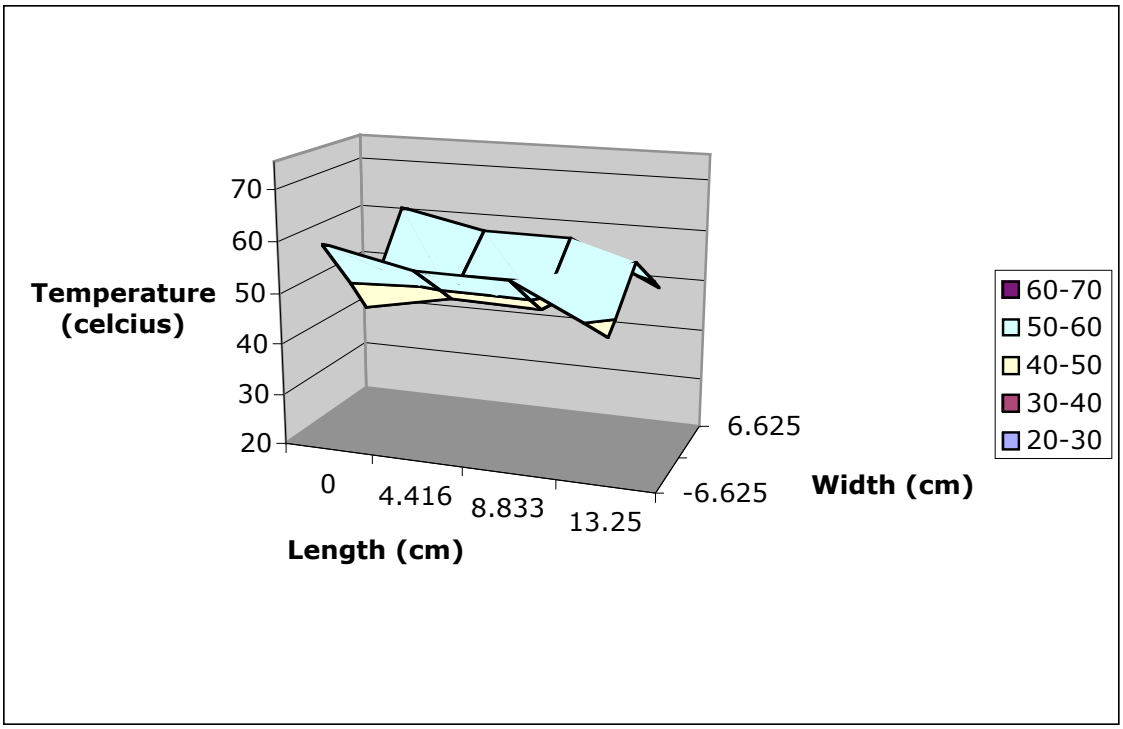

Figure 18: Temperature distribution, 99% Helium + 1% CF4 after 5 seconds operation

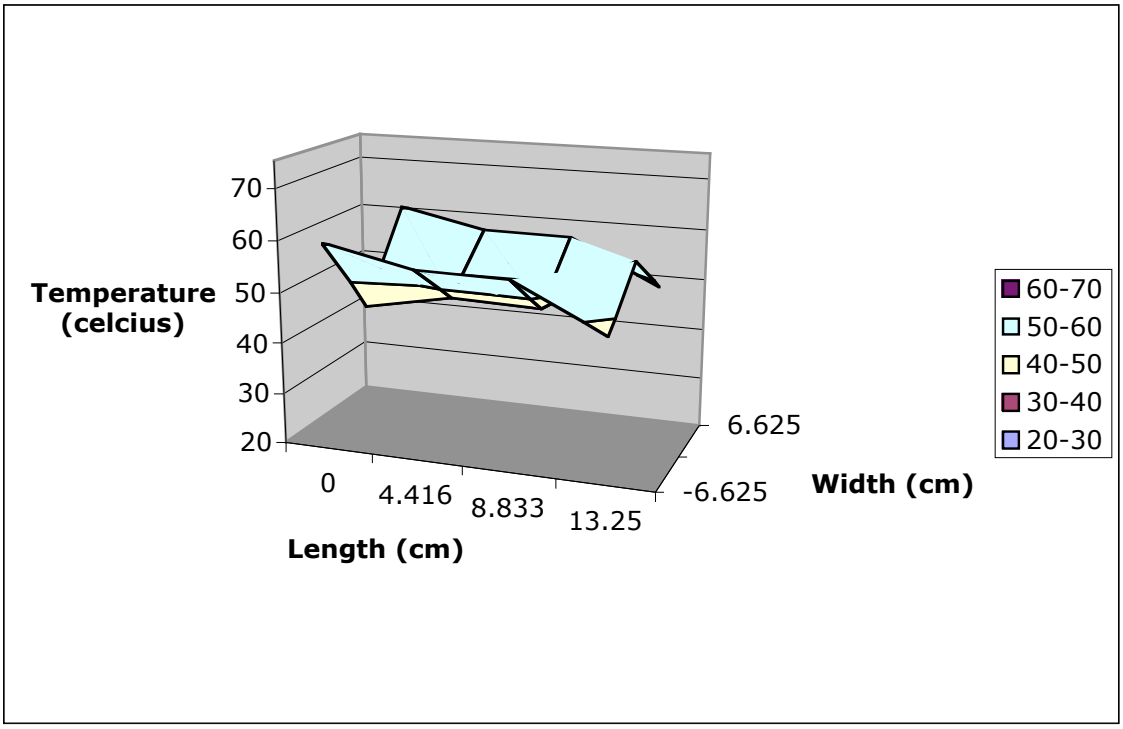

Figure 19: Temperature distribution, 99% Helium + 1% CF4 after 15 minutes operation

When increasing the percentage of CF_4 to 2%, a different distribution is observed. For the 5 second operation (Figure 20) the temperature distribution is quite uniform in the 30-40^{o}C range, however, after 15 minutes of operation there is a strong gradient from the edges towards the center, with the edge temperature approaching 70^{o}C (Figure 21), and the center remaining in the 50-60^{o}C range. It appears that stronger reactions take place with extended operation time and more dissociative processes lead to higher collisionality of electrons with dissociated fluorine, fluorine ions or CF_3 molecular species.

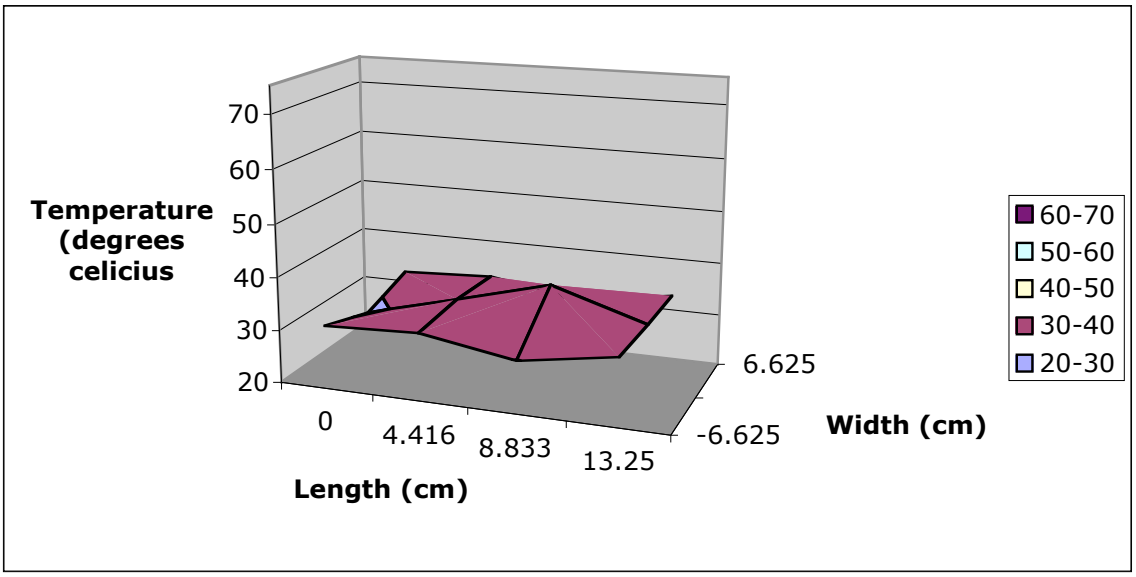

Figure 20: Temperature distribution, 98% Helium + 2% CF4 after 5 seconds operation

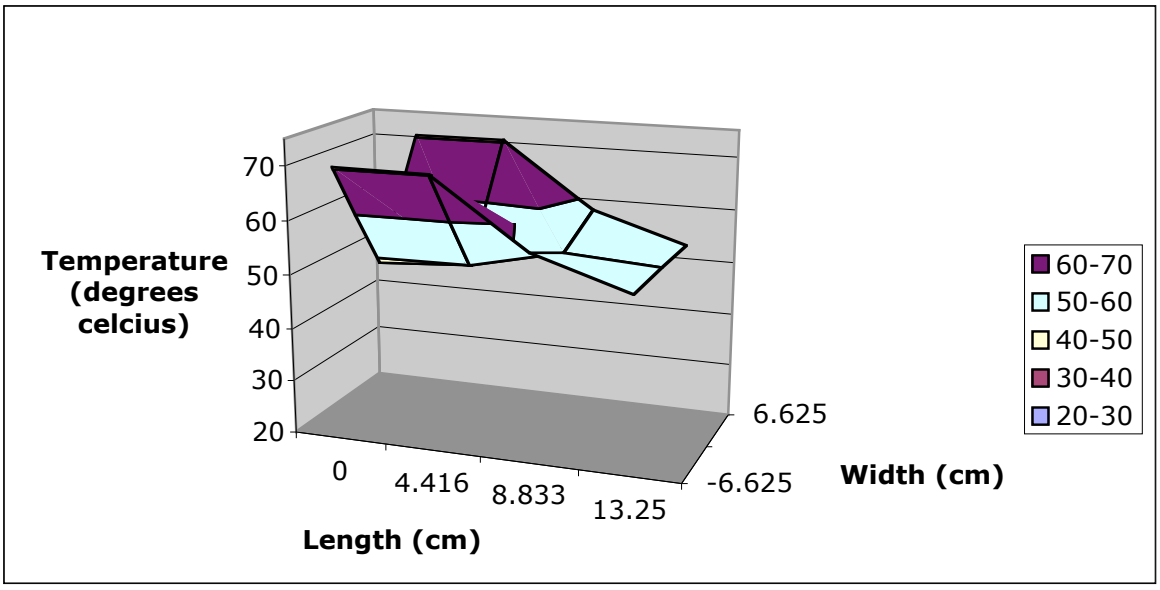

Figure 21: Temperature distribution, 98% Helium + 2% CF4 after 15 minutes operation

A mixture of O_2 and CF_4 with the helium plasma shows temperature profiles much similar to the case of 2% O_2, as shown in Figures 22 and 23. This is due to the fast recombination of dissociated fluorine ions or molecular fluorine with oxygen, thus the oxygen content dominates the collisional processes and the distribution appears similar to the oxygen case.

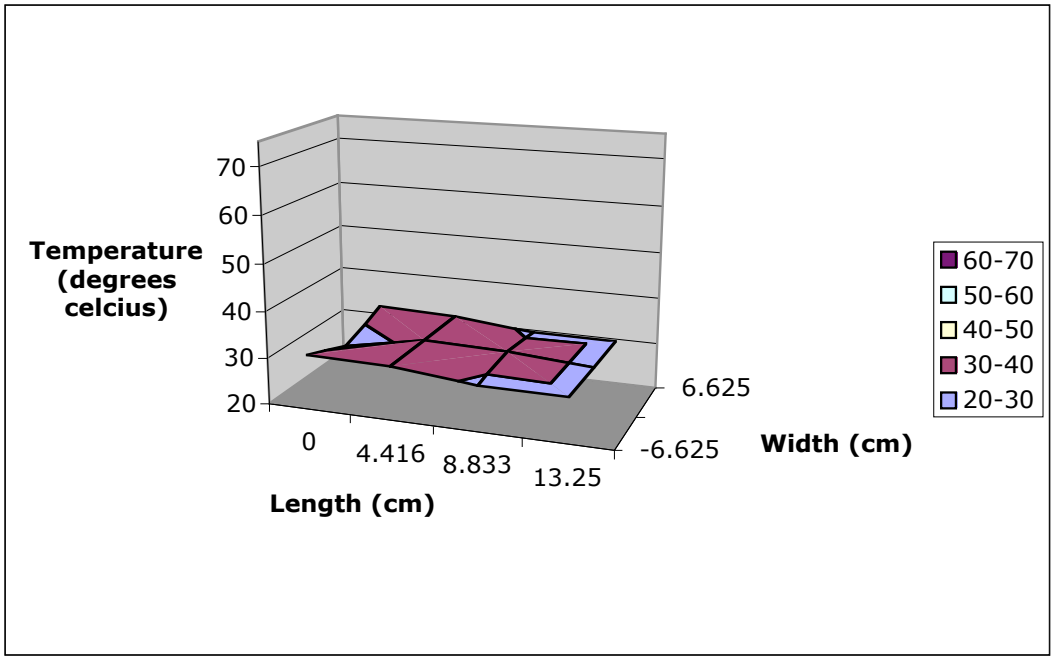

Figure 22: Temperature distribution, 98% Helium +1% O2 + 1% CF4 after 5 seconds operation

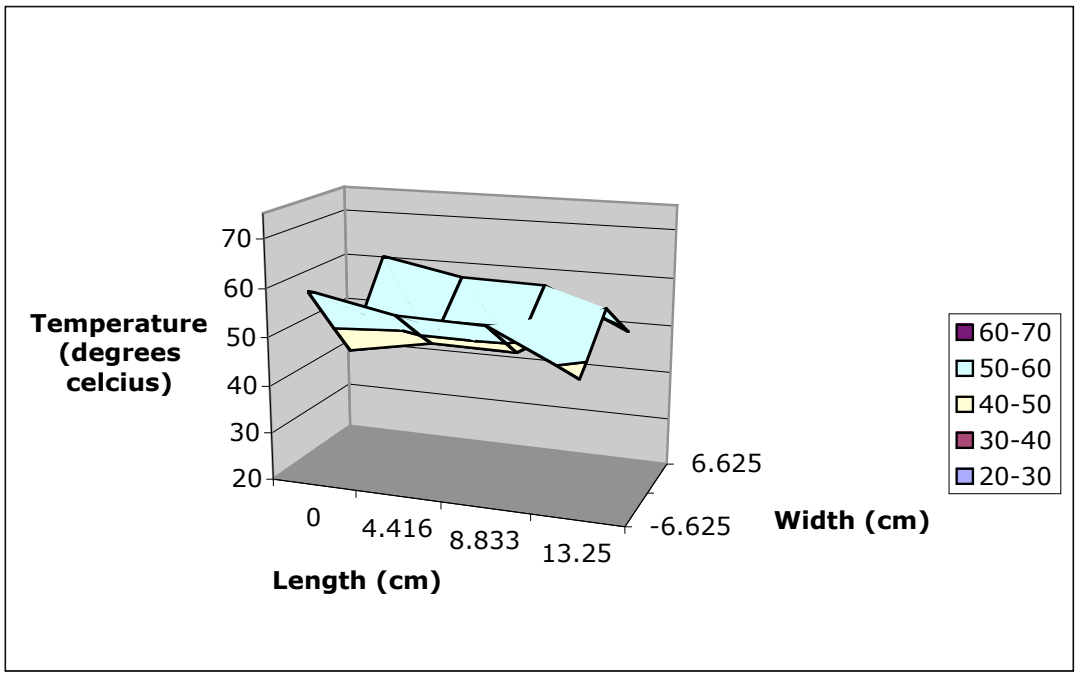

Figure 23: Temperature distribution, 98% Helium + 1% O2 + 1% CF4 after 15 minutes operation

A comparison between all of the different gases at 15 minutes reveals a similar overall profile of the temperature distribution in the test cell. At a time only five seconds after the electrodes have been turned on, the gas temperature remains around room temperature and the distinctive gas profile seen after 15 minutes is significantly less pronounced. All the gases exhibit a lower temperature at y=0, x=0, the center of the cell. As can be seen from the figures, the horizontal line, y=0.0, remains at a temperature lower than that of the surrounding gas and gas near the cell walls. This is due to incoming gas flowing into the closed-geometry test cell and mixing with the generated plasma, thus cooling the center. Incoming gas enters the cell at the center of the wall at location (-13.25 cm, 0.0 cm) at room temperature with a pressure force in the horizontal, positive x-direction. The flow is more laminar and less turbulent and thus the incoming flow pushes the plasma towards the walls, creating hotter boundaries. This is also shown by the increase in temperature along the walls or the y=6.25 cm and y=–6.25 cm lines. Despite the similarities between gas temperature profiles for the center of the cell, the shapes do differ at the far edges, at x=13.25 cm. Here, the outer temperatures, at y=6.25, are similar to those found along the center at the y=0.0 cm line. This is observed for all the gases and suggests that the incoming gas is exiting the system at these locations. It therefore does not reside within the cell long enough to increase the temperature to that close to the cell walls. However, at x=13.25 cm, y=0.0 cm, the temperature distribution falls into one of two groups for all gases, either the temperature increases to that of the side walls, or the temperature is uniform at the far wall. The cases of 1% O_2 and 1% CF_4 additions all fall into the category of gradient with increase towards the walls, while the 2% CF_4 and 2% O_2 gas mixes maintain a uniform distribution. This may suggest that the additional percentages homogenize the plasma

formation and thus the collisional effects are more uniform for the entire distribution.

3.3 Plasma Models

3.3.1 Electron Number Density

The electron number density is a key parameter in determining the nature of plasma, including the plasma frequency, the plasma electrical conductivity, the shielding mechanism and the Debye length. For a quasi-neutral plasma, the number density of electrons and ions are equal $n_e \sim n_i \sim n$, and hence the calculated electron number density is also a measure of the ion number density ($n_e = \sum_j n_j$) where n_j is the population of the jth ionic species. Ions play a large role in etching, and changing the surface functionality of substrates as they attach (crosslink) to open sites during substrate activation by the plasma.

To develop a model to determine the electron neutral collision frequency, one may start from the equation of the plasma dielectric constant, which is given by:

$$k_p = \left[1 - \frac{\omega_{pe}^2}{\omega(\omega - j\nu_{en})}\right]$$

For plasma generated between two parallel planar electrodes, the model could be taken from an equivalent circuit element, a capacitor. However, no circuit is completely capacitive and all plasma possesses resistive behavior and inductive components. Additionally, the dielectric materials that house the copper electrodes have a capacitive effect. Three electrical circuit models for analyzing the plasma are displayed in Figure 24 through 26.

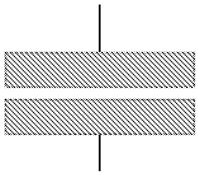

Figure 24: Single capacitor model equivalent plasma and insulators

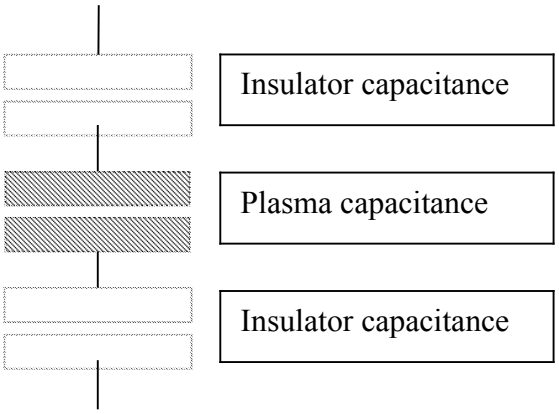

Figure 25: Triple capacitor model representing plasma and insulators' capacitances

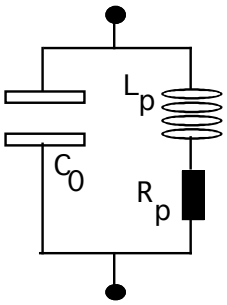

Figure 26: Complex inductor, resistor, and capacitor plasma model

Although the model containing all three electrical elements provides the most complete picture of the plasma, the single or triple models may still be used effectively. The single capacitive model neglects the capacitive effect of the dielectric barrier material and thus, the triple capacitor was chosen for analysis and data calculations.

The triple capacitor can be represented by three capacitors in series, where C_p is the plasma capacitance and C_D is the capacitance of the dielectric material:

$$\frac{1}{C_T} = \frac{2}{C_D} + \frac{1}{C_P} = \frac{2C_P + C_D}{C_P C_D}$$

And thus the admittance is given by $Y_p = \frac{1}{Z}$ where $Z = \frac{1}{j\omega C_T} = \frac{1}{j\omega \frac{C_P C_D}{2C_P + C_D}} = \frac{2C_P + C_D}{j\omega C_P C_D}$

$$Z = \frac{2K_P \frac{A_P}{\delta_P} + K_D \frac{A_D}{\delta_D}}{j\varepsilon_0 \omega K_P \frac{A_P}{\delta_P} K_D \frac{A_D}{\delta_D}} = \frac{2K_P A_P \delta_D + K_D A_D \delta_P}{\varepsilon_0 j\omega K_P A_P K_D A_D}$$

hence, $K_P = \frac{K_D A_D \delta_P}{2A_P \delta_D - j\varepsilon_0 Z\omega A_P K_D A_D}$

Substituting for the plasma dielectric constant and solving for electron plasma frequency:

$$\omega_{pe}{}^2 = -\left(\omega^2 - j\omega\upsilon_{en}\right)\left(\frac{2K_D A_D \delta_P A_P \delta_D + j\varepsilon_0 K_D{}^2 A_D{}^2 \delta_P Z\omega A_P}{4A_P{}^2 \delta_D{}^2 - Z^2 \varepsilon_0{}^2 \omega^2 A_P{}^2 K_D{}^2 A_D{}^2} - 1\right)$$

With electron plasma frequency $\omega_{pe}^2 = \frac{n_e e^2}{m_e \varepsilon_0}$

Then the electron number density would be expressed as:

$$n_e = \frac{\left(\omega^2 - j\omega\upsilon_{en}\right)m_e\varepsilon_0}{e^2}\left(1 - \frac{2K_D A_D \delta_P A_P \delta_D + j\varepsilon_0 K_D{}^2 A_D{}^2 \delta_P Z\omega A_P}{4A_P{}^2\delta_D{}^2 - Z^2\varepsilon_0{}^2\omega^2 A_P{}^2 K_D{}^2 A_D{}^2}\right)$$

from which the number density is

$$n_e = \frac{m_e\varepsilon_0\omega^2}{e^2}\left[1 - \left(\frac{2K_D A_D \delta_P A_P \delta_D + \upsilon_{en} K_D{}^2 A_D{}^2 \delta_P Z A_P \varepsilon_0}{4A_P{}^2\delta_D{}^2 - Z^2\varepsilon_0{}^2\omega^2 A_P{}^2 K_D{}^2 A_D{}^2}\right)\right]$$

Where K_D is the dielectric constant of the insulator (dielectric barrier);, A_D and A_p are the cross sectional areas of the dielectric and the plasma, respectively; δ_D and δ_p are the thicknesses of the dielectric and the plasma, respectively, ν_{en} is the electron-neutral collision frequency, and Z is the impedance determined by the amplitudes of the discharge voltage and current $Z = \frac{\left|\widetilde{V}_{RF}\right|}{\left|\widetilde{I}_{RF}\right|}$.

All of the quantities in the above equation are known since Z is determined by measuring the voltage and current, except for the collision frequency ν_{en}, which is either taken as a constant value or must be separately calculated. The electron-neutral collision frequency can be calculated as a function of the number density, the kinetic temperature of plasma electrons as it is related to the collisional cross section, and the average velocity over a Maxwellian distribution.

3.3.2 Electron Neutral Collision Frequency

The electron-neutral collision frequency is an important parameter. It represents the number of times an electron will collide with a neutral gas molecule within a given time (collisional time). Since electrons are small and respond to the instantaneous changes in the

electric field, they are able to absorb high levels of energy (often expressed in units of electron volt, eV).

Due to the dense nature of atmospheric plasmas, the mean free path (or time between collisions) is relatively short. This means that an electron will rapidly collide with other species in the plasma. The dominant species within atmospheric plasma is the neutral gas, so most collisions will take place between the high energy electrons and the plentiful gas molecules. These collisions are generally elastic but may result in the transfer of sufficient energy to the gas molecule to cause excitation, dissociation, or ionization.

The electron neutral collision frequency is defined as:

$$\nu_{en} = n_n \sigma \langle u \rangle$$
$$n_n = number\ density\ of\ \ neutrals$$
$$\sigma = collision\ cross - \sec tion$$
$$\langle u \rangle = average\ velocity\ (Maxwellian)$$

The values for the n_n, σ, and $\langle u \rangle$ can be approximated using the ideal gas law, solid sphere collision model, and the average velocity of a neutral gas molecule for a Maxwellian distribution.

3.3.2 Solid Sphere Collision Model

The solid sphere collision model assumes that the colliding particles can reach each other in a 'true' collision, and thus the cross section may be taken as the sum of the diameters of the particles, as shown in Figure 27.

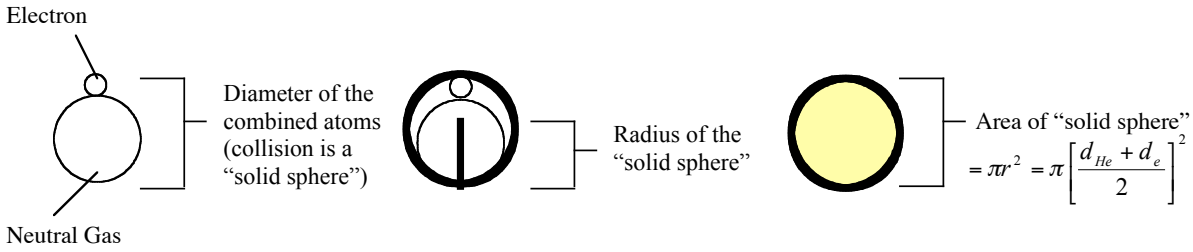

Figure 27: Illustration of the solid sphere collision model

Thus the collisional cross section in the solid sphere collision model can be defined as:

$$\sigma = \pi r^2 = \pi \left[\frac{d_{He} + d_e}{2} \right]^2$$

This cross section can be calculated from the tabulated known sizes of the electron and the atoms with which collision takes place.

3.3.2.2 Maxwellian Velocity Distribution Function

The Maxwellian distribution, also known as Maxwell-Boltzman velocity distribution function, describes the distribution of particles with respect to velocity $f(v) = \frac{dn_v}{dv} = \frac{4n}{\pi^{1/2}} \left(\frac{m}{2kT} \right)^{\frac{3}{2}} v^2 e^{-\frac{mv^2}{2kT}}$ and hence the total number of particles is the integral of the distribution function over velocity space $n = \int_0^\infty f(v) dv$. Figure 28 shows a graphic representation of the distribution function and various kinetic temperatures.

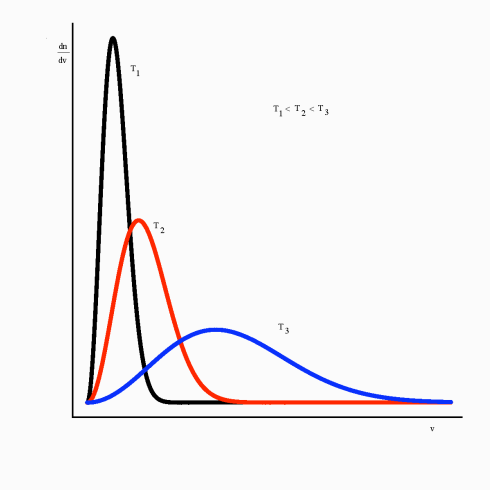

Figure 28: Maxwellian velocity distribution function

The average velocity <*v*> of a Maxellian distribution is given by

$$< v >= \sqrt{\frac{8KT_e}{\pi m_e}}$$

where

K = *Boltzmann's constant*

T_e = *kinetic temperature of electrons*

m_e = *massof electrons*

The average velocity of the electrons will be used to solve the plasma model.

3.3.2.3 Ideal gas Law

The ideal gas law relates the pressure and volume to the number of particles and their respective temperature. $PV = nRT$, where P is the pressure, V is the volume, n is the number of moles of gas molecules, R is the ideal gas constant and T is the kinetic temperature.

Using the ideal gas law into the equation for the electron neutral collision frequency,

the electron-neutral collision frequency can be expressed as:

$$\nu_{en} = \frac{P_{gas}}{kT_{gas}}$$

This approximation for electron-neutral collision frequency is a function of the neutral gas temperature. Thus the ability of the LABVIEW data acquisition system to monitor the real-time ambient temperature of the plasma becomes important for calculating the electron number density.

For helium plasmas, a typical value of the electron neutral collision frequency is approximately 4.89 x 10^{11} sec^{-1}. This value agrees with the electron neutral collision frequency tabulated for other similar atmospheric pressure plasma devices [7].

3.3.3 Electron Number Density Model

As previously shown in Section 3.3.1 for the three-capacitor model, and upon substitution for the impedance *Z* and the collision frequency ν_{en}, the electron number density could now be expressed by:

$$n_e = \frac{m_e \varepsilon_0 \omega^2}{e^2}\left[1 - \left(\frac{2K_D A_D \delta_P A_P \delta_D + \frac{P_{gas}}{kT_{gas}} K_D{}^2 A_D{}^2 \delta_P \left|\frac{\tilde{V}_{Rf}}{\tilde{I}_{Rf}}\right| A_P \varepsilon_0}{4A_P{}^2 \delta_D{}^2 - \left|\frac{\tilde{V}_{Rf}}{\tilde{I}_{Rf}}\right|^2 \varepsilon_0{}^2 \omega^2 A_P{}^2 K_D{}^2 A_D{}^2}\right)\right]$$

All values in the above model are either known or directly measured. When typical values are plugged into this model, an electron number density of 9x10^{12} / m^3 is obtained,

which is consistent with values obtained by other researchers [7].

3.3.4 Electron Number Density Model Data

The electron number density model is a function of temperature, voltage, and current. All of these parameters are subject to change over time and therefore an electron density profile can be obtained using the corresponding changes in these parameters inside the test cell. The density profile can be graphed to show the spatial distribution by employing the same grid system previously used (Figure 11) for plotting the ambient temperature profiles. However, it is important to note that voltage and current are averaged spatially over the entire discharge by LABVIEW. Therefore the only changes in these parameters will be due to time effects. Temperature, however, has been obtained both spatially and temporally for the entire cell.

This gas temperature data were used to solve for the electron neutral collision frequency. As an example of density distribution over various operational times and different gas concentration, plots of the electron number density distribution are shown in Figure 29 through 31 for 1% CF_4 gas. In Figure 29, the electron number density for helium + 1% CF_4 is shown at 5 seconds, in which the density peaks to ~ $10^{13}/m^3$ at the edges and drops to ~9.5 x $10^{12}/m^3$ in the middle. On average, one may consider that the density is almost uniform (9.5 x 10^{12}-1.1 x 10^{13}/ m^3).

Extending operation time to 5 minutes, Figure 30, shows a smoothed distribution with the number density 8.5 x 10^{12}-9.5 x $10^{12}/m^3$, almost uniform. The reason for density slightly dropping is the etching mechanism, followed by recombination processes. Etching due to CF_4 induces various dissociation processes and produces F, F^+, possible F^- and CF_2, all of

which enhance recombination rates and cause a drop in electron number density. This is also evident when extending operation time to 15 minutes at the same CF_4 concentration (1%), as shown in Figure 31 where the number density is almost uniform but slightly lower (8.5 x 10^{12}-9.0 x $10^{12}/m^3$).

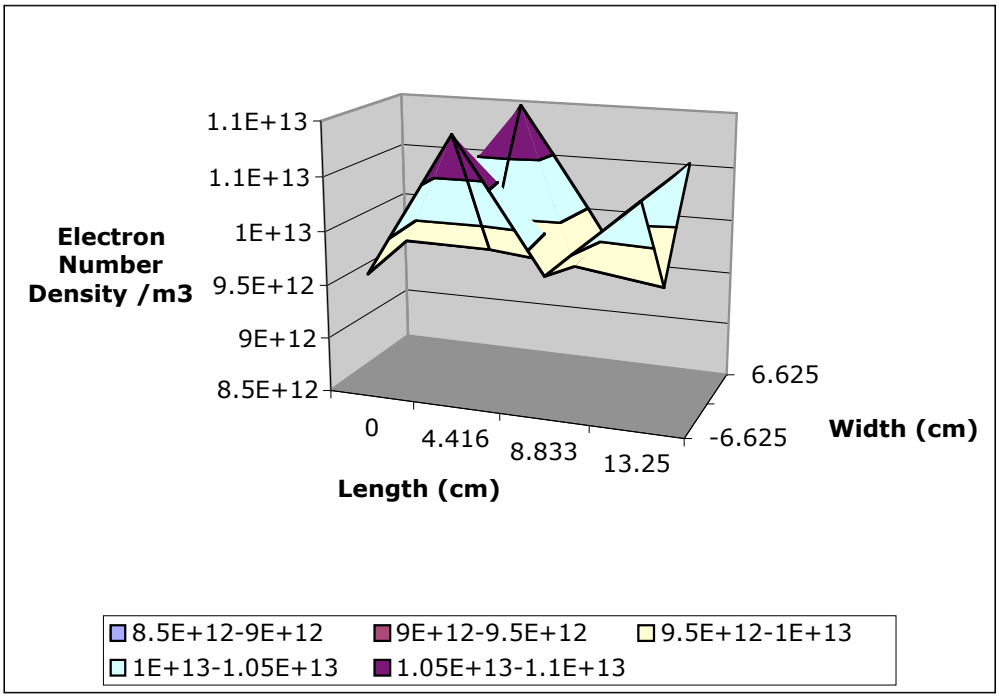

Figure 29: Density distribution for 1% CF4 at 5 seconds

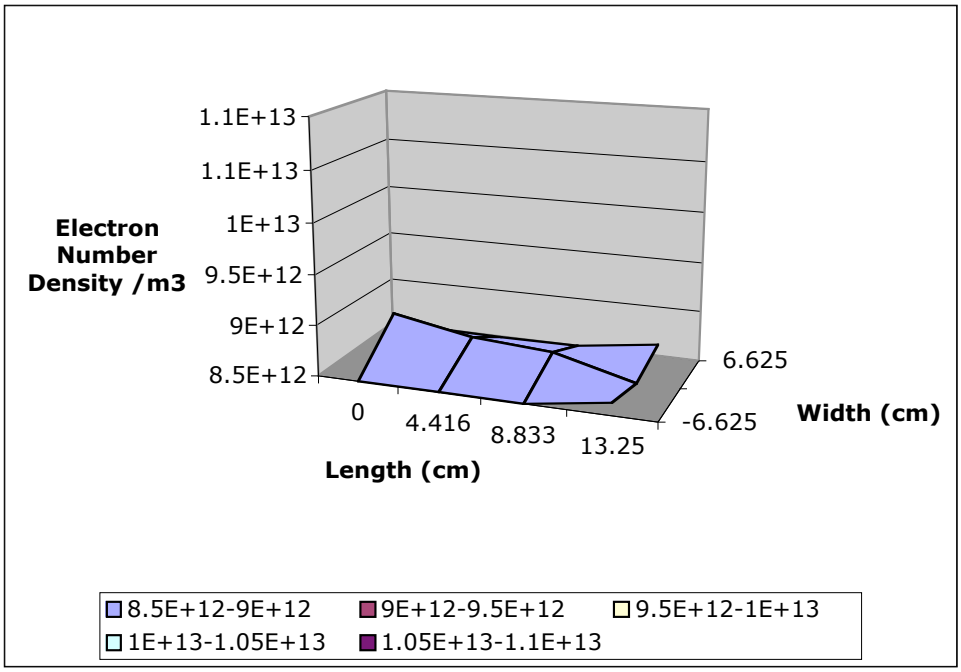

Figure 30: Density distribution for 1% CF4 at 5 minutes

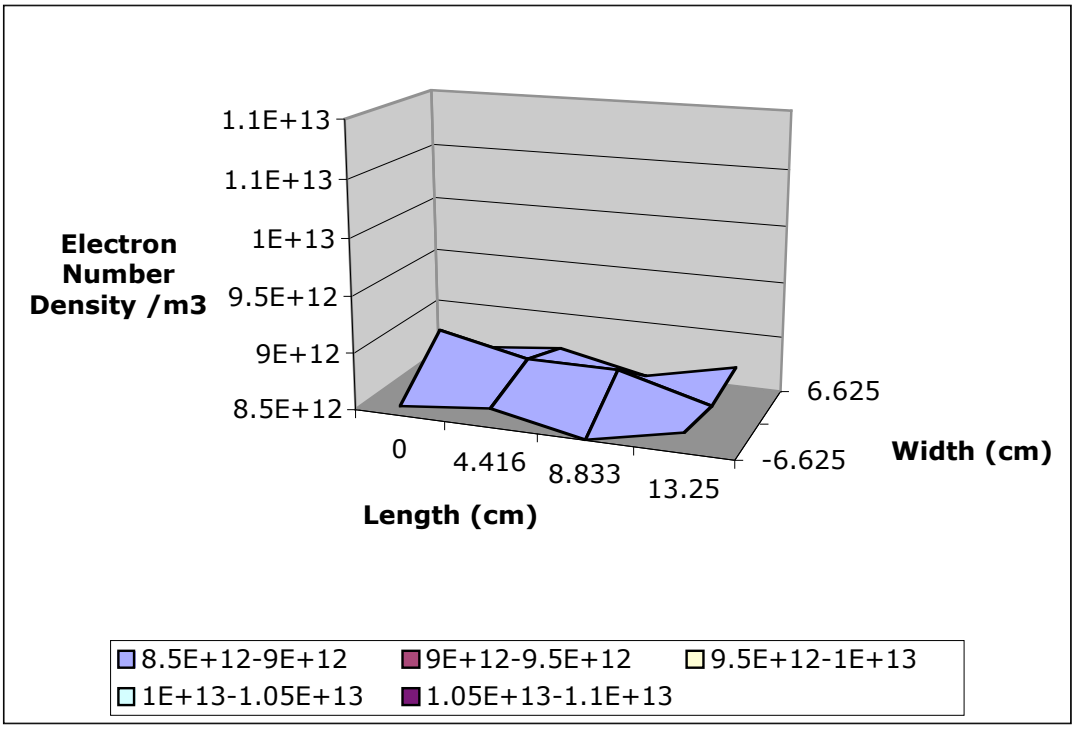

Figure 31: Density distribution for 1% CF4 at 15 minutes

The increase in gas concentration from 1% to 2% CF_4 has no dramatic effect on density distribution, and all distributions are similar for similar operational times as seen in Figures 3.23, 3.24 and 3.25. For the shorter operation time of 5 seconds, there is density gradient from edges towards the center, but for extended operation time of 5 and 15 minutes, the density profiles are uniform and within the same ranges previously observed for the 1% CF_4 concentration.

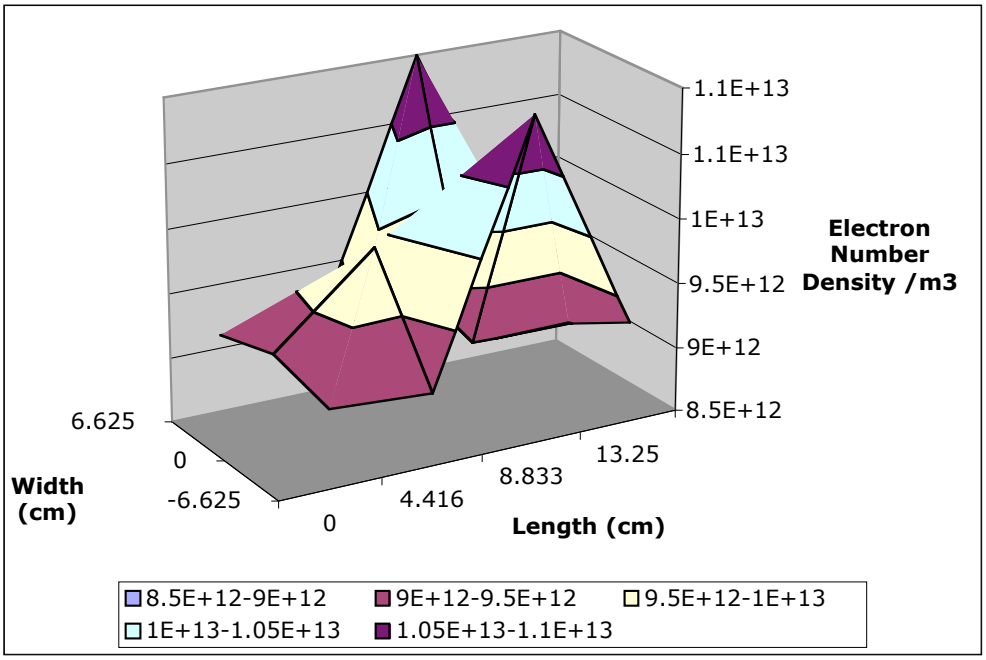

Figure 32: Density distribution for 2% CF4 at 5 seconds

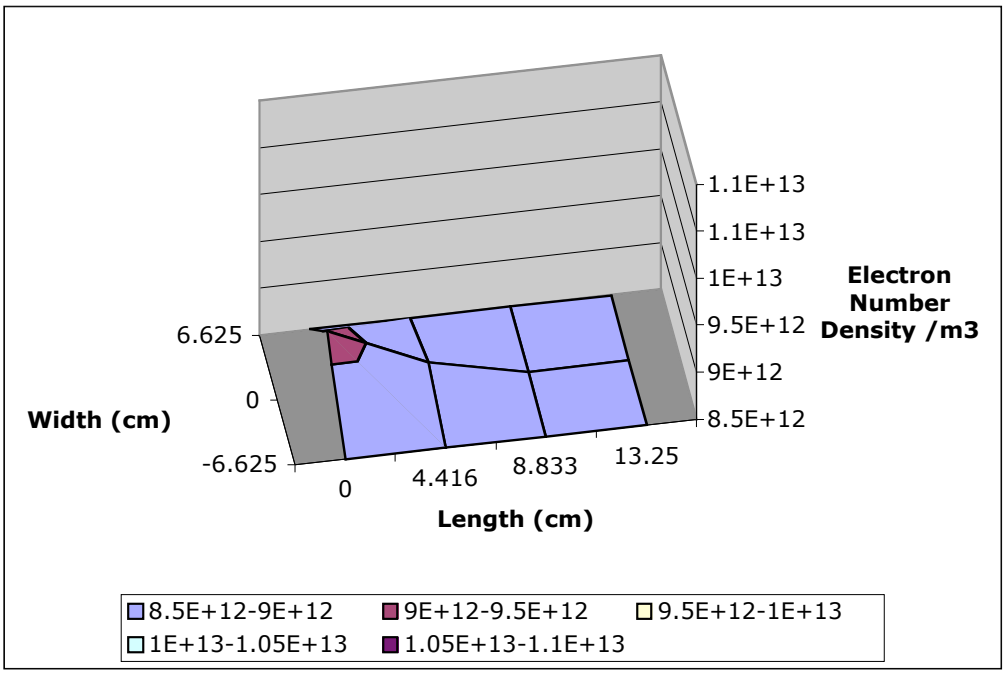

Figure 33: Density distribution for 2% CF4 at 5 minutes

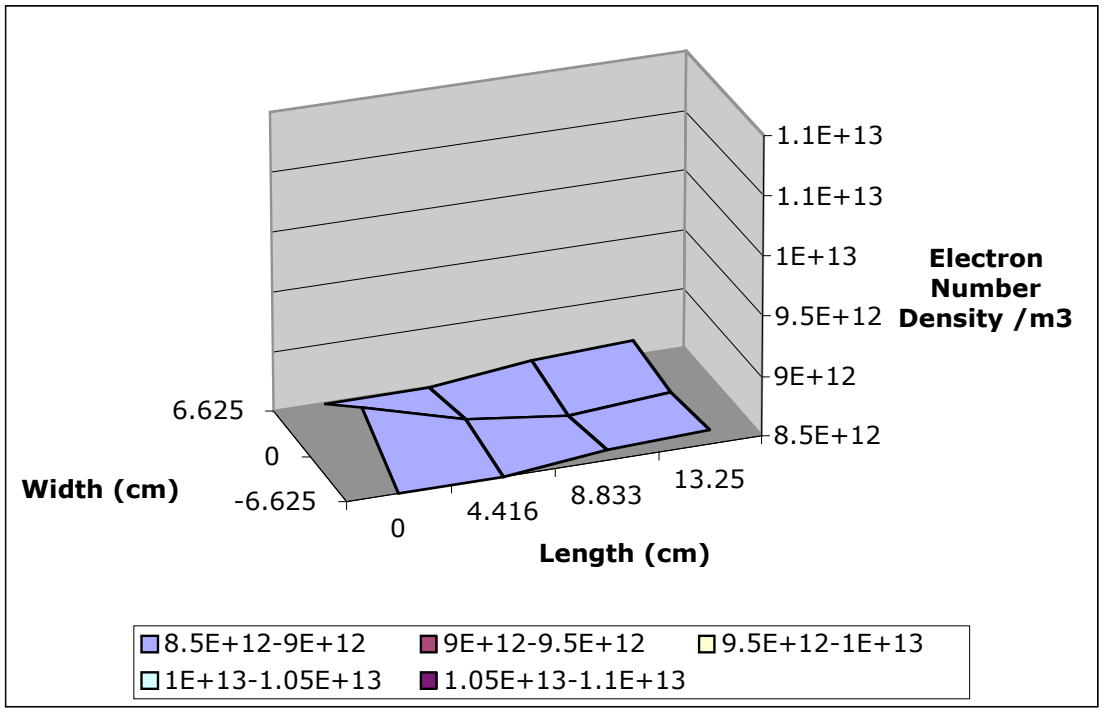

Figure 34: Density distribution for 2% CF4 at 15 minutes

3.4 Optical Emission Spectroscopy

3.4.1 Introduction

Optical emission spectroscopy is a method of determining the composition of an excited gas by measuring the emission wavelengths of excited electrons. Spectroscopy is a science based on observations by Plank about black body emissions and from the rules of Bohr's atomic model. Bohr's atomic model dictates that atoms and molecules contain electrons that can move only via discrete energy levels (often thought of as electron shells). Plank found that each energy portion, called quanta was inversely proportional to wavelength. Thus, as an electron de-excites, it will emit electromagnetic radiation of a characteristic wavelength and as it becomes excited, it will absorb energy of a particular wavelength. Since humans perceive wavelengths as color (visual spectrum), this identifying energy is associated with a particular color as well as wavelength.

In plasmas, gases are constantly undergoing changes in energy. Electrons in the gas mixture are frequently reacting with neutral gas molecules to cause ionization and dissociation. Later, gas molecules may recombine to form neutral particles. The most common gas reactions for the experimental gases used in the atmospheric plasma experiment are shown in Table 5.

Table 5: Common processes in helium, oxygen and carbontetrafluoride plasmas [11]

	Oxygen	**Carbontetrafluoride**
Dissociation Ionization	$e + O_2 \rightarrow O_2^+ + 2e$ $e + O_2 \rightarrow O + O^+ + e$	$e + CF_4 = CF_4^+ + F + 2e$
Dissociation	$e + O_2 = O + O + e$	$e + CF_4 = CF_3 + F + e$ $e + CF_4 = CF_2 + F_2 + e$
Dissociation Attachment	$e + O_2 \rightarrow O + O^-$	
Detachment		$e + F^- = F + 2e$
Polar dissociation	$e + O_2 \rightarrow O^+ + O^- + e$	
Dissociation Recombination	$e + O_2^+ \rightarrow O + O^*$	
Possible Species Formed	$O, O_2, O_3, O^+, O_2^+, O_4^+, O_3^-, O_2^-, O^-$	$CF_3, CF_2, F^-, F, F_2, C_2F_6, C_2F_5, C_2F_4$

Electron Impact Detachment	$e + O^- \rightarrow O + 2e$ $e + O_2^- \rightarrow O_2 + 2e$	
Association	$O^- + O \rightarrow O_2 + e$	$CF_2 + F^- \rightarrow CF_3 + e$
Detachment	$O^- + O_2 \rightarrow O_3 + e$ $O_2^- + O \rightarrow O_3 + e$ $O2^- + O_2 \rightarrow O_4 + e = 2O_2 + e$	

Optical emission spectroscopy relies on radiation emitted by the plasma or particles within the plasma to determine plasma parameters and composition. When plasma is at local thermodynamic equilibrium (LTE), electron plasma temperature can be obtained without knowing the plasma density from the relative method by measuring the intensity of identified emission lines.

$kT_e = \frac{E_{m1} - E_{m2}}{\ln\left(\frac{I_2\lambda_2^3}{I_1\lambda_1^3}\frac{g_1 f_1}{g_2 f_2}\right)}$, where E_{m1} and E_{m2} are the upper and lower level state energies, λ_1 and $\lambda 2$ are the wavelengths of corresponding emission lines, g_1 and g_2 are the corresponding statistical weights, f is the oscillator strength and I_1 and I_2 are the measured emission intensity at the corresponding wavelengths. A Boltzmann plot can be constructed from $\ln\left(\frac{I\lambda}{gA}\right) = C - \frac{E_i}{kT_e}$, where λ is the wavelength, I is the relative intensity, g is the statistical weight of the upper level, A is the transition probability, Ei is the energy of the upper level, k is Boltzmann's constant, T_e is the electron kinetic temperature, and C is an arbitrary constant

[12]. Thus, electron plasma temperature can be determined from the slope of a plot constructed between the Boltzmann's factor $\ln\left(\frac{I\lambda}{gA}\right)$ and the upper energy level E_i.

The electron number density can also be obtained from spectral measurements if line broadening is determined. For plasma at LTE, Stark (pressure) broadening can be observed and thus the equation of line broadening can be used $\Delta\lambda = 2W\left(\frac{n_e}{10^{16}}\right) + 3.5A_1\left(\frac{n_e}{10^{16}}\right)^{\frac{1}{4}}$, where W is the electron impact width parameter and A_1 is the ion-broadening parameter and can be neglected for non-hydrogenic plasmas [13].

Atmospheric pressure plasma does not satisfy LTE or coronal equilibrium, and thus these plasmas are classified as 'non-equilibrium' plasmas. Neither relative line intensity, nor line broadening can be used for atmospheric plasmas. The technique shown to be most useful is the neutral remsstrahlung technique[14,15]. This technique depends on calculating the power radiated Q_ per unit volume by neutral remsstrahlung in a low energy atmospheric plasma at a particular wavelength:

[illegible], where E is the initial energy of the decelerated electron, [illegible] is the neutral gas density, [illegible] is the electron density, [illegible] is the energy of the photon emitted at the given wavelength, and v is the electron velocity. To obtain the electron temperature (T_e) and electron density (n_e), the value of Q_ has to be calculated for each wavelength of the spectrum, then the best fit with the measured spectra can be found by varying the values of n_e and T_e. The results obtained by other researchers using similar atmospheric plasma devices revealed a range of temperature between 0.8 to 2.3eV, and

electron number density in the range 1.7 to 4.2 x 10^{12} m^{-3}. These results are in good correlation with results obtained from the plasma model (8.5 x 10^{12}-1.1 x 10^{13} m^{-3}). In this research, neutral bremsstrahlung was not used and the spectra were only used to identify the plasma elemental composition. However, based on results obtained on similar devices the above temperature and density can be considered valid.

3.4.2 Experimental

Line spectra were obtained for gas mixtures used in this research to identify the plasma composition. An Ocean Optics HR2000 Near Infrared Spectrometer (600-1025nm) was used to obtain the spectra. It was connected to a 5mm collimating lens and a 400 micron fiber was placed accessible to the plasma. A background correction was performed by removing all external light and the resulting data were processed using Ocean Optics software (OOI Base 32). The data were calibrated in both wavelength and power with a resolution of approximately 0.45nm. Only one average was used for the emission spectra, though five were collected for future use on Neutral remsstrahlung techniques.

3.4.3 Optical Emission Data

Optical emission spectra were taken for the various gas mixtures. Figures 35 through 40 shows the spectral data. As seen in Figure 35, the spectra taken for a pure helium discharge, neutral helium lines dominate, however neutral nitrogen and oxygen are also detectable. The nitrogen and oxygen lines are contamination lines, due to the fractional air present in all atmospheric plasma discharges. Inclusion of either 1% or 2% oxygen (Figures 36 and 37)

does not change the spectra, and the plasma composition is the same except for the appearance of an oxygen line at 926.6nm as a result of increased concentration.

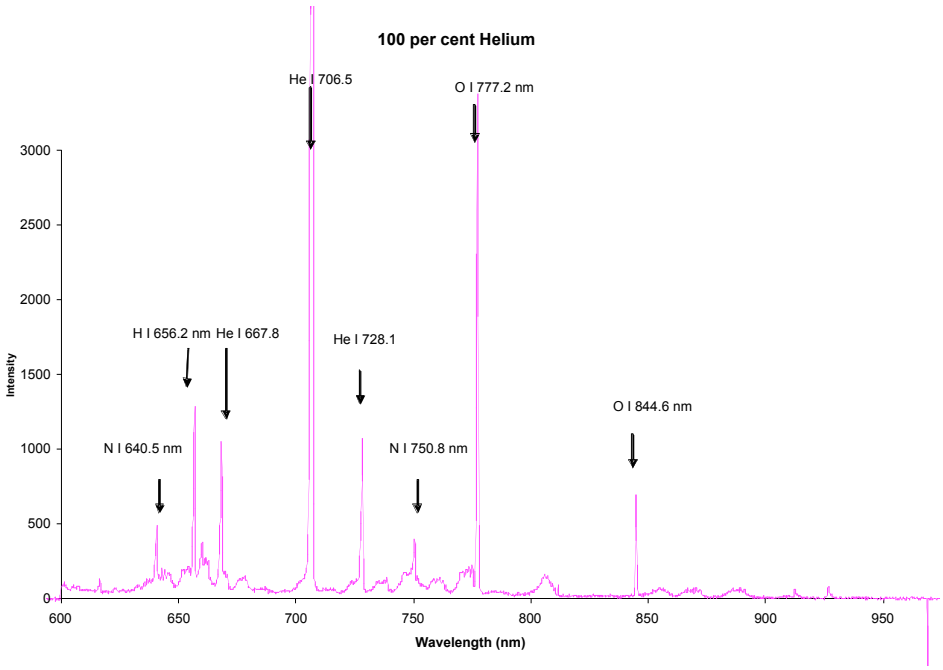

Figure 35: Spectra for a 100% helium discharge

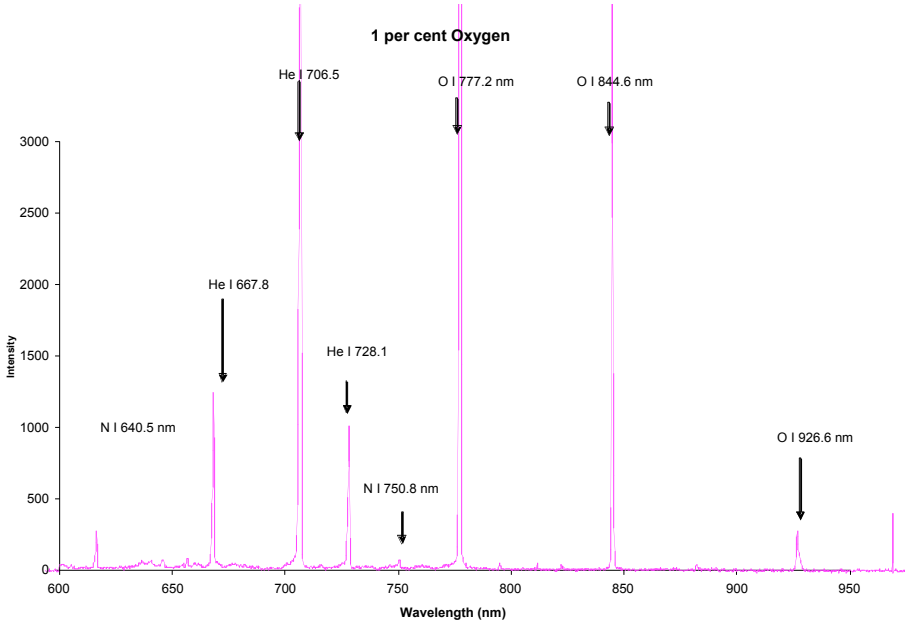

Figure 36: Spectra of a 99% He + 1% Oxygen discharge

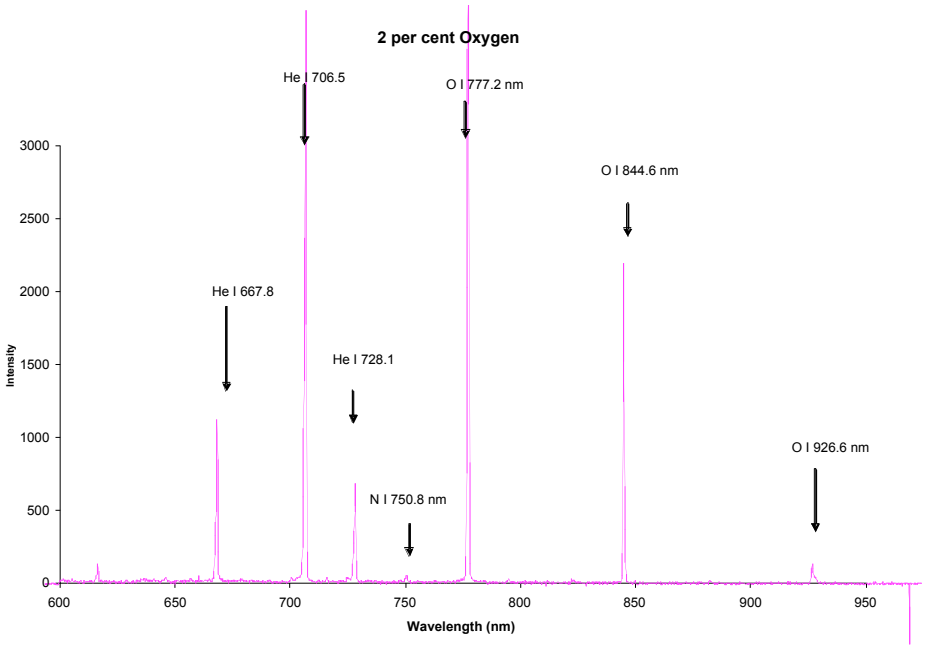

Figure 37: Spectra of 98%He + 2% Oxygen discharge

Addition of CF_4 to the discharge shows a 740nm fluorine line for the 1% CF_4 (Figure 38) and the 2% CF_4 (Figure 39). The mixture of oxygen and CF_4 at 1% each does not show the 740nm fluorine line but shows a stronger 926.6nm oxygen line. This is probably due to recombination of fluorine, which reduces its emission, and more dissociation of O_2, thereby increasing the intensity of the 926.6nm line.

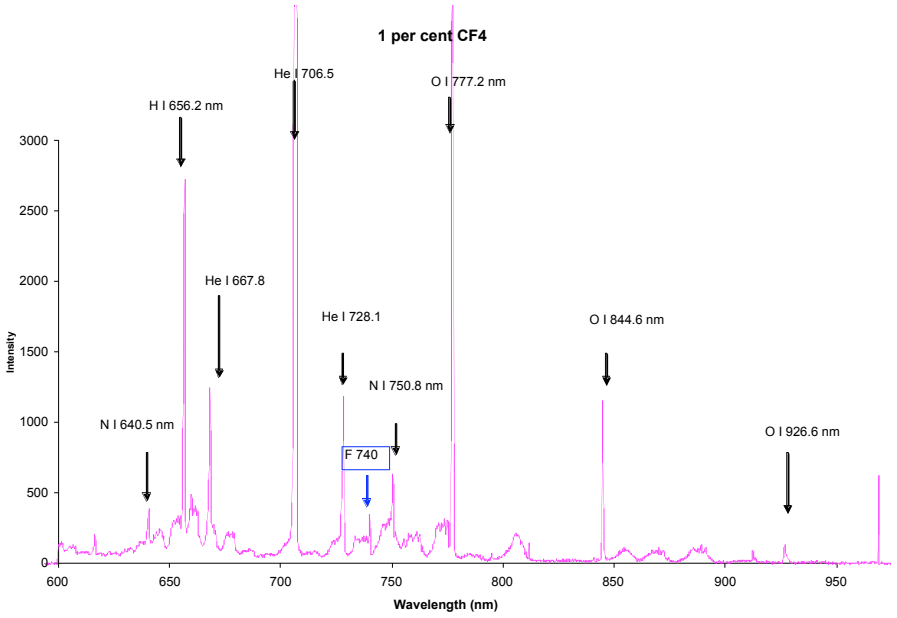

Figure 38: Spectra of 99% He + 1% CF4 discharge

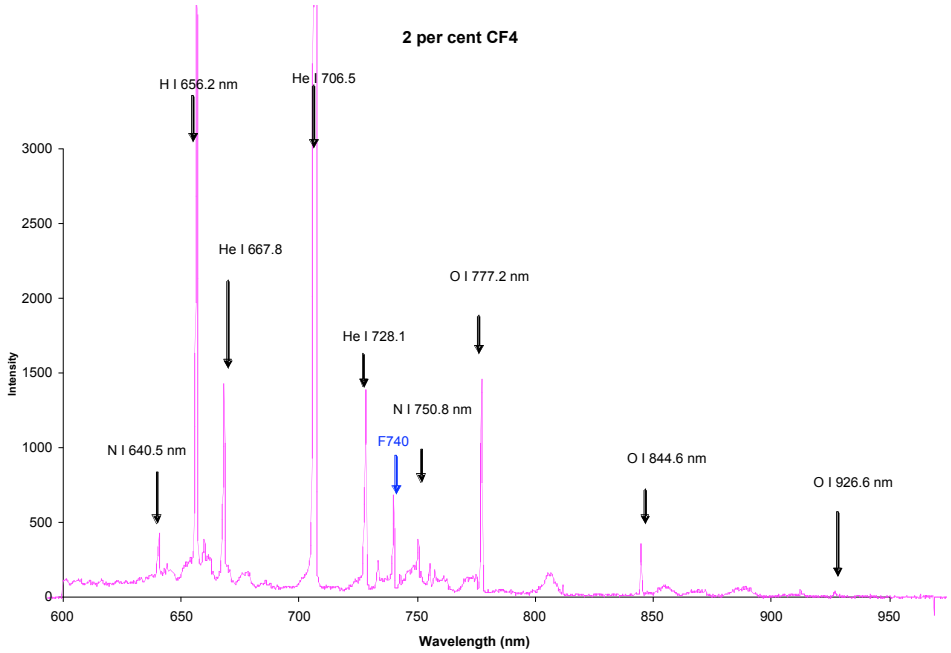

Figure 39: Spectra of 98% He + 2% CF4 discharge

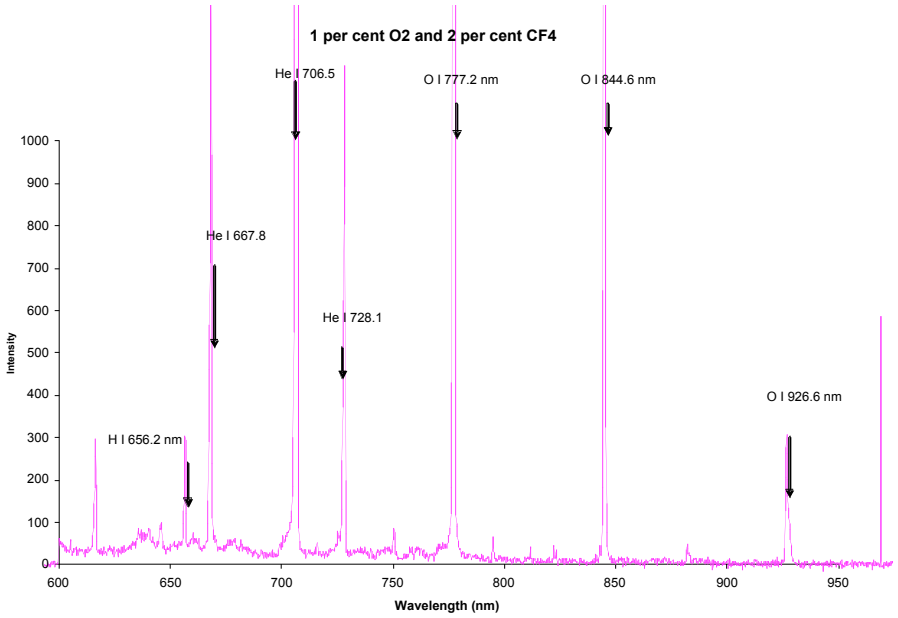

Figure 40: Spectra of 98% He + 1% Oxygen + 1% CF4 discharge

Of interest is the change in the intensity of H_α line when changing the gas composition. As seen in Figures 35-40, the intensity of H_α for the 100% He discharge is about 1292, while the addition of 1% CF_4 increases the intensity to 2734 and further increase of CF_4 to 2% increases the H_α intensity to about 3000. When adding 2% O_2, the H_α line totally disappears, reducing O_2 to 1% showed an increase in H_α intensity to 100, but adding an additional 1% CF_4 increases the intensity to 300. It appears that the CF_4 has a hydrogen impurity, and that's why the H_α intensity increases with increased CF_4 concentration. However, for oxygen addition the intensity of H_α decreases due to recombination and formation of OH. This is obvious from the intensity observed in the 100% helium discharge because under all circumstances there will be a fraction of air, and possible humidity. Thus, when adding more oxygen into the helium discharge, higher recombination rates would take place the H_α should decrease in intensity. This is well observed when comparing the initial

helium discharge (H_α intensity ~1292) to reduction in the intensity to 100 when adding 1% O_2, then down to zero when adding 2% O_2.

4. Plasma Interaction with Substrates

4.1 Plasma Modification of Substrates

Plasmas are used to modify various substrates due to the availability of electrons, ions, excited atoms, neutral atoms, metastables, and free radicals. Each species can interact with the substrate in one or multiple processes. The combinations of these species formed within the plasma will be determined by the applied voltage, the current flowing into the discharge, the frequency with which the electric field oscillates, and the operational pressure. The application of the electric field to the plasma is important, and if it is oscillating in time, it will provide a cyclic effect as the cycle oscillates between peak positive and peak negative. Additionally, the spatial distribution of the electric field will determine the uniformity of the treatment. A strong gradient is not desirable for surface treatment of textiles, since uniformity over the entire surface is preferred.

The interactions of the plasma with the substrate can cause significant changes to the substrate's characteristics. However, these are surface changes and rarely occur more than 5μm into the depth of the substrate. For this reason, plasma is an excellent method of modifying surface characteristics of a material without affecting bulk properties. Plasma surface modifications include, but are not limited to, surface coatings, deposition and etching, surface radicalization, and the creation of new surface functional groups [16].

4.1.1 Etching

Etching can be subdivided into four categories, sputtering, chemical gasification, energetic ion-enhanced etching, and inhibitor ion-enhanced chemistry. In all of these processes, part of the surface is removed and the removal depth depends on both the energy of the ions and the surface binding energy. Plasma, unlike chemical processes, can accomplish controlled, and even selective methods of etching [17]. Figure 41 illustrates the four basic plasma etching processes: (i) sputtering, (ii) pure chemical etching, (iii) reactive ion etching, and (iv) ion inhibitor etching.

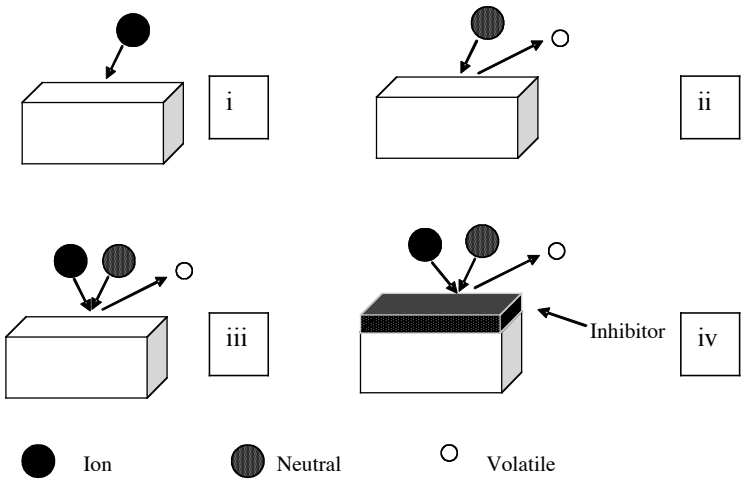

Figure 41: Illustration of basic plasma etching processes

Sputtering is a process that occurs when an ion collides with a substrate with enough energy to eject an atom from the surface of the material. This process is typically induced in a direct current plasma system in which the ions are accelerated across the plasma sheath towards the target material. The ion impact on the surface physically ejects atoms that later are allowed to fall on the surface of another material (substrate) to produce a deposited layer

[18]. Since sputtering is a process during which energy transfer takes place, the etching rate is a function of the ion's energy, the physical structure of the substrate, and the strength of the substrate's intermolecular bonds. Etching will occur at any location where sufficiently energized ions impact the surface. For this reason, sputtering is not a selective form of etching and is not particularly efficient. Generally, etching occurs in a one to one ratio, where one atom is ejected per each accelerated ion impacting on the material's surface.

Chemical gasification utilizes the dissociative abilities of the plasma to create chemically reactive neutral species that interact with the substrate in a purely chemical process. When plasma electrons collide with the neutral gas atoms or molecules, dissociation into new gaseous species takes place. In chemical gasification, at least one of those species is able to react through pure chemistry with the substrate and produce a volatile product. The creation of the volatile product decreases the molecular weight of the substrate, thus etching the surface. Since etching is now a function of chemistry rather than particle energy, the process is more efficient than that of physical sputtering. Since chemical reactions can occur at any point on the substrate and are isotropic, chemical gasification is also isotropic. However, a dissociated gas must be chemically reactive with a given substrate and moreover with the exact chemical structure of the surface at the point of contact. This limits applicability of the technique to a few niche substrates, but allows for great selectivity [18].

Energetic ion-enhanced etching is a combination of both sputtering and pure chemical etching. As with pure sputtering, highly energized ions react with the surface of the substrate. However, they are not responsible for direct removal of atoms or molecules from the substrate, but rather depositing their kinetic energy onto the surface to "damage" the intermolecular bonds of the substrate. Damage can refer to the introduction of defects into

the crystalline structure of the material, or to chain scission, which results in the creation of bonds, like hairs, jutting off the surface. The exact mechanism of damage varies from one compound to another, but in all cases results in a reduction of surface bonds and thereby creates a more reactive surface. This surface becomes receptive to the neutral gas, and a purely chemical reaction proceeds as in chemical gasification. The properties are similar to those found in chemical gasification.

Lastly, ion inhibitor etching is similar to reactive ion etching, but with the addition of an inhibitor. The inhibitor is placed (via gas or resist) over a non-uniform surface. The ions bombard the surface with a horizontal uniformity, removing the inhibitor and allowing for a subsequent chemically reactive neutral to react with the substrate surface. However, in troughs or peaks where the inhibitor has coated a vertical sidewall, the reactive ions will not remove the inhibitor and thus no chemical gasification reactions can occur. Therefore the chemically reactive neutral will be unable to react in vertical regions. The result is an anisotropically etched surface with very straight, vertical walls for all peaks and troughs [18].

4.1.2 Redeposition and Backscattering

Redeposition and backscattering are methods by which the released volatile or non-volatile products return to the surface of the substrate. Redeposition refers to the immediate deposit of the etched material, whereas backscattering includes interactions between the etched material and the gaseous plasma before returning to the substrate surface.

Redeposition commonly occurs in surface crevices where the product is non-volatile and redeposits along the walls. Volatile products will not redeposit, even if released in

confined areas, but will bounce of the surface of the sidewalls in a series of collisions until escaping from the recessed surface feature. Once free of the surface, volatiles and non-volatiles that do not redeposit will interact with the plasma gases, and may eventually return to the surface of the substrate. This process is known as backscattering.

4.1.3 Radical Formation

Exposure to plasma also causes the creation of free radicals as a result of surface activation and release of excited atoms or molecules. These radicals exist in sufficient quantities to be observed by Electron Spin Resonance (ESR) only seconds after exposure to plasma [19]. The radicals are also quite long-lived, showing very little sign of decay after 20hours, even when stored in an air environment [20].

Radicals can form in several places on a polymeric substrate. They can react with the terminal end of a polymer, interrupt a polymer mid chain, or exist on a stable monomer. Generation of the radical may lead to subsequent reactions, such as graft polymerization, cross-linking by activated species of inert gas (CASING), or the creation of new surface functional groups [19]. There are two concepts concerning the creation of radicals. One is electron bombardment, which can occur when an electron comes in contact with the surface of a substrate. Clearly electron bombardment only affects a very thin surface layer of the polymer, the outermost layer in which the electron can come in contact. However, studies have shown that radical formation is not limited to the surface of substrates, but occurs deep within the bulk of the polymer as well. Thus some mechanism for transporting the radical

inside the polymer must exist. Currently UV plasma generated UV radiation is the most plausible explanation as a possible mechanism [20].

4.1.4 Chain Scission and Cross-linking

Chain scission and cross-linking are competing reactions involving the radicals formed by the plasma. Chain scission occurs when a larger molecule is divided into two separate molecules, each with a free radical. Alternatively, cross-linking occurs when two separate molecules with radicals combine to create one large molecule. Some of the possible reactions are shown in Table 6.

Table 6: Examples of chain scission and cross-linking

Chain Scission	$R_3 - C - C - R_3 \rightarrow R_3 - C^* + {}^*C - R_3$ $R_3 - C - H \rightarrow R_3 - C^* + {}^*H$ $R_3 - C - N - R_2 \rightarrow R_3 - C^* + {}^*N - R_2$
Cross-Linking	$R_3 - C^* + {}^*C - R_3 \rightarrow R_3 - C - C - R_3$ $R_3 - C^* + {}^*H \rightarrow R_3 - C - H$ $R_3 - C^* + {}^*N - R_2 \rightarrow R_3 - C - N - R_2$

During plasma exposure, both chain scission and cross-linking are occurring simultaneously, though one type of reaction often dominates. The type of reactions that occur, their reaction rates, and the dominance of one reaction over the other will all be a function of the plasma gas type and the substrate. In order to induce chain scission, an electron or ion impacting on the substrate (polymer, monomer, etc) must have sufficient energy to break a bond. Bond energy for the most common bonds is shown in the Table 7.

In addition to having sufficient energy to break a bond, the types of formed radicals will be influenced by stearic hindrance, and the overall number of particular bonds (electrons and ions are not selective).

Table 7: Dissociation Energy of Typical Bonds

Bond Type	Bond Dissociation Energy (bond breakage energy in eV)
C-C	3.47
C-H	4.12
C-O	3.5
C-N	2.91
O-H	4.61
N-N	3.9

When cross-linking and chain scission occur, changes in the characteristics of a substrate will follow. Extensive chain scission can damage a fiber, reducing its strength and other tensile properties. This damage can be beneficial or detrimental depending on the desired application. Alternately, cross-linking can strengthen a substrate, causing cross-linking between monomers. However, gelation, or one cross-link per every monomer, may cause an undesired increase in stiffness [19].

4.1.5 Plasma Deposition/Polymerization

Plasma deposition is simply an extension of the process of chain scission and cross-linking. A monomer is typically introduced into the plasma and then undergoes a chain scission reaction. The products all exist as radicals for a sufficient duration to move around

within the plasma. Eventually, they recombine in a new order to form a large molecule that deposits or forms on the surface of the polymer. An illustrated example is shown below:

$$A-B+C-D-F+\underset{Plasma}{\rightarrow}A^{*}+B^{*}+C^{*}+{}^{*}D^{*}+{}^{*}F\rightarrow C-D-F-A-B$$

The rate of plasma polymerization is typically linear $R = kF$, where R is the rate of plasma polymerization, k is a reaction constant and F is the plasma gas flow rate; and can be approximated with this simple formula for most gases [20].

4.1.6 Hydrophilicity and Oleophilicity

Hydrophilicity and oleophibicity are relationships between a substrate and water or oil. If a substrate is hydrophylic, it will readily absorb water and will also wet rapidly. To the contrary, if a substrate is hydrophobic, it will repel water. Oleophobic compounds wet in non-polar solvents and do not absorb water. In fact, water will form balls and sit indefinitely on the surface of oleophobic compounds. These compounds will not wet with water as a solvent, or may take a very long time to wet, thus increasing the time and reducing the efficacy of chemical reactions. Plasma has been shown to be able to easily modify the properties of hydrophobicity and oleophobicity on the surface of a substrate. The type of gas used will determine the functionality. For example, oxygen will form oxygen-free radicals that attach themselves to a polymer in the form of –CO-, -COOH, -COO-, -C=O, -O-COO- groups on the surface of the substrate [21]. Since oxygen is highly polar, these groups will significantly increase the hydrophilicity of a non-polar compound. In a similar manner, CH_4 gas will cause a plasma polymerization of CH_2 polymers capped with CH_3 end groups [22].

4.2 Substrate Characterization

Two materials were chosen for testing plasma effects, wool and cellulosic paper, to determine the how atmospheric pressure plasmas interact with substrates. These two materials are different from each other in their structure and in their susceptibility to plasma ions and excited plasma atoms. Wool is animal-based material while cellulosic paper is plant-based.

4.2.1 Wool

Wool is a natural fiber obtained by shearing the fur coat of an animal. Many different animals produce wool including, sheep, alpaca, llama, camel, and even rabbits. Though all these animal fibers do have at least a niche function within industry, sheep's wool dominates the market. It can be found in apparel, such as high-end suits and coats as well as in carpeting.

The chemical structure and morphology of wool cause it to have distinct and useful characteristics. Wool is a naturally wavy textile, with any where from 0-12 crimps per cm. Natural crimp is beneficial in the spinning process where it aids in warmth of the fiber by trapping air pockets. In addition, the surface of wool fibers is covered in a system of overlapping scales. The size and length of the scales vary with animal and breed, but can be found on all wool fibers. These scales act as a natural 'Velcro', hooking with each other and further improving the adhesion of wool during spinning and felting processes. However, unintended felting may also occur during routine washing presenting a problem to consumers.

The structure of wool can be divided into three parts, the cuticle, the cortex, and the medulla; a cross section of a wool fiber is shown below.

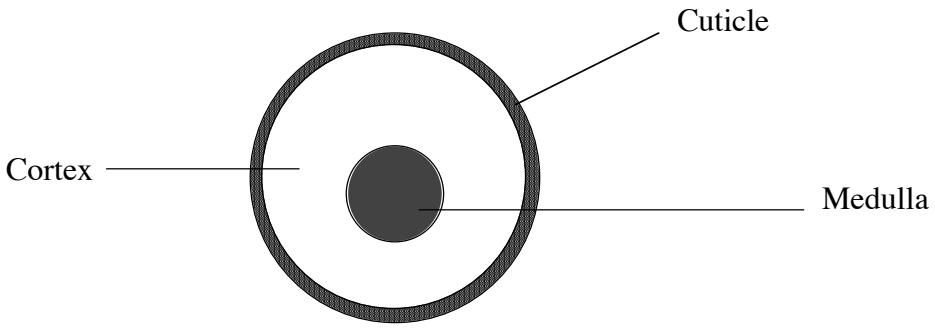

Figure 42: Wool fiber cross-section

The cuticle is composed of a series of overlapping cells. These cells form the scales of the wool fiber and encase the inner cortex and medulla. The scales are unidirectional and thus the coefficient of friction for wool fabric will depend on the machines alignment with or against the scales. Inside of the cortex are two different types of cortical cells, orthocortical and paracortical. The presence and abundance of these two cells is also specific to breed and species. Differences in chemical structure cause the orthocortex to dye more easily by basic and acidic dyes. Inside of the cortical cells is an amorphous collection of rods called macrofibrils. These are more tightly packed in orthocortical than paracorticals cells. The macrofibril can be further divided into the microfibril and into helical arrangements of 10 protein chains. Each chain consists of an intertwined triple helix of peptide chains (alpha helixes). These alpha helixes contribute to wools elastic ability and shape retention.

Cytoplasmic trash can also be found within the cortex, and in greater quantity within the paracortical cells. The structure of wool is shown below.

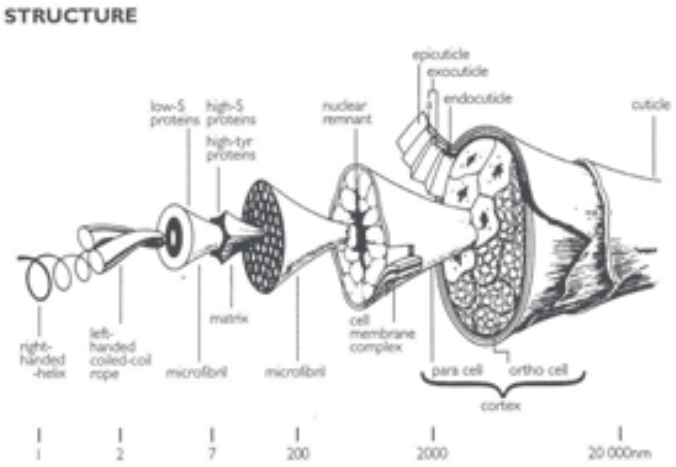

Figure 43: Structure of a wool fiber [23]

The medulla is located within the center of the cortical cells through the length of the fiber. It can be continuous, broken, or even non-existent in some breeds and species. It is very porous and filled with air. Interactions between light and the medulla also cause fibers that contain the structure to appear lighter in color than their medulla lacking counterparts. This is due to the unique ability of the medulla to reflect incoming light.

Chemically, wool fabrics are composed of α-keratins. Keratin is a group of protein structures that can be found in the form of alpha helixes within the structure of wool. Figure

44 shows the chemical structure of wool.

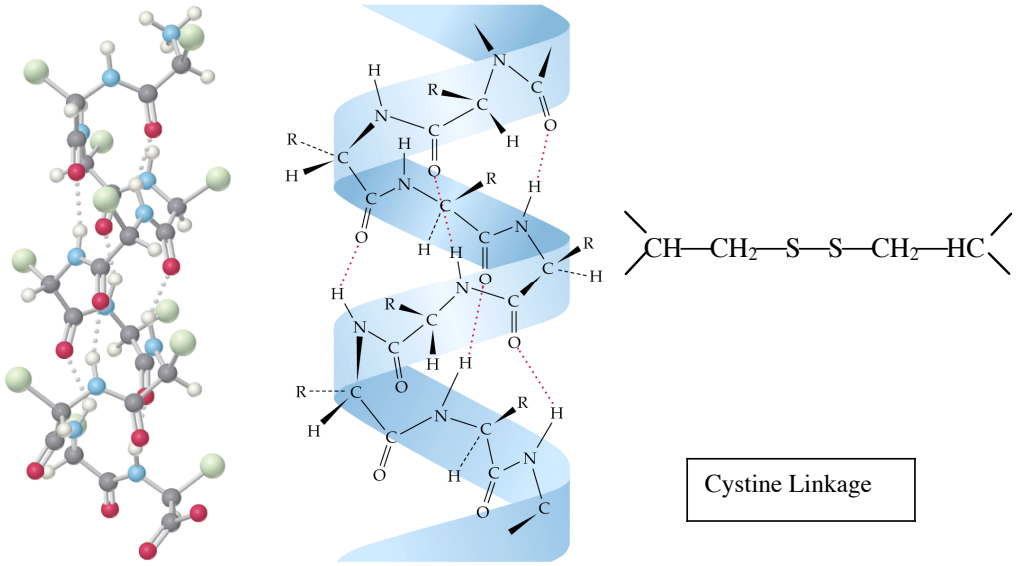

Figure 44: Chemical structure of wool [24]

The alpha helix chains are linked to parallel chains by di-sulfide bonds in the form of cystine linkages that are composed of disulfide bonds. These bonds can easily be broken and reformed, causing wool to have significant problems with shrinkage and wrinkling. In addition, the high sulfur content gives out the distinct malodor when burned. Large amounts of amines (NH) can also be found within the keratin structure, which takes on a positive charge in acidic conditions and thus allows for easy dye-ability by negatively charged acid dyes [9,10].

Table 8 lists some of the important properties of wool

Table 8: Some of the important properties of wool [9,10,25]

Dielectric Constant	-1.2
Cross-section	Circular
Specific Gravity	1.314 gm/cm^3
% Moisture regain at 65% RH	Over 80%
Glass Transition ©	---
Melting point C	Does not melt
Burning Point C	200ºC -decompose
Heat degradation	140ºC

4.2.2 Cellulosic Paper

Paper is primarily made out of cellulose, a material found in plants. Cellulose is found within the cell walls of plants and function both as a structural and supporting medium as well as a method of fluid transportation. On a molecular level, cellulose is a polymer consisting of six-membered ring saccharide monomers connected to each other by glycosidic oxygen bonds. On a macroscopic level, cellulose is composed of fibrils, long chains of molecules that line up end to end. The properties of these fibrils including their high tensile strength and wet ability make cellulose desirable for papermaking. The basic structure of cellulose and its derivative is shown in Figure 45.

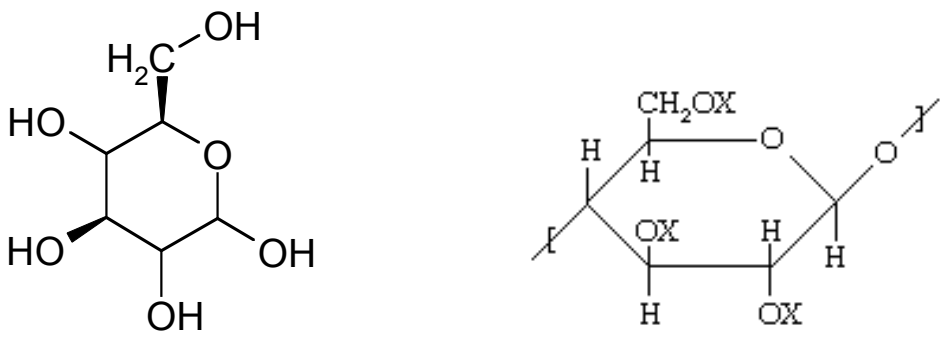

(a) (b)

Figure 45: Basic chemical structure of cellulose (a) and with its derivatives (b) [26]

Historically, paper was made from four different types of fibers: seed hair fibers (cotton), bast fibers (flax), grass fibers (straw or esparato), and wood fibers. Today, wood fibers make up 95% of all cellulose used in papermaking. The trees used fall under two categories: deciduous and hardwood. Typical deciduous trees include the pine, spruce, and fir. Hardwood trees are more numerous in species, including the oak, sweet gum, maple, and aspen.

After the trees have been selected and trucked into an appropriate facility, the papermaking process can begin. First, trees are debarked, chipped, and then they are pulped, either chemically, mechanically, or in a combination process. The purpose of pulping is to isolate the cellulosic material and remove the other chemical components, primarily a glue-like compound called lignon. Chemical pulping uses a cooking process (high steam and water) in conjunction with either an alkaline process (sodium sulphate and caustic), or an acid process to dissolve the lignon and separate it from the cellulose. While "cooking," pulps are often bleached with chlorine gas, calcium hypochlorite, hydrogen peroxide, or chlorine dioxide. These chemicals react with the remaining color-bearing lignon components and

either destroy or dissolve them. Pulps are then squeezed through rollers, blown with dry air, and formed into sheets. A desired finish may then be applied based on the intended application of the paper [27].

Though paper is most commonly associated with books, and other printed media, it is just as prevalent in the storage industry where it is used for boxes that hold chemicals, books, foods, and many other items. If the items within these boxes are subject to attack by microbial agents, then these paper boxes can benefit by the application of a permanent anti-microbial finish. Most anti-microbial finishes are toxic and thus entirely unsuitable for food items, so care must be taken in choosing the finish. A method of applying a non-toxic anti-microbial finish to cellulosic paper will be examined in the experimental section of this thesis. One of the natural antimicrobial agents is chitosan, a derivative of chitin, which was used in this thesis research and is explained in the following section (4.2.3).

4.2.3 Chitosan

Chitosan is a derivative of chitin, a material found naturally in the exoskeleton of crustaceans. Chitin is biodegradable and one of the most abundant natural polysaccharides. The most interesting feature of chitin and its derivative chitosan is the combination of anti-microbial properties and complete harmlessness to humans.

Chitosan does occur naturally as well, mostly found in specific types of fungus, but not an in an easily accessible form [28]. As a result, chitosan is produced commercially from the deacetylation of chitin, a procedure summarized in Figure 46.

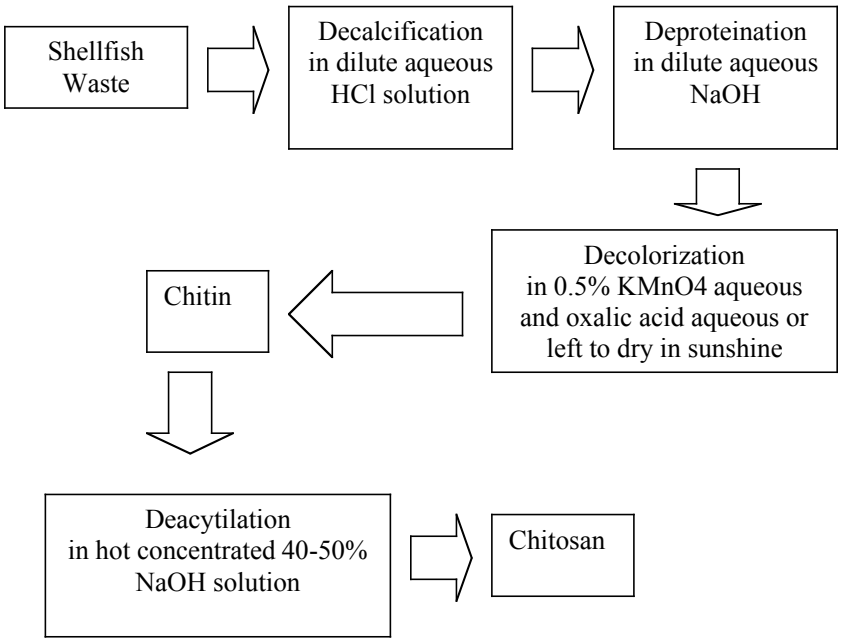

Figure 46: Processing of shellfish waste into chitin and deacetylation into chitosan [29]

The chemical process for deacetylation of chitin into chitosan is shown in Figure 4.5 in which a hot concentration of NaOH (40-50%) is used.

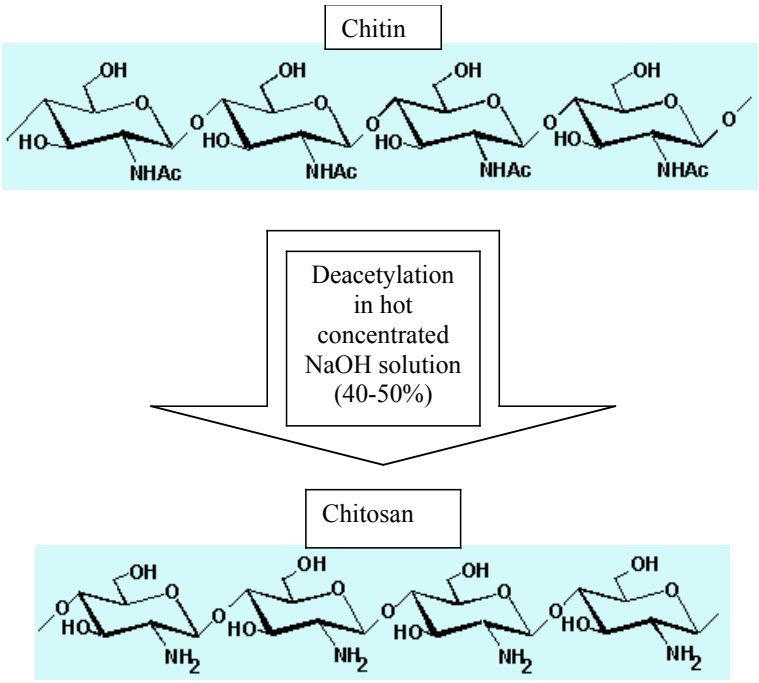

Figure 47: Deacetylation of chitin to produce chitosan [29]

As seen in Figure 47, chemically chitin and chitosan are very similar. However, they do differ chemically in the amine functional group. As a result, chitosan is more soluble than chitin, and the amine group will become a cation in acidic solutions, providing the best anti-microbial functionality. In addition to deacetylation, further modification of chitosan can be done to improve water solubility and antimicrobial properties. This includes the creation of HTCC (N-(2 hydroxy) propyl-3-trimethylammonium chitosan chloride), a reaction between chitosan and GTMAC (glycidyl trimethyl ammonium chloride). The chemical structure of synthesized HTCC is shown in Figure 48.

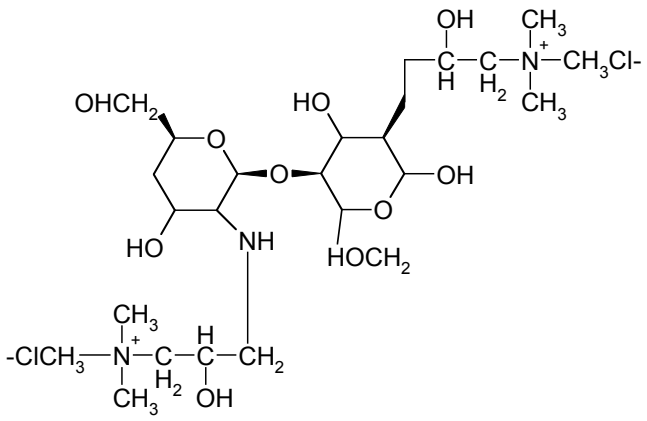

Figure 48: Chemical Structure of synthesized HTCC

4.3 Characterization Methods

4.3.1 Weight Change

Change in weight, usually expressed as a percent weight change can show the loss or addition to substrate due to a process. In order to get an accurate measure of weight changes, a substrate must be exposed to controlled conditions, especially if it is hydrophilic and can absorb moisture from the surroundings. Conditioning of a substrate involves a constant temperature, pressure, and humidity for a sufficient time (generally 24-48 hours), to allow the substrate to acclimate, or for the weight to become constant with little or no perturbation.

Weight changes due to plasma treatment can be attributed to the different plasma effects discussed earlier, such as etching, deposition, scission and cross linking, etc. A dry weight, obtained from samples treated in a humidity free environment will provide information on the etching and deposition processes due to exposure to plasma. A decrease in weight will represent a predominance of etching and a weight increase can be attributed to

deposition (both redeposition of materials etched from the substrate and bonding of gas molecules to the substrate). To create a humidity free environment requires heat above 100° C or a chamber filled with a desiccant.

Standard wet textile conditions are 21°C and 65% humidity. A reduction in wet weight indicates both etching/deposition (which can be assessed by dry weight measurements) and changes in the surface functional groups. If the groups become more hydrophilic or hydrophobic, the moisture regain of the substrate will be altered. The % weight change is measured by taking the difference between the final and initial weights in percentage change $\%\ weight\ change = \frac{W_f - W_i}{W_i} \times 100$, where W_f and W_i are the final and initial weights, respectively.

4.3.2 Scanning Electron Microscopy (SEM)

All scanning electron microscopy was conducted using a Hitachi S-3200 Scanning Electron Microscope. It is a variable pressure scanning electron microscope with controllable vacuum chamber.

4.3.3 Energy Dispersive X-ray Spectroscopy (EDS)

Energy Dispersive X-ray Spectroscopy is used in conjunction with scanning electron microscopy to determine the elemental composition of the substrate. Electrons bombarding the substrate cause the emission of x-rays. The energy of each x-ray photon is characteristic

of the element that generated it. An example of EDS for a cotton sample is shown in Figure 49, where the elemental composition is determined by the peaks of each detected element and their concentration is determined by the integration of the area under each peak.

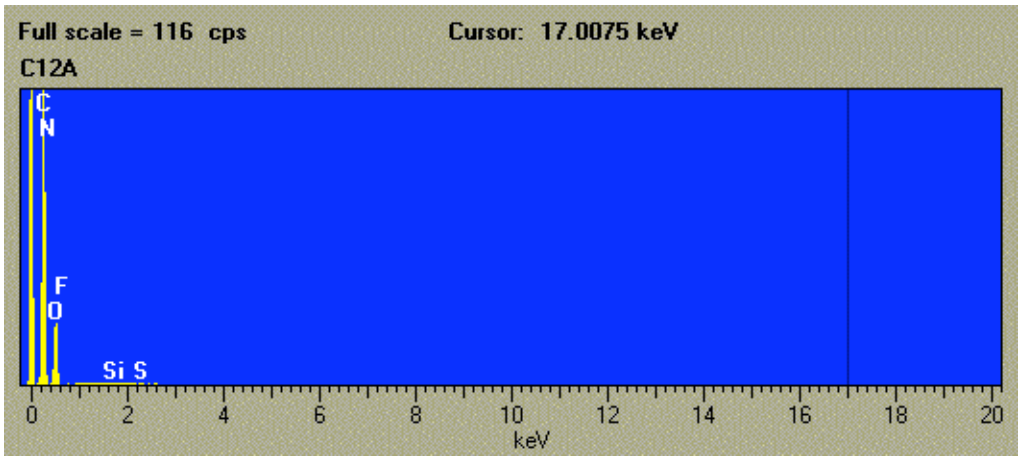

Figure 49: Example of EDS Spectra taken for cotton fabric

4.3.4 Tensile Testing

Tensile Testing is a method of characterizing specific substrate properties, such as peak load and energy, strain, and elongation at peak load. Peak Load is the maximum load a material can withstand before breaking. For textile materials, at the peak load, the fiber will have stretched to a certain characteristic length, called elongation. The relationship between this new length and the original gauge length of the fabric yields the % strain at peak load. The integral of the peak load curve up to its maximum value gives the energy at peak load. Tensile testing is a bulk property unlike plasma, and unless severe etching, chain scission, or cross-linking has occurred, then the tensile properties of a substrate exposed to plasma should not vary significantly from unexposed ones. Different

materials have different tensile characteristics, and an example is shown in Figure 50 for cotton and wool.

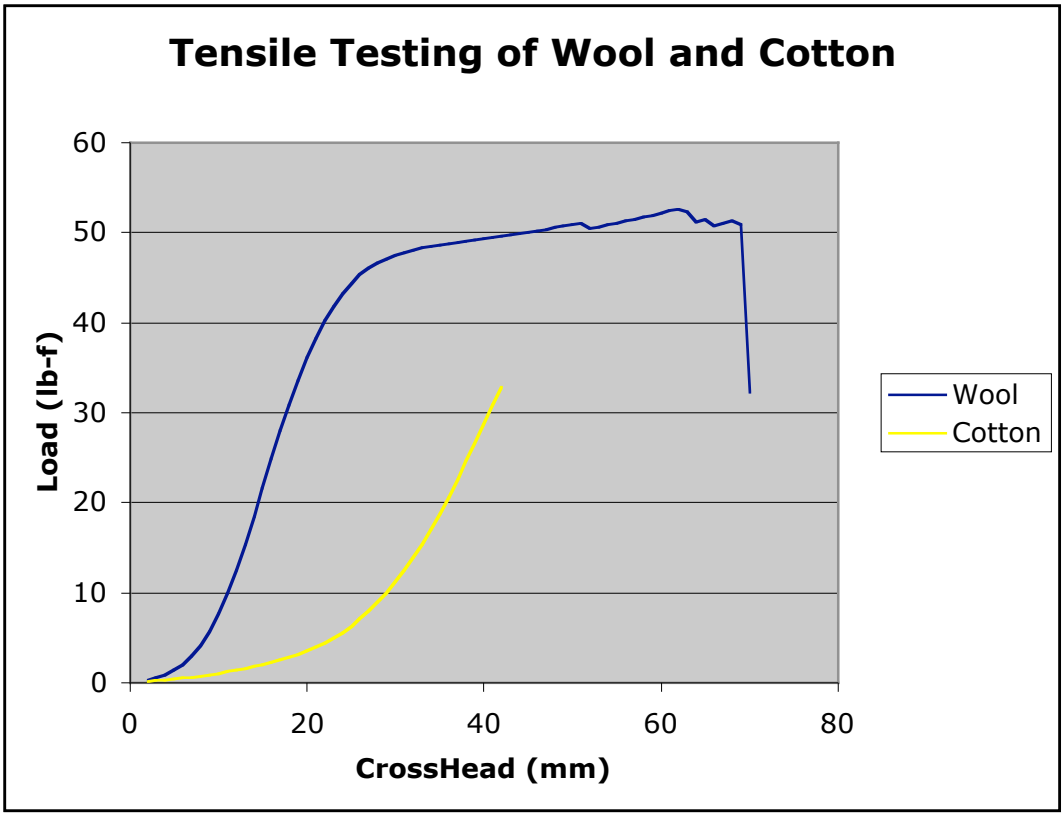

Figure 50: Tensile testing of cotton and wool

The features of the graph demonstrate the differences between the internal structure of wool and of cotton. Wool is made up of alpha helixes, coils that can be stretched significantly before damaging the internal structure. This ability to elongate can be seen in Figure 50 as the crosshead increases dramatically with little change in the load. Alternately, cotton is made of flat molecules and has no ability to stretch. It will not elongate to the extent of wool and is a weaker fiber, breaking at a lesser load.

4.3.5 Contact Angle and Absorption Time

Contact angle is a method of measuring the hydrophobicity or hydrophilicity of a substrate. When measuring the contact angle, a liquid, frequently water, is applied to the surface of a fabric in a very small quantity. Due to the free surface energy of the particle and to its composition (polar versus non polar), the water molecule will form a sphere or half-sphere on the surface of the fabric. If the substrate is non-polar and has a high surface free energy the water form a ball, avoiding the surface. If the substrate is polar and has a low surface free energy, the water will hydrogen-bond with the substrate and will partially, or completely, sink into the surface of the substrate and thus the sphere flattens or is completely absorbed. The extent of the hydrophobicility or hydrophilicity can be measured by obtaining the angle the water forms with the surface of the fabric. In addition, if a substrate is hydrophilic and readily absorbs the water droplet, a measure of the time to absorb rather than contact angle is also useful in characterizing the degree of hydrophilicity. Figure 51 illustrates the contact angle diagram showing a hydrophilic surface (left image) and a hydrophobic surface (right drawing) and the change in contact angle between them.

Figure 51: Contact angle for hydrophilic (left) and hydrophobic (right) surfaces

4.3.6 Fourier Transform Infrared Spectroscopy

Infrared Spectroscopy is a technique that can be used to determine the functional groups within a chemical. It is a non-destructive process that uses the infrared energy range

to induce vibrations and rotations in chemical structures. Chemical bonds are responsive to specific frequencies or energy levels. When they are exposed to these frequencies they respond by vibrating and stretching. There are many types of possible vibrations, including wagging, twisting, and rocking.

Fourier Transform Infrared Spectroscopy (FTIR) works by subjecting a substrate to a beam of infrared light. The amount of light absorbed at a given wavelength is measured and recorded. Thus an energy spectrum (in the form of absorbance or transmittance) can be generated with peaks or troughs corresponding to the vibrations or rotations of a bond. This technique is particularly effective on organic compounds and is used for location functional groups (such as –COOH or $–NH_2$). Samples were evaluated using a Nexus® 470 FTIR in conjunction with a Nicolet® Omnisampler.

4.1.7 Colorimetry

Colorimetry is a new, qualitative method developed for identifying a positively or negatively charged functional group using acid and basic dyes. Acid dyes are composed of basic compounds that react with acidic (positive) functional groups to create a bond. Basic groups are exactly opposite -acids that bond to basic compounds. When the reaction occurs, the dye is bound to the substrate and will not easily be removed by water.

Anti-microbial finishes are frequently compounds containing a positively charged amine functional group ($-NH_3^+$). This functional group has been shown to be undesirable for the growth of bacteria and microbes. Since the positive amine group is cationic in nature, it will chemically react with nucleophilic compounds. Thus basic dye colorimetry can be used on substrates reacted with these positive amine functional groups (and thoroughly washed) to

identify whether grafting has successfully occurred. The test is simple and requires observing the depth, uniformity, and existence of color on a dyed substrate. If grafting is not successful, there will be no color visible and thus the substrate has not dyed and no cationic functional groups are present. Non-uniform distribution of the dye may indicate patchy (spotty) grafting. Some substrates may naturally contain acidic groups and will dye regardless of cationic grafting. In these cases, the depth or shade of the color may be used to determine whether grafting has occurred [30].

4.4 Wool Research

4.4.1 Experimental

Wool samples were exposed to the atmospheric pressure plasma with six different gas mixtures and the addition of a wool substrate, 100% helium, 99% helium + 1% O_2, 98% helium + 2% O_2, 99% helium + 1% CF_4, 98% helium + 2% CF_4, and 98% helium + 1% O_2 + 1% CF_4. All operational parameters were kept constant except exposure time to plasma, which was varied from 1 to 5 minutes in one minute increments with the addition of a 30 second exposure. The wool substrate used was 100% worsted garbadine wool #541 obtained from Test Fabrics. The 62" wide fabric was cut into 4″x6″ samples for batch treatment. Wool samples were conditioned before and after plasma exposure in a Fisher Scientific Iostherm Programmable Oven, Model 818F at standard pressure and 105°C (zero humidity) and in a conditioning chamber at 21°C, 65% humidity, at standard pressure. After treatment, the samples were tested for changes in strength due to crosslinking or chain scission (tensile testing), changes in hydrophobicity and hydrophilicity due to the formation

of new functional groups (contact angle/ absorption time), and the new functional groups were identified using EDS.

During exposure to plasma, operational parameters and plasma number density were monitored via LABVIEW interfaced to the data acquisition boards. The system was warmed up for 15 minutes using a pure helium discharge prior to exposure and the temperature was allowed to drop until 80-85°F. For each test, two wool samples were placed inside the cell and exposed to the desired gas mixture for the desired duration. The Teflon-coated thermocouple was positioned at the center of the cell to monitor temperature changes. For all plasma gas mixtures and exposure durations, at least two trials were conducted with two samples per trial.

4.4.2 Plasma Characterization

The addition of a wool substrate to the plasma changes the plasma behavior as a result of the change in dielectric constant due to the inclusion of the wool into the plasma. Thus monitoring the changes in the dielectric constant, through the plasma model solver yields a measure of the change in the plasma parameters due to inclusion of the substrate.

4.4.3 Temperature Characterization

Ambient temperature within plasma is an important parameter when using a substrate with relatively low glass-transition or melting points. If temperatures within the plasma rise to a high value, permanent damage to the substrate may occur. Although it was previously seen that the gas temperature in profile did not exceed non-acceptable levels, it is possible

that the introduction of a substrate may cause changes in the overall gas temperature beyond acceptable limits.

When a substrate is introduced into the plasma, it may create new gaseous species (ions or radicals) through processes such as etching. Considering the closed geometry of the plasma cell, these ions/radicals will not rapidly escape the system and may exist for extended periods of time. Figure 52 illustrates temperature change inside the test cell with and without a wool sample for 100% helium discharge for 300 seconds duration. The temperature rises by about 3^{o}C in the first 5 seconds and continues to rise to 5^{o}C at 300 seconds.

This temperature rise may be attributed to a change in the relation between temperature, pressure and the number of moles in the ideal gas law $T = \frac{PV}{nR}$. Volume remains constant, however the formation of new ions and radicals from the etched surface can cause pressure increase and thus temperature increase. The alternative is a reduction in the number of moles *n*, as a result of mixing evolved atoms from the substrate with the plasma gas followed by recombination processes.

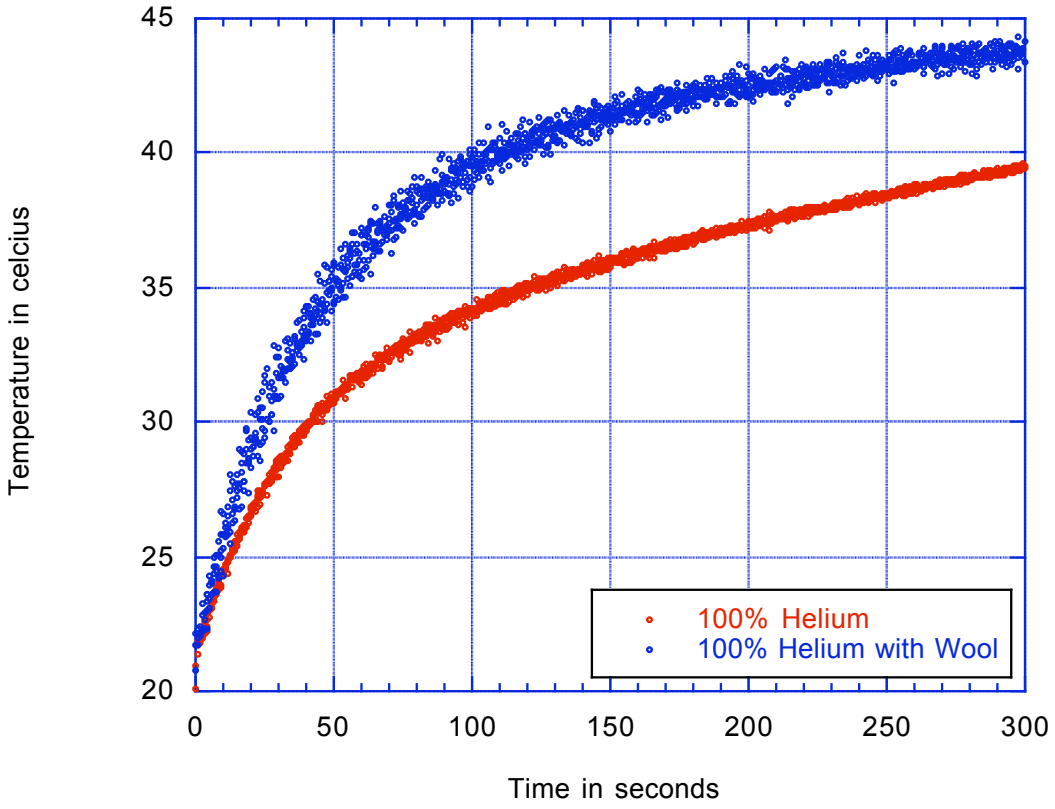

Figure 52: Temperature change for a 100% helium discharge with and without wool substrate for 300 seconds duration

When adding 1% O_2 to the helium discharge, Figure 53, the temperature changes, similar to the pure helium discharge, but at a lower rate. It actually reaches a stable condition after 100 seconds and remains at a plateau. The temperature increase in a 300 seconds time frame is about 4°C. In this case, while etching and radical formation may take place, the inclusion of oxygen allows for additional reactions between oxygen ions and excited atoms (even negative oxygen ions) and the substrate, and higher recombination rates can be

expected. Further increase in oxygen content, Figure 54, increases etching and radical formation, however the rate of recombination also increases and re-deposition takes place. As a result, the increase in the ambient temperature with wool substrate exposed to plasma starts to decrease and temperature drops back to same level as without the substrate.

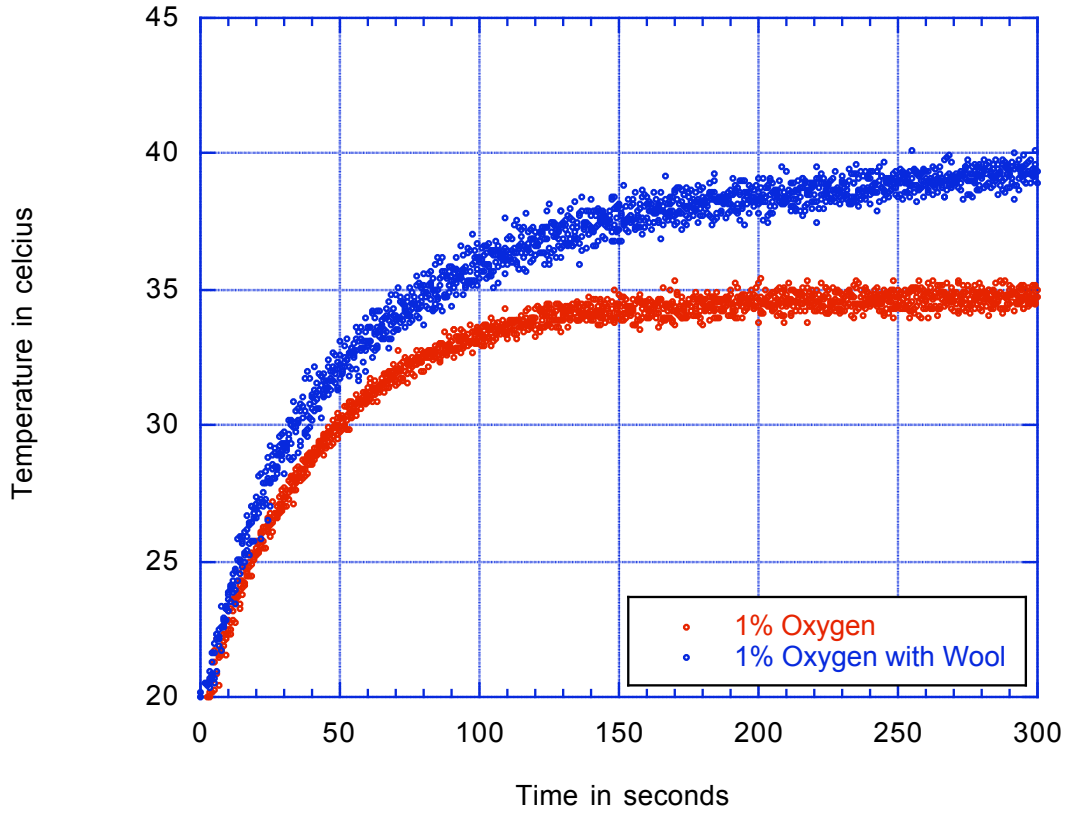

Figure 53: Temperature change for a 99% helium + 1% O2 discharge with and without wool substrate for 300 seconds duration

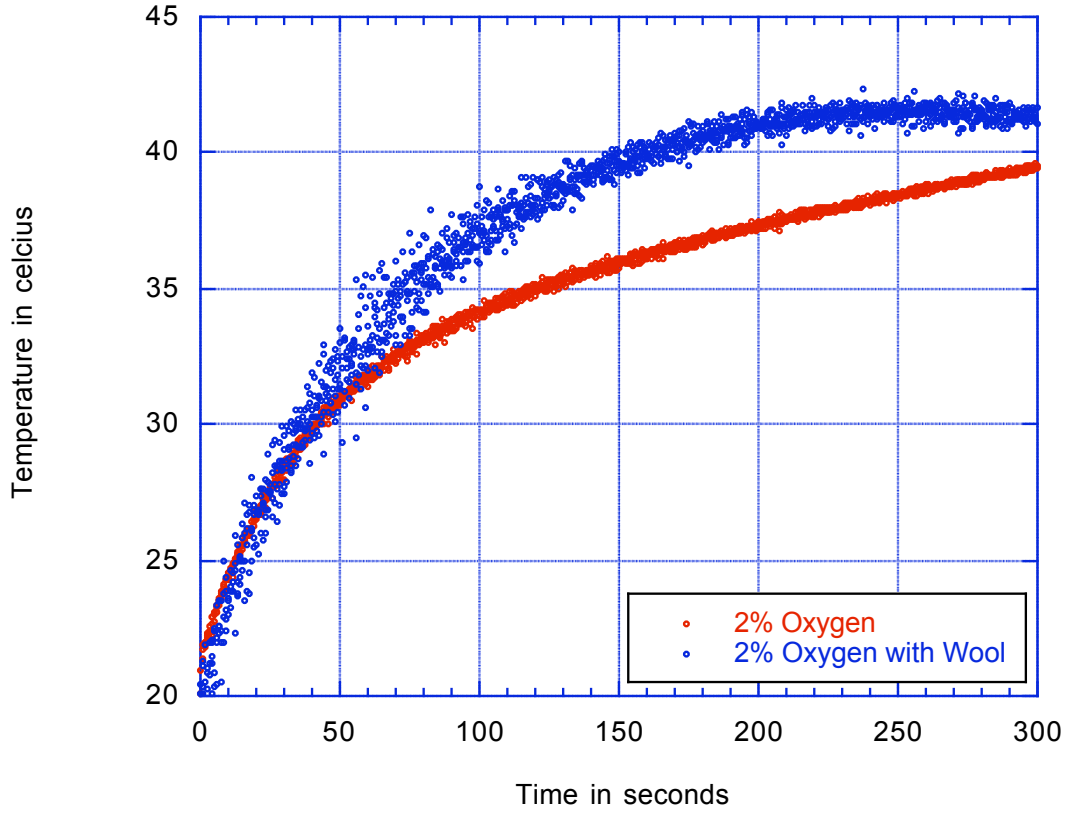

Figure 54: Temperature change for a 98% helium + 2% O2 discharge with and without wool substrate for 300 seconds duration

Experiments with 1% CF_4, Figure 55, have shown little to no change, and the temperature does not rise above the limits of CF_4 discharge without substrate. This behavior may be attributed to strong etching mixed with strong re-deposition, or surface fluorination without actual change in the ideal gas model. However, increasing CF_4 concentration to 2%, Figure 56, shows a slight temperature increase but levels off at 300 seconds to that without substrate. It is quite possible that dissociation processes of CF_4 into F, F^+, F^- or CF_3 may allow for mixed etching and re-deposition with near-equal rates and hence no major change

in the number of moles of gas molecules *n* would be expected.

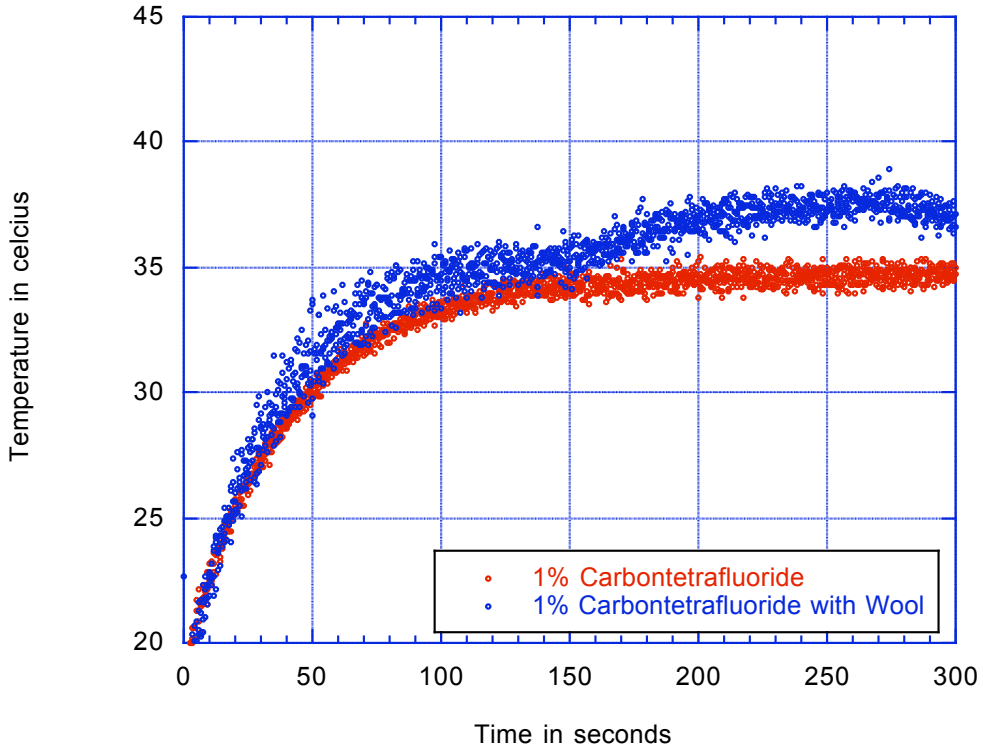

Figure 55: Temperature change for a 99% helium + 1% CF4 discharge with and without wool substrate for 300 seconds duration

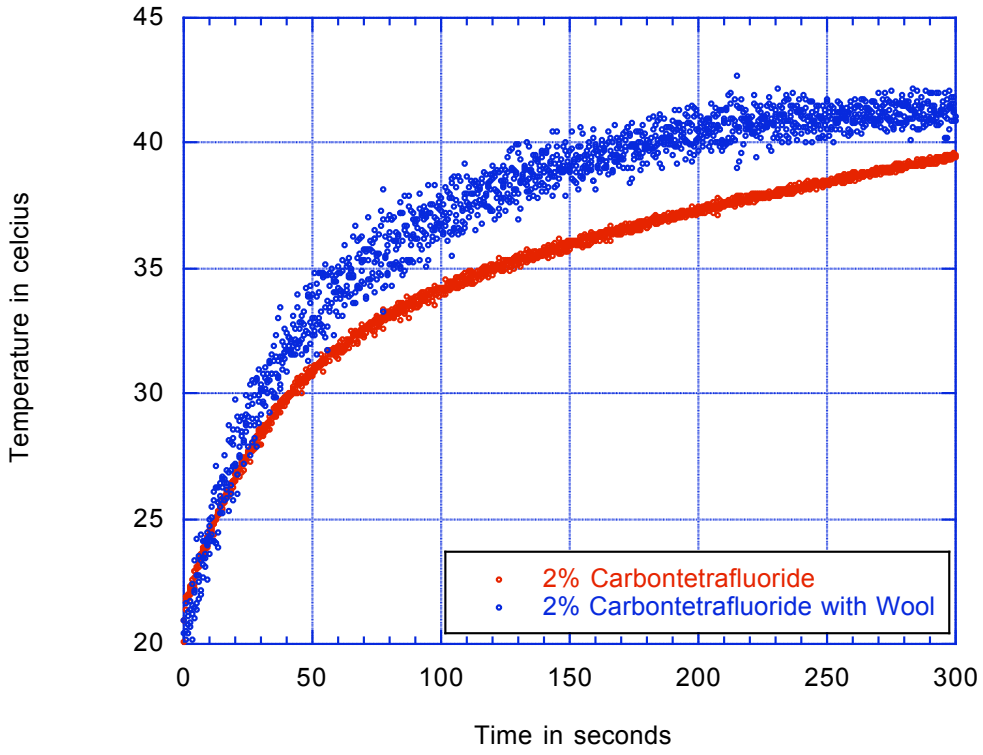

Figure 56: Temperature change for a 98% helium + 2% CF4 discharge with and without wool substrate for 300 seconds duration

Experiments with 1% O_2 + 1% CF_4, Figure 57, have shown changes similar to that of pure helium, and close to that of 1% O_2 without CF_4. It appears that the effect of O_2 on the discharge dominates over CF_4, and hence the result is similar to that of oxygen-only inclusion in the helium stream.

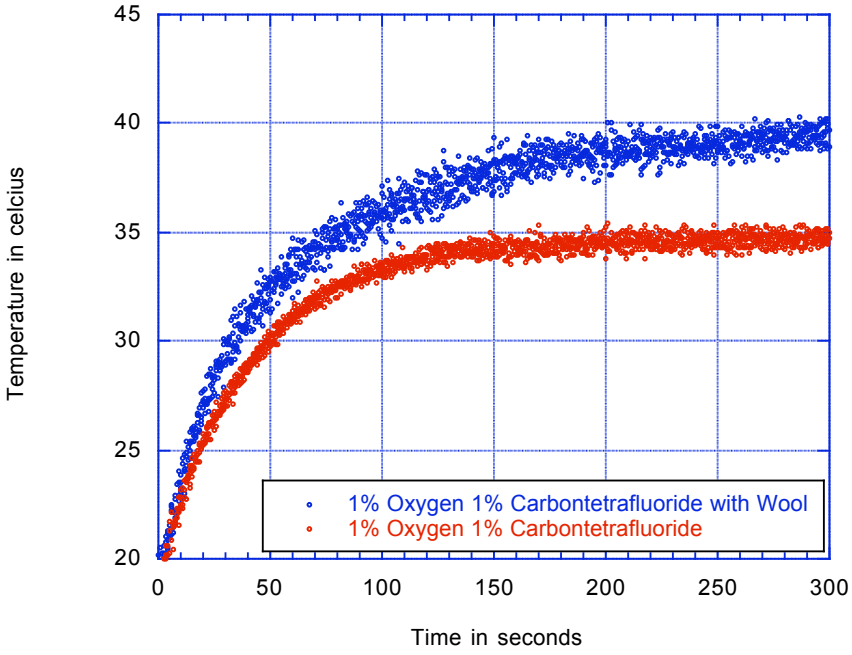

Figure 57: Temperature change for a 98% helium + 1% O2 + 2% CF4 discharge with and without wool substrate for 300 seconds duration

A summary of all temperature changes with wool substrates inside the plasma for all gas types is shown in Figure 58. Obviously, introducing a wool substrate into the plasma chamber increases the temperature at the center of the test cell. This difference in temperature is negligible at sixty seconds, but becomes more pronounced between 60 and 120 seconds. At 300 seconds, the temperatures appear to level off for most gas mixes. Of interest is the effect of pure helium discharge on the temperature change, since it is the highest of all the gas mixtures. This is because helium is an inert gas and does not recombine with free radicals evolving from the substrate due to etching by helium ions. A comprehensive model of the effect on temperature changes is recommended, however, it is outside the scope of this thesis.

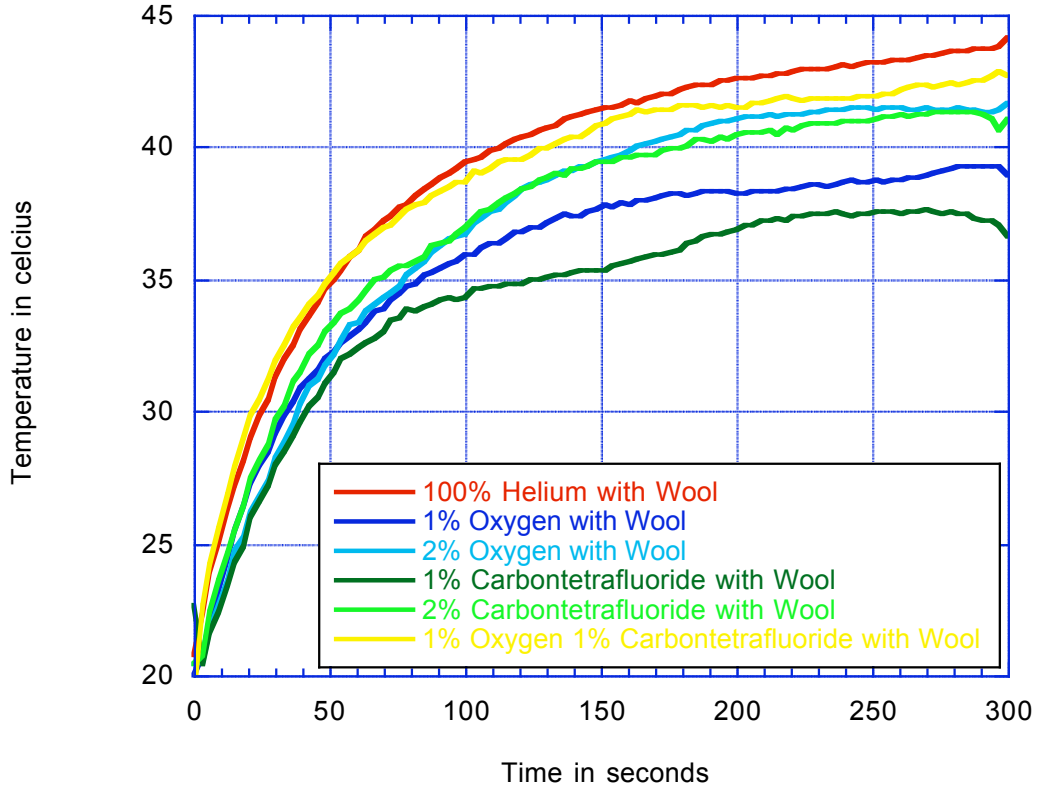

Figure 58: Temperature change with wool substrate in the plasma for all gas mixtures

4.4.2.2 Electron Number Density Characterization

The electron number density is determined from the model with data collected using the LABVIEW solver. Since plasma is quasi-neutral, this number density represents the number of electrons and ions in the discharge, even when fractional ionization is very low. In presence of a substrate, the electron number density may change as a result of interactions between plasma and the substrate. Electrons can impact the surface of the substrate (wool), causing chain scission, etching, re-deposition, fluorination, etc., and thus the number density may accordingly change. Since most surface functionalization is caused by ions, knowledge

about the relative ion number, which is equal to the electron number density, gives critical information about the kinds of reactions that can occur.

The electron number density model, in conjunction with LABVIEW data, can be used to solve for the electron number density. The electron number densities of the plasma with and without a wool substrate were obtained for all gas mixtures. Discharge voltage and current are averaged spatially over the entire area of the discharge and therefore changes are only temporal.

The electron number density of a pure helium discharge with and without a wool substrate is shown in Figure 59. After an initial 30 seconds of operation, the electron number density in the pure helium discharge levels off and becomes constant for extended plasma exposure durations, thus indicating stable plasma at a constant fractional ionization. The fractional ionization of atmospheric pressure plasma is very low as shown by the simple form of the Saha equation, which relates the number density of ionized species to the neutral density density $\frac{n_i}{n_n} \approx 2.4 \times 10^{21} \frac{T^{3/2}}{n_i} e^{-\frac{U_i}{kT}}$, where n_i is the ion number density (equals electron number density for a quasi-neutral plasma), n_n is the neutral gas density, T is the gas temperature, and U_i is the ionization potential. When solved using appropriate values, it can be seen that the fractional ionization at room temperature is extremely low. The number density without substrate in the plasma is 9.5 x 10^{12}/m^3, and drops to 7.5 x 10^{12}/m^3 in 300 seconds with the substrate in the plasma, indicating a fast recombination process. The drop in electron number density with a wool substrate suggests that the new radicals generated by etching processes with the partially ionized helium gas are recombining with electrons in the discharge and reducing the overall electron number density. This is consistent with the

observed increase in gas temperature, previously discussed, as a result of increased pressure due to recombination effects.

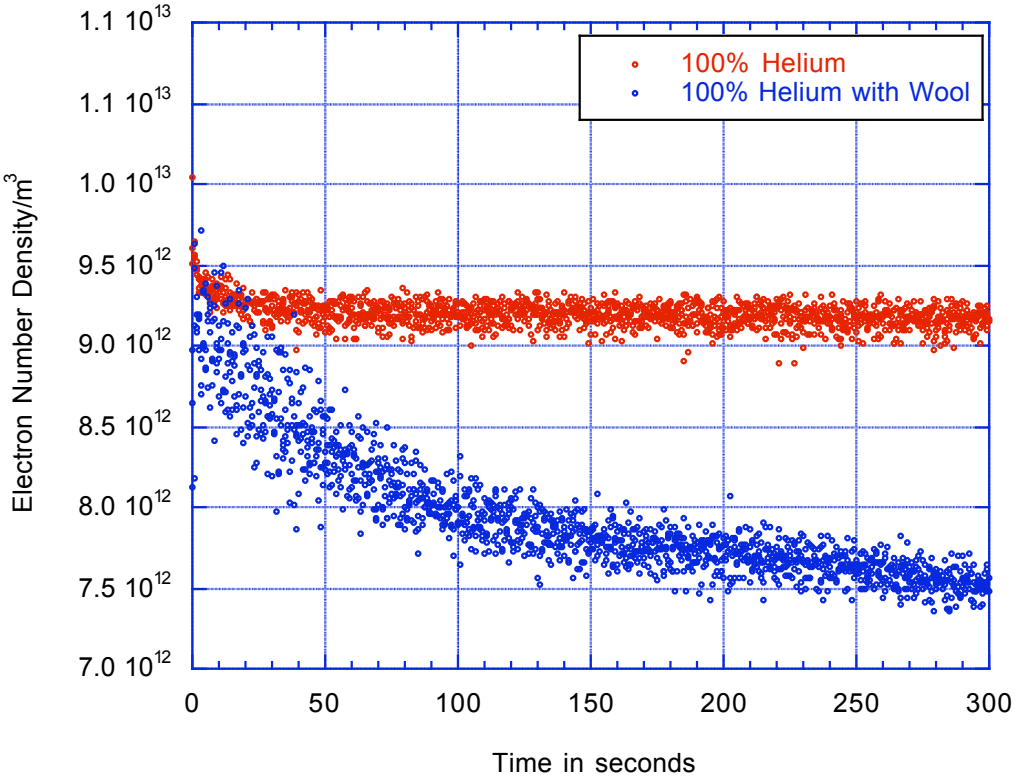

Figure 59: Change in electron number density for a 100% helium discharge with and without wool sample

When 1% oxygen is included into the helium discharge and a wool substrate is introduced, the electron number density slightly increases in the beginning up to 15 seconds then drops to ~8.0 x $10^{12}/m^3$ in 300 seconds. As seen in Figure 60, a 1% addition of oxygen does not vary significantly in electron number density from the pure helium plasma. However, the introduction of the wool substrate does not cause as significant a decrease in the electron number density for 1% oxygen as for 100% helium. This is attributed to the formation of

free radicals due to etching by oxygen.

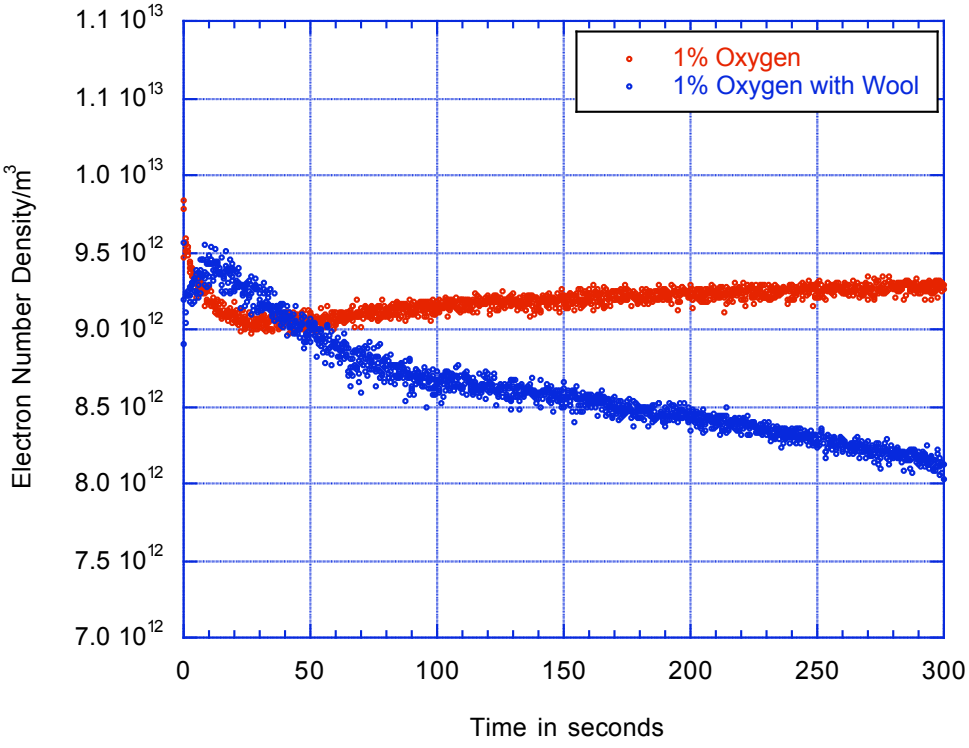

Figure 60: Change in electron number density for a 99% helium + 1% oxygen discharge with and without wool sample

The addition of 2% oxygen into the discharge allows for higher ionization and the number density without substrate is ~1.1 x $10^{13}/m^3$, as shown in Figure 61, then drops to 9.4 x $10^{12}/m^3$ in 300 seconds due to higher recombination rate. When the substrate is inserted into the discharge the number density increases due to increased etching and subsequent ionization, however, it drops to 9.6 x $10^{12}/m^3$ in 300 seconds, still higher than without a substrate. This observed increase suggests that the greater the oxygen content, the more ionization and free radicals will be created due to strong etching by oxygen ions.

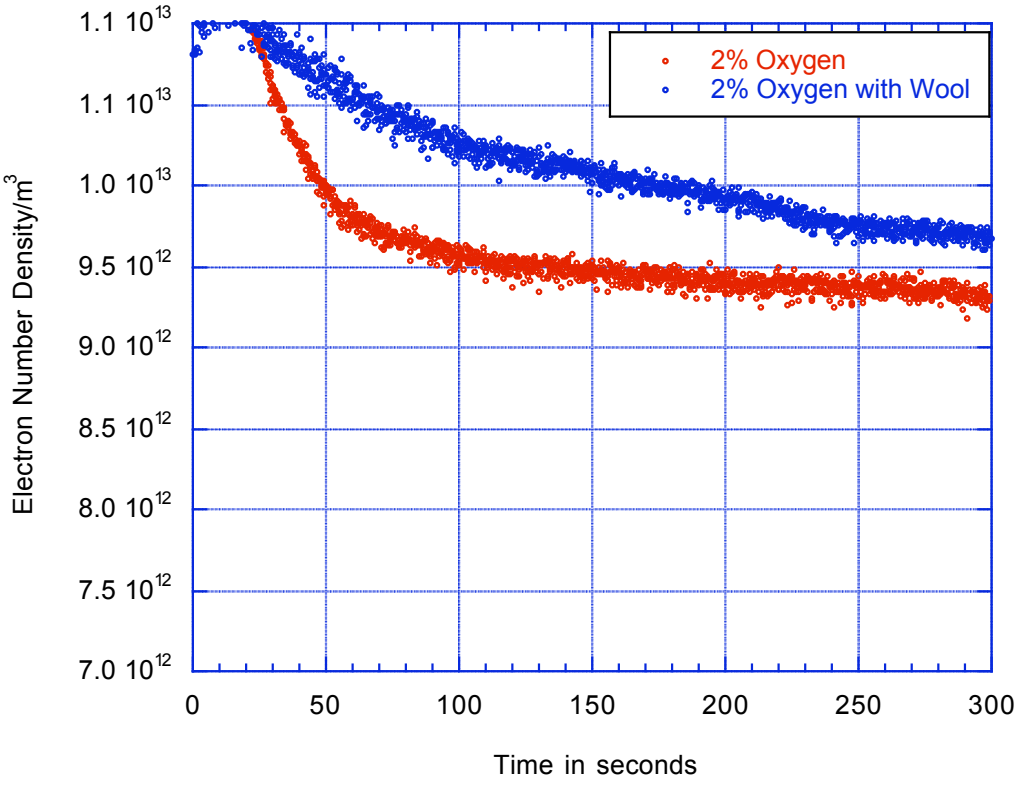

Figure 61: Change in electron number density for a 98% helium + 2% oxygen discharge with and without wool sample

The addition of carbontetrafluoride to the helium discharge is similar to the pure helium case and the 1% oxygen case, as seen in Figures 62 and 63. Without a substrate, the electron number remains constant at 9 x $10^{12}/m^3$, similar to a pure helium plasma. The addition of the wool substrate causes a reduction in electron number density, a result of the dissociation and ionization of the CF_4 gas and the interaction between the plasma active species (ions and excited atoms) with the substrate. This reduction is similar to that of the 1% oxygen case. However, a wool substrate in 2% CF_4 plasma does not show an increase in electron number

density when compared to a pure helium discharge after 300 seconds. The 2% CF_4 case takes much longer to reach a plateau than does the pure helium. This is due to more formation of radicals and ions due to dissociative processes of the CF_4 gas. However, the addition of CF_4 beyond 1% does not increase the rate of dissociation or ionization -it actually reduces it over time. Thus further increase in CF_4 concentration may not be desirable.

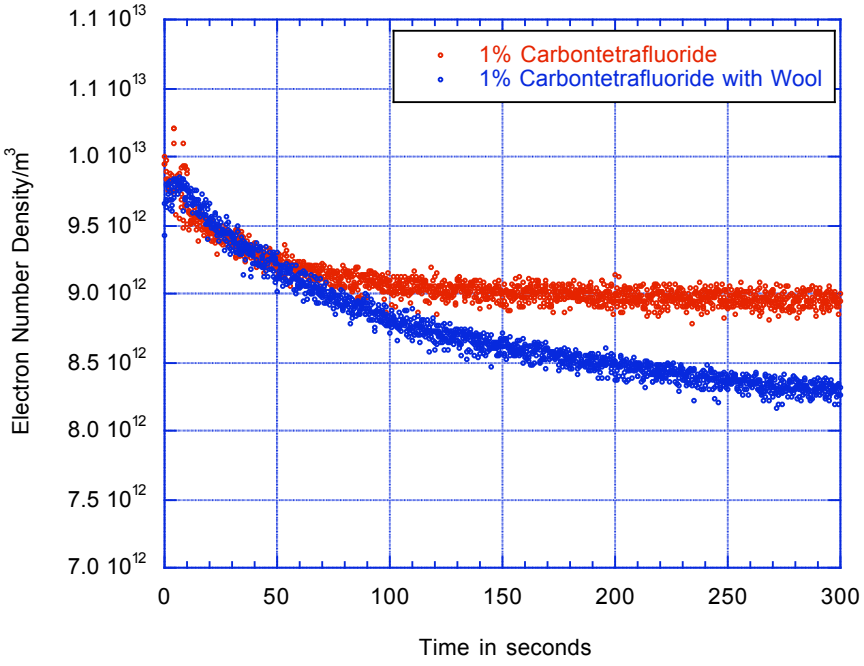

Figure 62: Change in electron number density for a 99% helium + 1% CF4 discharge with and without wool sample

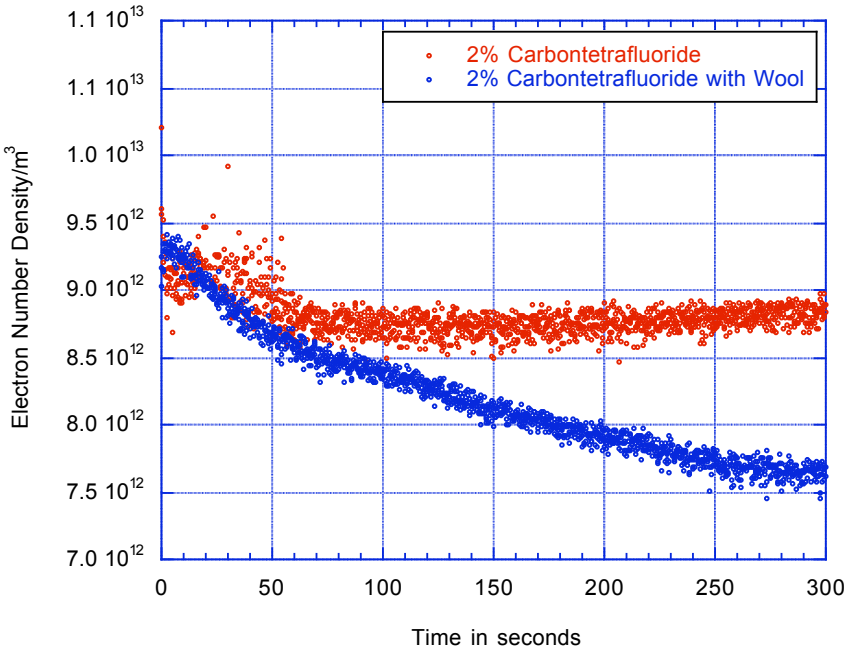

Figure 63: Change in electron number density for a 98% helium + 2% CF4 discharge with and without wool sample

When helium is combined with both 1% O_2 and 1% CF_4, as in Figure 64, the electron number density levels at 9 x $10^{12}/m^3$ in 100 seconds, then slightly drops to at 8.6 x $10^{12}/m^3$ in 300 seconds. Inclusion of the wool substrate causes a reduction in the electron number density to 7.7 x $10^{12}/m^3$ in 300 seconds. The combination of O_2 and CF_4, induces dissociation and ionization of multiple species, but also allows for stronger recombination processes between ionic species such as O^+, O^-, O_2^+,F^+, F^- and CF_3^+ additional to etched atoms/molecules from the surface of the wool substrate.

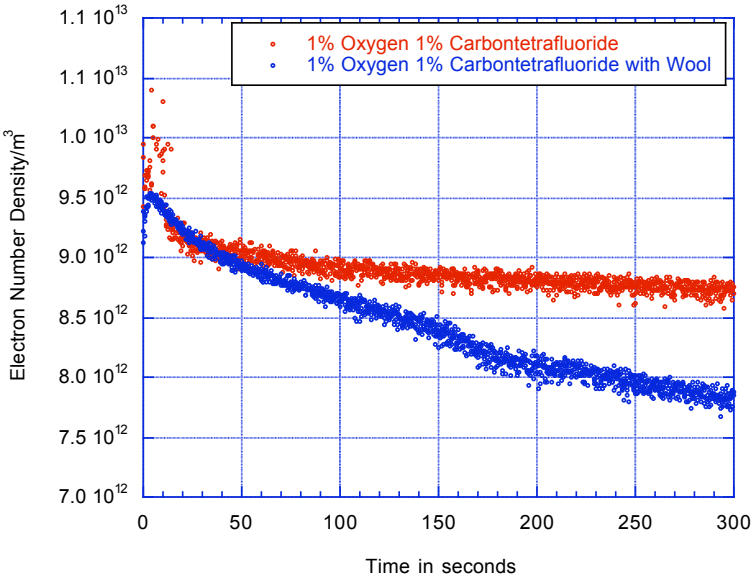

Figure 64: Change in electron number density for 98% helium + 1% O2 + 1% CF4 discharge with and without wool sample

The changes in electron number density for all gases with wool substrates are summarized in Figure 65. The changes are relatively similar with exception of the 2% oxygen case. As shown, the 2% oxygen gas mixture has an electron number density significantly higher than all other gases, even higher than the plasma without a wool substrate. This is a result of ionization and radical formation greater than the rate of recombination, as previously mentioned, oxygen ions and excited atoms interact with the substrate in chemical reactions at the plasma-substrate interface. Overall, helium gas shows the greatest decrease in electron number density and this can be attributed to the recombination of the electrons with the ions etched from the substrate without chemical reactions taking place.

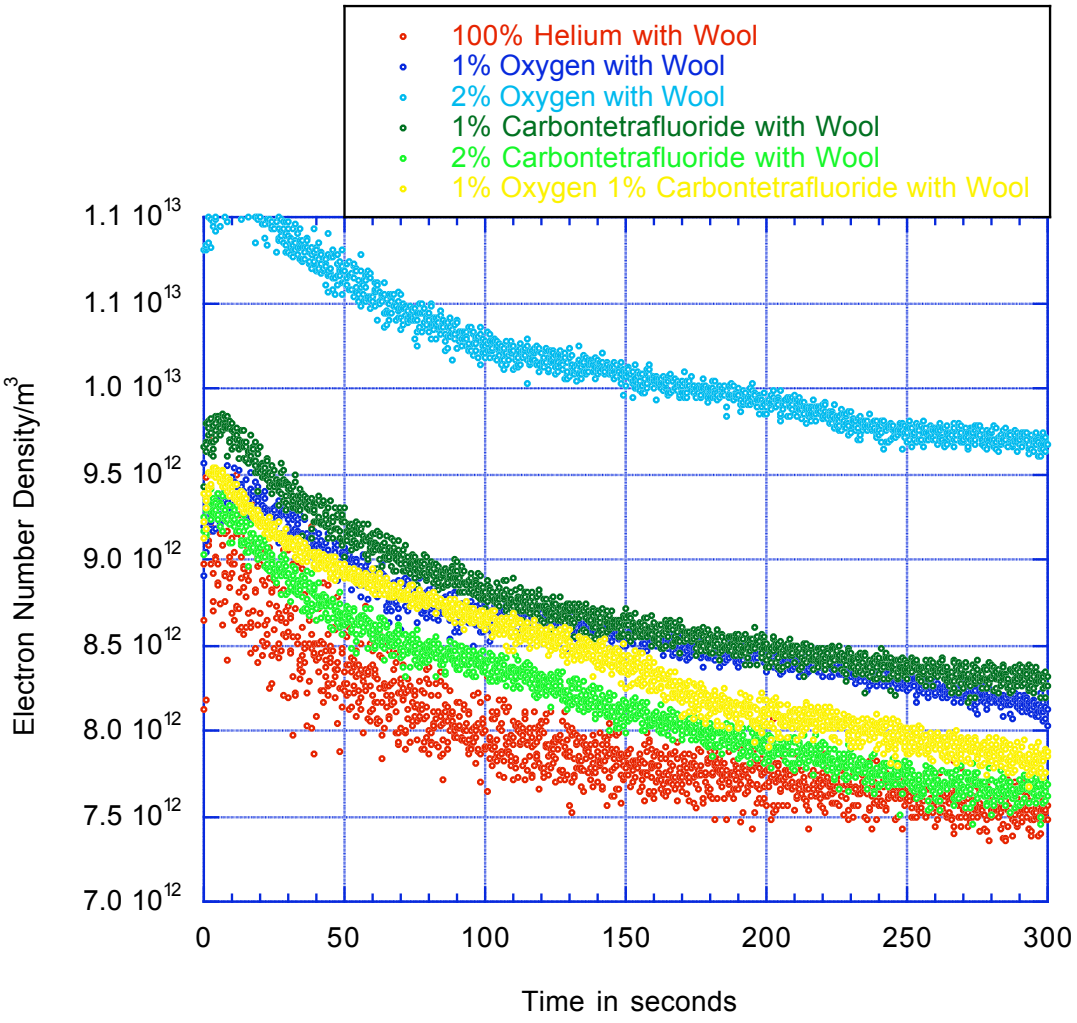

Figure 65: Change in electron number density for all plasma gases with a wool sample

4.4.2.3 Weight Change

All samples were conditioned for 24 hours at constant temperature and humidity conditions before and after plasma exposure to prevent deviations in mass due to variations in ambient humidity. Conditioning occurred inside of a Fisher Scientific Isotherm Programmable Oven Model 818F at ambient pressure and 105°C. Since the evaporation

point of water is above 100°C, the relative humidity is assumed to be 0%. Measurements were made on an Ohaus Explorer E00640 microbalance. The changes in weight due to exposure to plasma may be attributed to plasma-substrate interactions including etching, oxidation, fluorination, radicalization, scission, cross-linking, and re-deposition. These changes are dependent on the substrate material, which is wool for the purposes of this experiment, and the plasma gas mixture. Gas mixtures dissociate, ionize, and react with the substrate by different mechanisms and thus cause unique changes in substrates. The choice of the wool fiber is also significant, because wool is a natural fiber and a great degree of variation can be expected between samples. Figure 66 shows weight change of wool samples exposed to various plasmas.

In the 100% helium plasma discharge, a wool substrate experiences a drastic loss in weight as a function of time. Because helium is a noble gas, it will not chemically react with the wool to form new functional groups, so etching and redeposition are the only substrate-plasma interactions expected. The most significant weight loss occurs at 30 seconds, but continues steadily over 240 seconds. This reduction in weight can be attributed to etching of the wool substrate by helium ions. Though this mechanism dominates the first 240 seconds, after 300 seconds the wool fabric experiences a significant weight increase due to re-deposition in the closed chamber geometry.

The addition of oxygen changes the plasma-substrate interactions because in addition to etching and re-deposition, oxygen can complex with the wool chemical structure and form new functional groups. Observations of weight change show only the cumulative effect and thus only the dominant mechanism. Etching is a dominant mechanism for the oxygen

plasma. As the concentration of oxygen increases from 1% to 2%, the weight of the wool decreases suggesting an increase in the etching process. The greatest decrease in weight, as with the pure helium case, is within the first 30 seconds, and the decrease in weight over time is not as significant as with a pure helium plasma suggesting that oxygen is bonding with the wool surface. For both concentrations of oxygen, a slight plateau is reached between 60 and 180 seconds. There is little change in weight for this time period, suggesting the processes of etching and functionalization or redeposition are in competition and occurring at approximately equal rates. However, after 180 seconds, the etching mechanism dominates and both substrates decrease significantly in weight. At the end of 300 seconds, the 2% oxygen plasma etches nearly twice the amount of weight off the wool fabric than does the 1% oxygen plasma. Thus, the greater the concentration of oxygen, the greater the amount of etching will occur.

Carbontetrafluoride (CF_4) added to the helium gas in small concentrations reduces the weight over time, suggesting etching is dominant. The decrease in weight is slightly less with 1% CF_4 than for the pure helium, suggesting that some form of re-deposition or surface functionality must be occurring (such as fluorination) or that the CF_4 is preventing substrate interaction by reducing electron and ion energy through collision without significant ionization or dissociation (as seen when examining changes in electron number density). However, 2% CF_4 shows an increase in etching over 1% CF_4, but not a significant change in etching when compared to a pure helium discharge. It can be concluded that at this concentration of CF_4, the etching processes dominate.

Gas mixture of 98% helium with 1% O_2 and 1% CF_4 cause reduction of weight, which is also a result of etching as both oxygen and fluorine ions are strong etchants.

However, the overall weight loss is very small compared to the other gas mixtures. The most significant decrease in weight occurs within the first 30 seconds, seen for most gases, followed by a plateau, and at 300 seconds re-deposition or surface functionalization occurs at a rate greater than that of etching. Two possibilities exist to explain this observed phenomenon. Either the ions and radicals produced by the oxygen and CF_4 are interacting with themselves and preventing processes such as etching to occur, or functionalization and re-deposition are occurring at a rate equal to the rate of etching after 30 seconds and greater than the rate of etching after 300 seconds.

As seen in Figure 66, all samples exposed to any of the gas mixtures primarily undergo etching. The greatest decrease in weight for almost all gases occurs after 30 seconds, and can be attributed to the etching of the waxy coating off the surface of the wool. This coating is different in chemical composition from the internal wool structure, the former an organic hydrocarbon and the later is a protein structure. The rate of etching varies for all samples, but the 2% oxygen plasma appears the most effective etchant after 300 seconds.

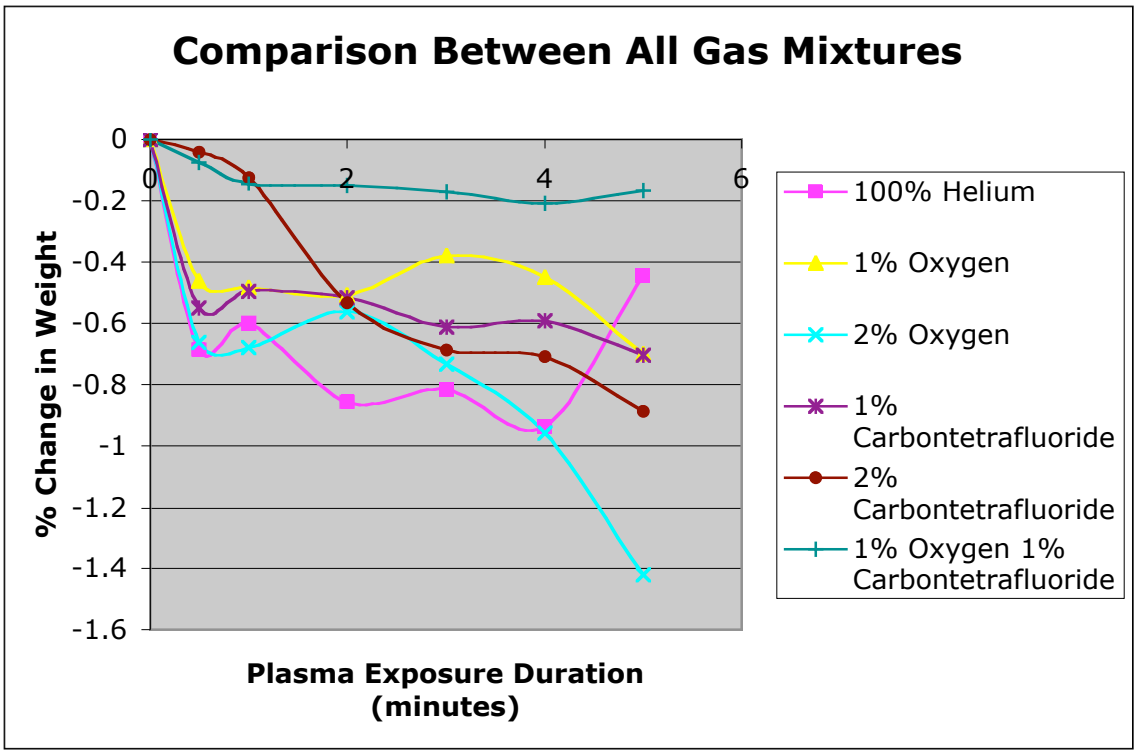

Figure 66: Change in weight of a wool substrate exposed to various plasmas

4.4.2.4 Contact Angle and Absorption Time

Contact angle was measured using a Model A-100 Rame-Hart, Inc goniometer. Sampling was conducted in ambient conditions at room temperature and standard humidity. Each sample was tested at five locations with 6µL of water for each drop. Both left and right angle were measured for each drop and results for each location and side were averaged.

Previous studies show that the contact angle of samples exposed to air can undergo an aging affect. Since all industrial textiles will be exposed to air and durability of any fiber finish is necessary, all contact angles were taken over a month after fabric treatment.

While measuring the contact angle of wool fabrics, it became apparent that many of the treated fabrics absorbed the water droplet before the right and left angle could be

determined. In addition, the gradual decrease in angle over time caused discrepancies between the right and left angle of the same water droplet, since both cannot be measured simultaneously.

For this reason, absorption time was measured in addition to contact angle. The water droplet was micro-pipetted onto the surface of the fabric, and time-to-absorb was measured. Upon contact, a stopwatch was used to record the time to absorb. The water droplet was observed through the magnifying glass for changes in contact angle. When the contact angle decreased to zero, the time was recorded. If absorption occurred within 200 seconds, no contact angle was recorded. If no changes in the contact angle were observed in 200 seconds, then a contact angle was measured.

The absorption and contact angle of the wool fabric represents a change in the hydophilicity of the wool, or its ability to absorb water from the humidity in the air. As hydrophilicity increases, the contact angle decreases and absorption time is reduced. Wool fibers are composed of an internal protein structure covered in a waxy, hydrocarbon coating. This coating is only a few μm thick and can easily be removed by etching processes when plasma-treated. These etching processes were examined by observing the changes in weight over plasma exposure duration for the various gas mixtures, and all showed signs of etching. However, as seen in Figure 67, after only 30 seconds of plasma exposure the absorption time of most gas mixtures has not significantly decreased from the control, nor has the contact angle, as seen in Figure 68. Some reduction has occurred, particularly for the 100% helium discharge suggesting that etching is dominant, but the substrate can still be characterized as hydrophobic at this exposure duration. Thus, though the most significant quantity of etching occurs in the first 30 seconds, some or most of the waxy coating of the wool still remains. In

addition, it can be summarized that the processes of surface functionalization, the other process leading to increased hydrophilicity, are not significant after 30 seconds due to the lack of reduction in absorption time. After 180 seconds, a notable difference in contact angle and absorption time is observed. Thus the etching processes have removed the waxy coating and functionalization of the surface with hydrophilic groups may be occurring. This trend continues after 300 seconds when all gas mixtures have modified the wool fabric from a hydrophobic to a hydrophilic substrate due to the reduction in absorption time and the lack of a contact angle. Overall, 1% CF_4 + 1% O_2 gas cause the least change in hydrophobicity. This may be attributed to the lesser extent of etching that occurs with this gas mixture as previously discussed. The observed reduction in contact angle and increased absorption has been observed by other researches, particularly for oxygen plasmas [31]. For these oxygen plasmas, decreased contact angle and absorption time may be partially due to the formation of hydrophilic functional groups such as –COOH, -C=O, etc. [32]. However, for other gases as well as for oxygen the most probable reason for the increased hydrophilicity is due to etching of the waxy and hydrophobic coating off the surface of the wool fibers [33].

A comparison between the gases suggests that some gases are more effective than others in producing hyrdrophilicity. The dependence of wool properties on gas mixture has been documented in literature, especially for changes in hydrophilicity [34].

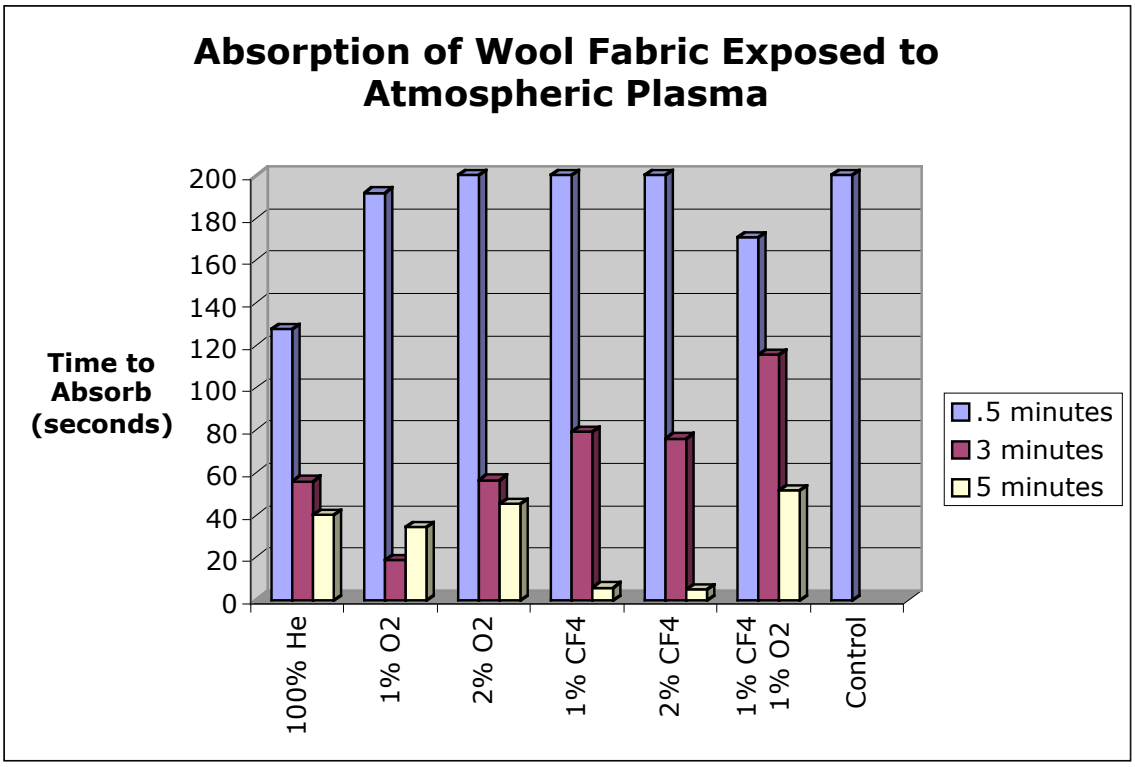

Figure 67: Absorption of wool fabric exposed to plasma

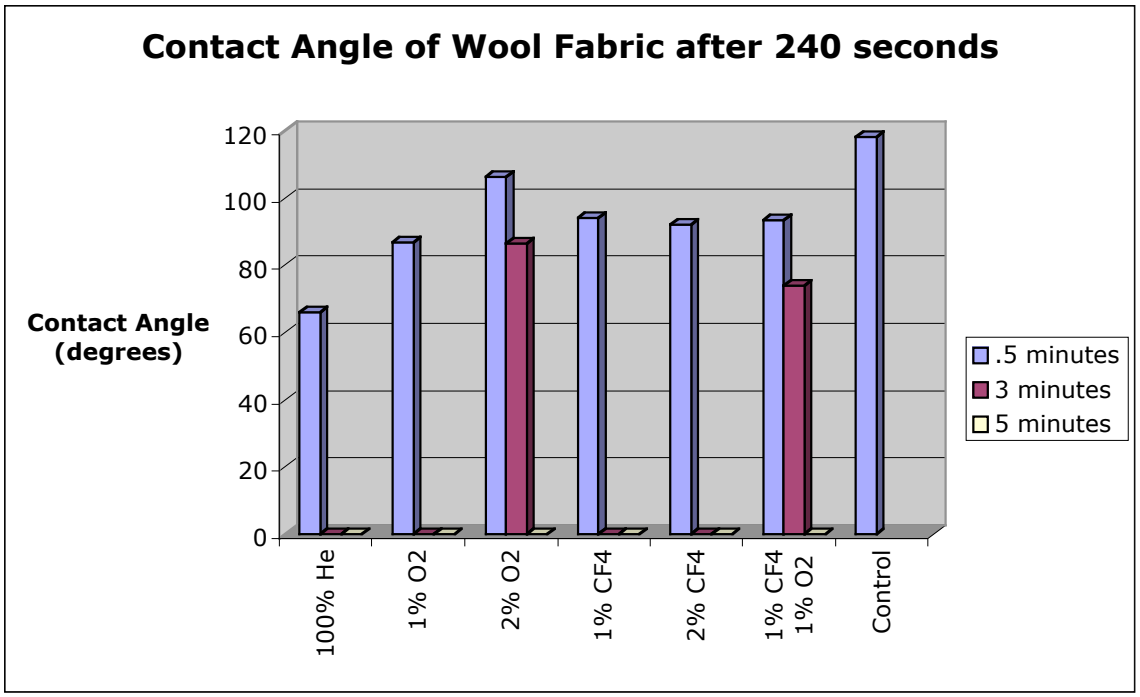

Figure 68: Contact angle of wool fabric exposed to plasma

4.4.2.5 Energy Dispersive X-ray Spectroscopy

A variable pressure scanning electron microscope, Hitachi S3200 series, was used in conjunction with an oxford Isis EDS system to conduct elemental analysis of the samples. The oxford Isis EDS system can detect elements with atomic numbers greater than Boron (A=5). Thus elements such as carbon, oxygen, and fluorine can all be identified and quantified by the system. An accelerating voltage of 5kV in conjunction with a 50μm aperture was chosen for the samples. The spot analysis function was used to measure the elemental concentration on a very small portion of a fiber within the sample. Analysis was conducted on three locations and averaged for each sample.

EDS analysis, illustrated in Figure 69 shows an increase in fluorocarbon concentration for samples exposed to CF_4 gas mixes. The control sample of wool contained no elemental fluorine, however, after plasma exposure fluorine is present in small quantities for all gases except for 1% CF_4+ 1% O_2 at 30 seconds. At 300 seconds the percentage of fluorine has increased in most cases (except the 2% CF_4 case, which shows a slight decrease).

It is also important to note that EDS analyzes the entire elemental content of the material, whereas plasma treatment is only a surface treatment. Plasma fluorination would result in increased fluorine concentration only on the surface of the fabric. EDS is not limited to the surface, but will average over the entire thickness of the fabric. Therefore a small increase in fluorocarbon with respect to the entire thickness of the fabric indicates a larger increase in surface fluorocarbon.

Due to the increase in fluorine content in the fabrics exposed to fluorocarbon plasmas, it can be concluded that some surface deposition and/or bonding of fluorine with the wool fabric is occurring. In addition, the data indicates that a longer plasma exposure time will result in a greater increase in surface fluorination.

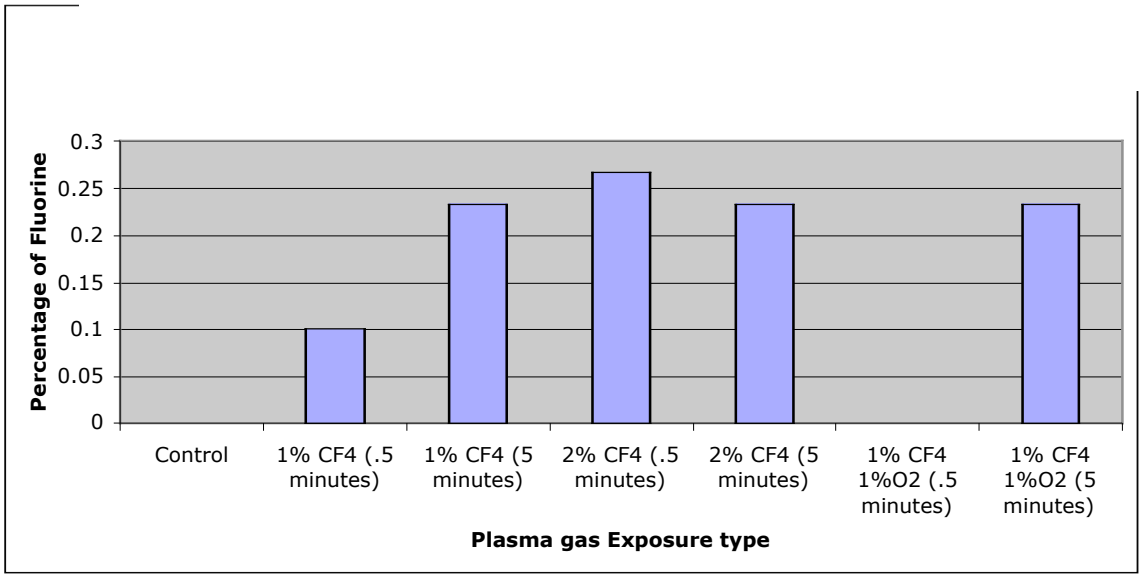

Figure 69: Fluorine content on wool samples exposed to plasma with percentage of CF_4

4.4.2.6 Tensile Testing

Tensile testing was conducted for all samples using a MTS Q-Test/5 with an Elite Controller attachment. A 250lb load cell was used with attached leather grips to prevent slippage. The system was connected to a computer running Testworks 4 software package, which analyzed and recorded the data. A strip test for the warp with a gauge length of 3" was conducted on the wool substrates. Two samples from each gas mixture and each plasma exposure duration were cut along the grain into 1" x 6" strips (3 strips per sample, 6 total). Each strip was then conditioned for 24 hours in the testing facility at 65% humidity, 21°C, at

ambient pressure. After conditioning, each strip was individually tested and averages were taken for each trial. The computer system automatically tabulated peak load, energy at peak load, % elongation, and the % strain at elongation.

The peak load is the maximum amount of weight the fiber could support before irrevocable damage, usually in the form of a rip or tear. . The control sample, at 0 seconds plasma exposure, is higher in value than most of the gas types. As can be seen from Figures 4.28 and 4.29, the samples exposed to the 2% oxygen show a distinct increase in peak load after only 0.5 seconds. The increase continues until 60 seconds then levels out. This increase in peak load could be due to significant increases in cross-linking or to the creation of hydrophilic groups. The increases in hydrophilicity trap water at the fibers surface where it can act as a lubricant and allow slippage in the woven fabric structure. Slippage allows for more even weight distribution and the ability to sustain more weight. This behavior is also noted for the1% O_2 case at about 240 seconds. Thus an increased percentage of oxygen suggests more rapidly increased strength, but the same strength can be achieved by a smaller dose at a longer duration. Studies on pressurized low temperature plasma systems that used oxygen revealed similar findings. These studies also show that wool treated in oxygen plasma will have an increase in tensile strength over time [35]. Other gases containing helium and oxygen exhibited a small decrease in the peak load in comparison with the control. At 300 seconds for the 2% CF_4 gas, the wool undergoes a sharp decrease in peak load. This suggests too much etching has occurred. Overall, the 1% CF_4 1% O_2 shows the most and worst effect on the peak load of all the gas mixtures.

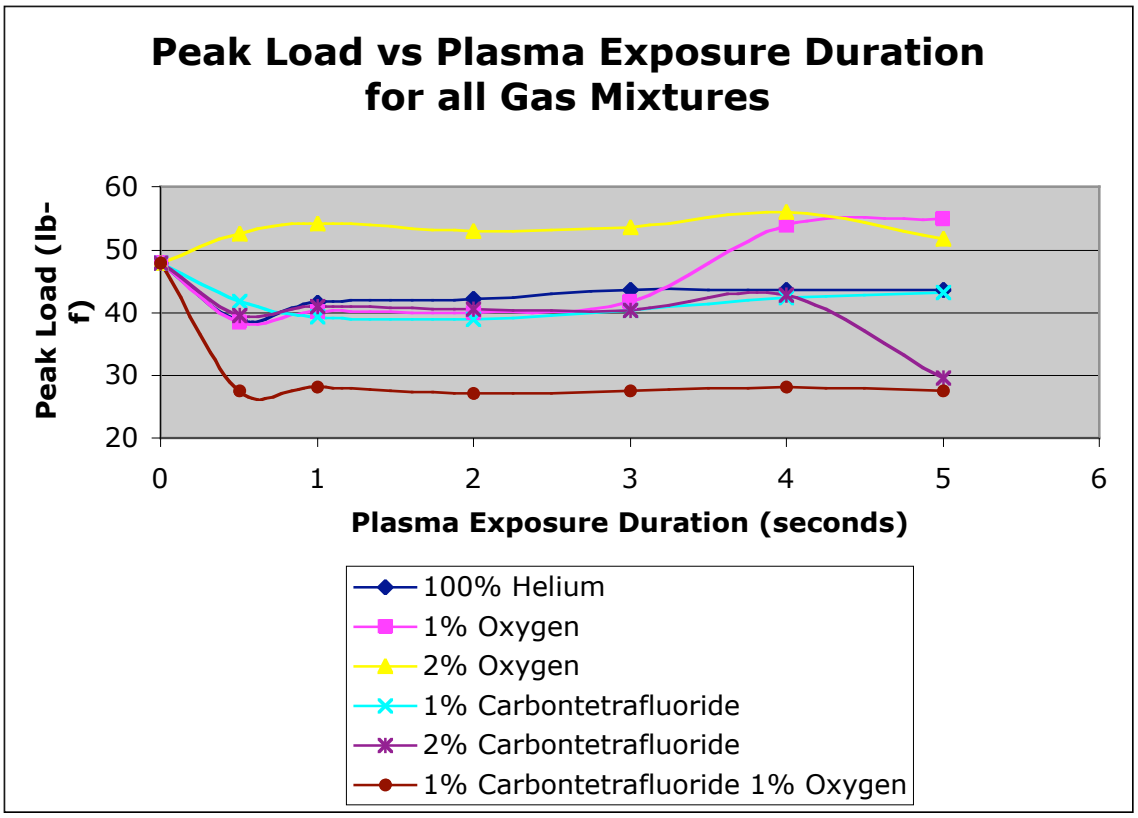

Figure 70: Peak Load of wool substrates for all plasma gas mixtures

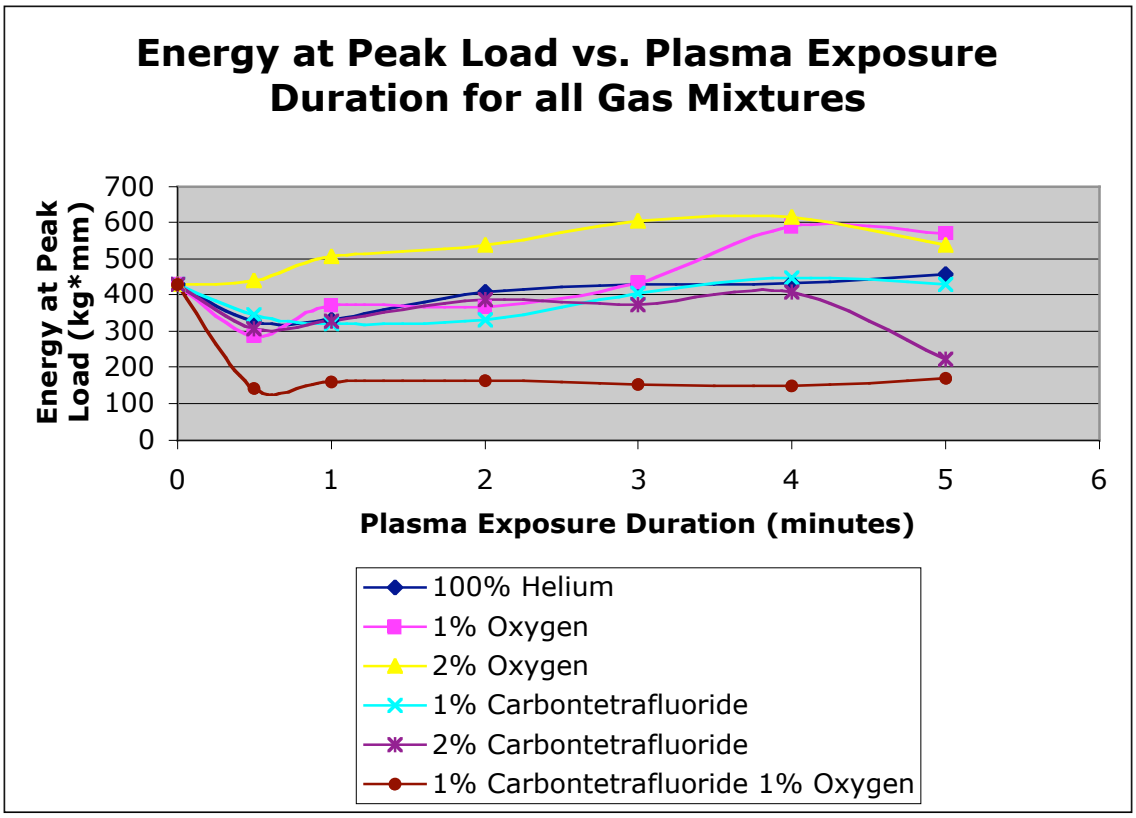

Figure 71: Energy at the Peak Load of wool substrates for all gas mixtures

The % elongation at break, and the% strain are attributed to a fabric's ability to stretch without being permanently damaged. Wool is known for its natural stretchiness, a result of its α-helix protein structure. As seen in Figure 72 and 73, after 0.5 seconds in plasma, all treatments show a significant decrease in elongation. This may be due to damage of the protein structure of wool due to etching. However, this is unlikely since previous data indicates the waxy coating on the surface of wool has not been etched away at this limited plasma exposure duration. All plasma gas mixtures, excluding 1% O_2 +1% CF_4, show recovery of the % elongation after 60-120 seconds of plasma exposure. Likewise, the etching rate of the wool surface for all cases excluding 1% O_2 +1% CF_4, increases with

continued exposure to plasma. The changes in % elongation can therefore be correlated to the etching, though the exact chemical mechanism and surface modification is not fully understood. As noted with changes in strength, the 2% oxygen case shows an improved elongation after 60 seconds of plasma exposure. The1% oxygen case eventually reaches the capabilities of the 2% oxygen case, but requires a much longer exposure time. Only the 1% O_2 +1% CF_4 mixture shows a significant and permanent decrease in elongation.

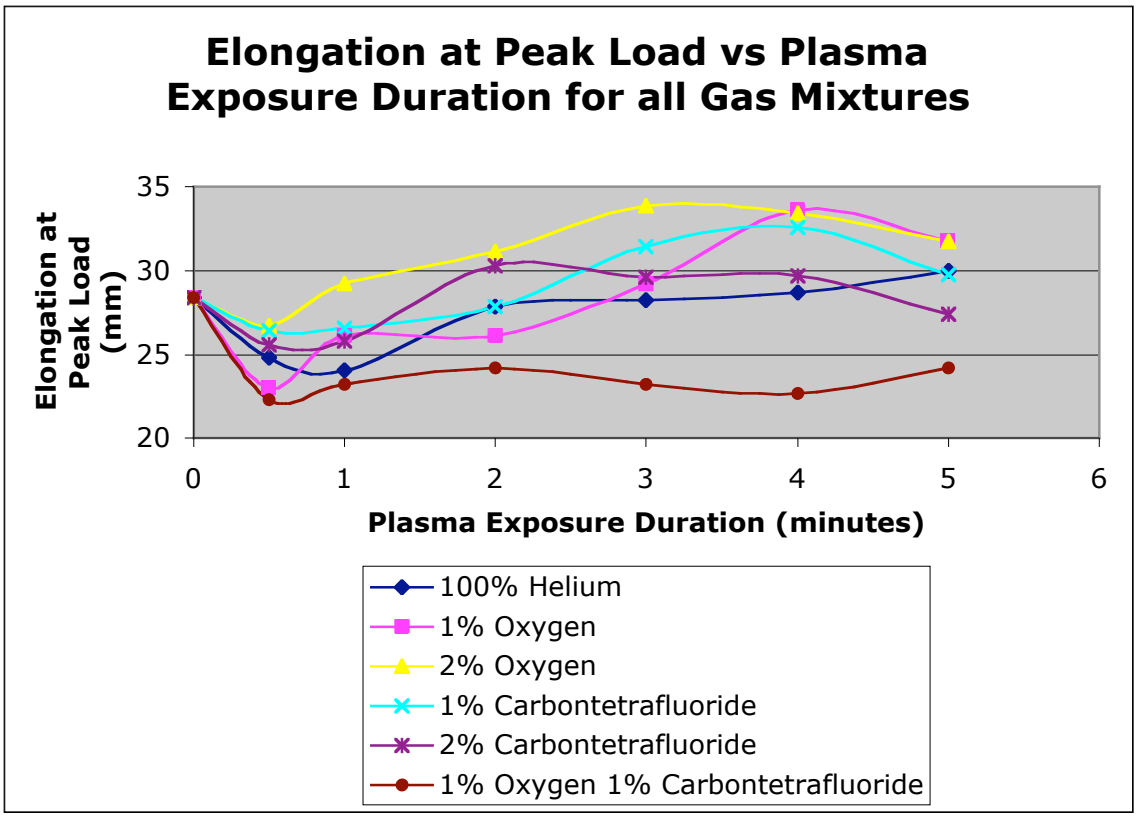

Figure 72: Elongation at the Peak Load of wool substrates for all plasma gas mixtures

4.5 Cellulosic Paper Research

4.5.1 Experimental

Cellulosic "kraft" paper was exposed to atmospheric pressure plasma with inclusion of the anti-microbial agent HTCC in order to create a permanent, safe, anti-microbial functionality on the surface of the cellulose. Cellulosic papers 12″ x 12″ with a thickness characteristic of chipboard were obtained and cut into 3″ x 3″ squares. Samples were conditioned at standard pressure, 21˚C, and 65% humidity for 24 hours. Next samples were exposed to the HTCC (5g/100mL) and plasma in three application procedures. For all application methods, the HTCC was applied via a spray application and the plasma gas was 99% helium + 1% oxygen with 120 seconds exposure time. The methods of application included:

1) HTCC spray followed by plasma exposure,
2) Plasma exposure followed by HTCC spray,
3) Plasma exposure followed by HTCC spray then a subsequent plasma exposure, and
4) Spray without exposure to plasma.

After plasma exposure, the samples were reconditioned and weighed then washed by dabbing with ethanol and water and re-conditioned. Changes in weight were tabulated and revealed weight increase for all samples and the control. In order to test the adhesion of the spray application, a small portion of each sample (1cm x 2cm) was then washed via soxhlet extraction for 24 hours in 100% ethanol. The samples were then reconditioned and weighed.

Application of HTCC after plasma exposure signifies that modifications to the

chemical structure of the exposed substrate will be limited to the cellulosic paper. Thus, the integrity of the HTCC chemistry is preserved, except for the bond it forms with the activated cellulosic paper surface. Furthermore, the plasma parameters will change only due to the dielectric property of the cellulosic paper and not due to the HTCC chemical. When the HTCC is introduced into plasma, it may radicalize, polymerize, and/or undergo chain scission. The dominant process has not been analyzed in this thesis, but must be understood in order to ascertain whether the anti-microbial functionality of the compound remains intact and to ensure a lack of toxicity or the production of carcinogens, etc.

4.5.1.1 Weight Change

Weight change analysis was conducted to determine from the % weight add-on if grafting of the HTCC to the cellulosic paper occurred. The data shows a significant increase in the weight of all samples including the control as seen in Figure 73. Although it is expected that the cotton will naturally absorb some HTCC due to its chemical structure, a 4.8% increase by weight without plasma exposure is unlikely. This suggests that the method of washing the cellulosic paper by "dabbing" is not sufficient. A more rigorous washing that does not significantly damage the surface of the cellulosic paper is necessary.

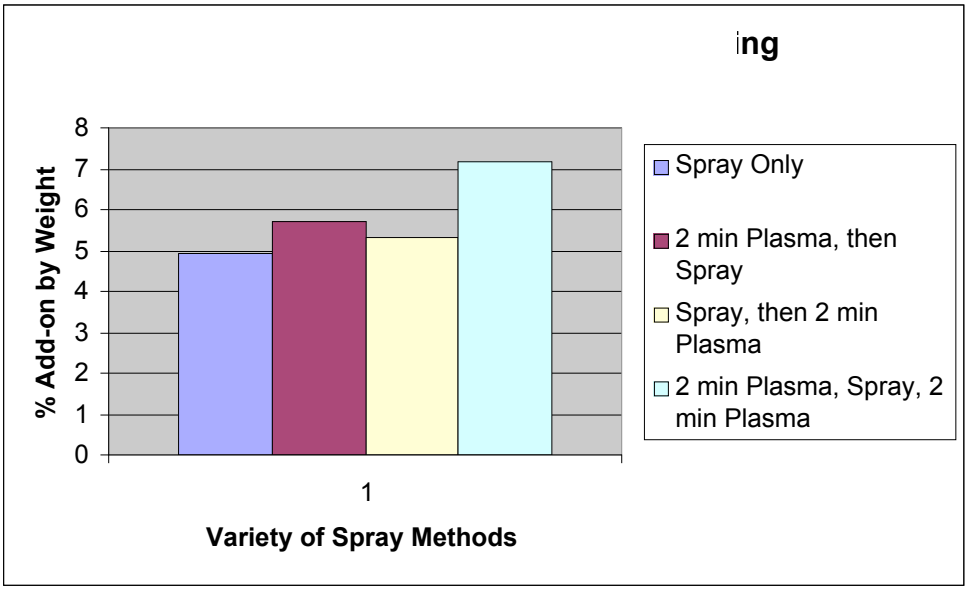

Figure 73: Add-on of HTCC after one washing

To address the inadequacy of dabbing as a method of washing and removing un-grafted HTCC, soxhlet extraction was used to wash the samples. Each sample was cut into smaller samples, conditioned and weighed, then exposed to soxhlet extraction for 24 hours in 100% ethanol solution, dried, reconditioned, and weighed. The weight loss that occurred during soxhlet extraction is shown in Figure 74, and represents the removal of un-grafted HTCC from the paper. Soxhlet extraction resulted in the removal of almost all the HTCC from the control sample (not treated in plasma). The other samples lost very little or no weight after soxhlet extraction suggesting the formation of a permanent and stable bond with the HTCC due to the plasma exposure

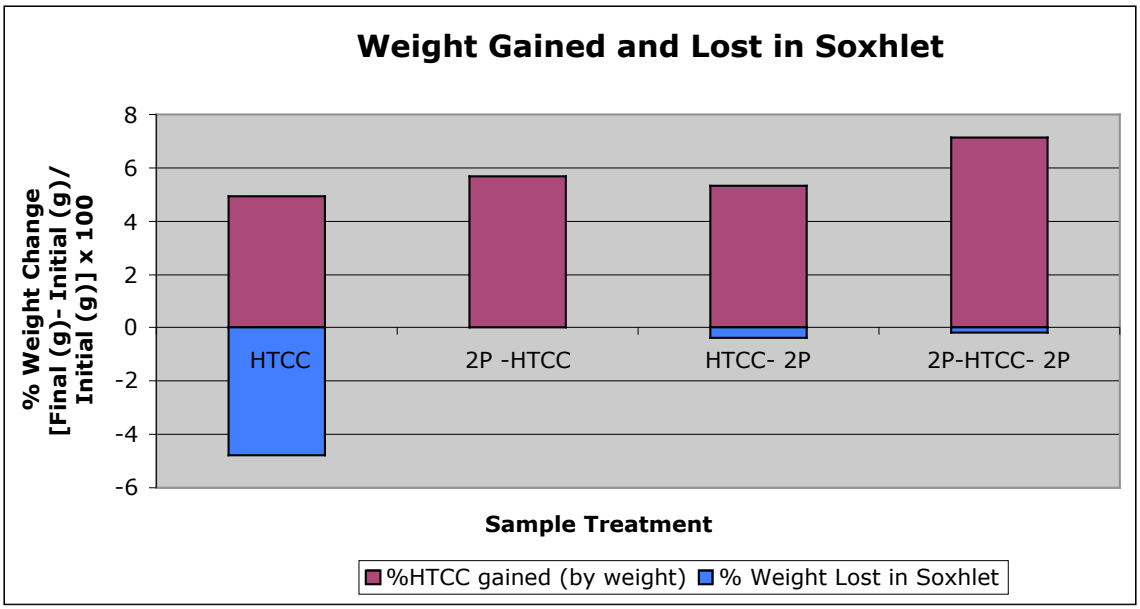

Figure 74: Weight change after soxhlet extraction

4.5.1.2 Scanning Electron Microscopy (SEM)

All scanning electron microscopy was performed using a Hitachi S-3200 Scanning Electron Microscope (SEM). All samples were mounted on a plate and sputter coated with silver for two minutes. Within the SEM, an accelerating voltage of 5kV, and a 50µm aperture were used to analyze the samples.

The photographs taken by the SEM clearly show the grafting of HTCC to the cellulose (Figure 75-77). The control shows a smooth cotton sample with little surface features and the sample sprayed with HTCC, but not plasma treated shows an increased surface roughness, probably due to the soxhlet extraction or dabbed washing and possible presence of some residual HTCC. The sample plasma treated and grafted with HTCC clearly shows the presence of a new material on the surface of the cellulosic fibers, visually confirming the grafting of the HTCC.

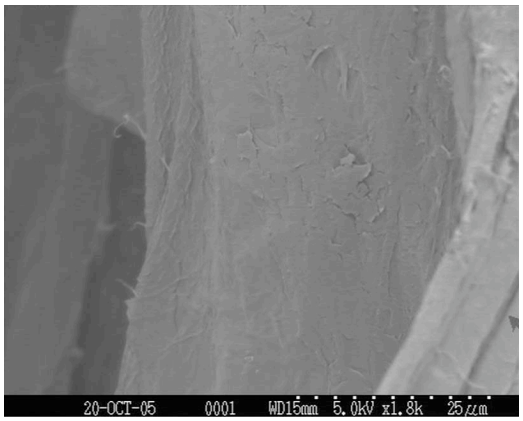

Control

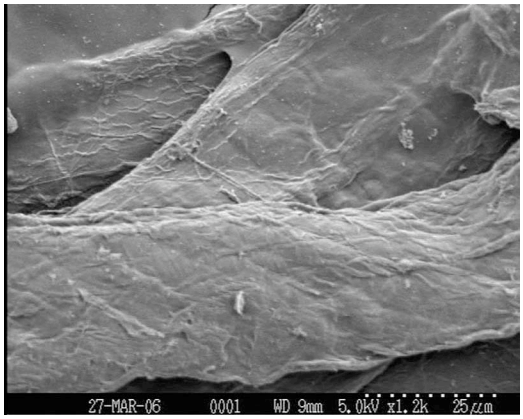

HTCC Spray Only

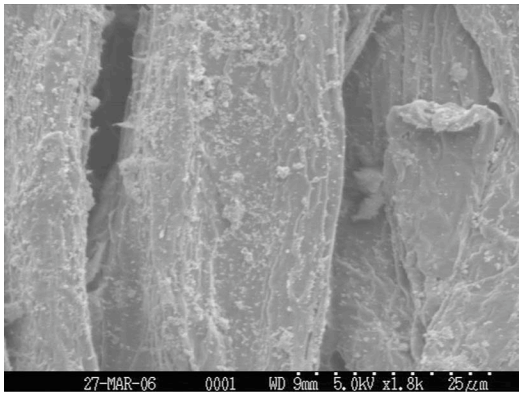

2 minutes Plasma-HTCC Spray

Figure 75: SEM photographs of cellulosic samples, control, HTCC sprayed and 2-minutes exposed to plasma with HTCC spray

4.5.1.3 Colormetric Testing

Colormetric testing was conducted using Dystar Telon Orange M-GSN, which is a basic dye. A solution was prepared with 1.0 gram of dye in 1.0 L of water and all samples were submerged for 15 minutes. After 15 minutes samples were run under cold water for 3 minutes to remove un-reacted dye, then air-dried and examined for dye adhesion and uniformity.

Colorimetry testing revealed the presence of positive groups, attributed to the positive nitrogen groups found in the HTCC structure on the surface of the cellulosic papers as can be seen in Figure 76. All of the samples sprayed with the HTCC, regardless of plasma exposure have been stained by the orange basic dye, signifying that all of the samples have some amount of HTCC on their surfaces. Since all samples have been washed via soxhlet extraction, this HTCC can be considered permanently bonded to the cellulosic chemical backbone. All plasma exposure methods show successful grafting of HTCC, and preservation of the quaternary amine functional group (which is the source of the anti-microbial effect) in addition to the sample that was not exposed to plasma. As discussed earlier, it is not unexpected that the cellulosic paper will retain some HTCC even without plasma treatment, due to the hydroxyl groups found inside the cellulosic chemical structure. However, the sample that was not plasma treated does show significant patchiness in comparison to the plasma treated samples suggesting smaller, and more unevenly bonded HTCC. In addition, its weight loss during soxhlet extraction was very significant in comparison to the other samples, suggesting plasma exposure increases bonding and results in a higher concentration of successful HTCC grafting.

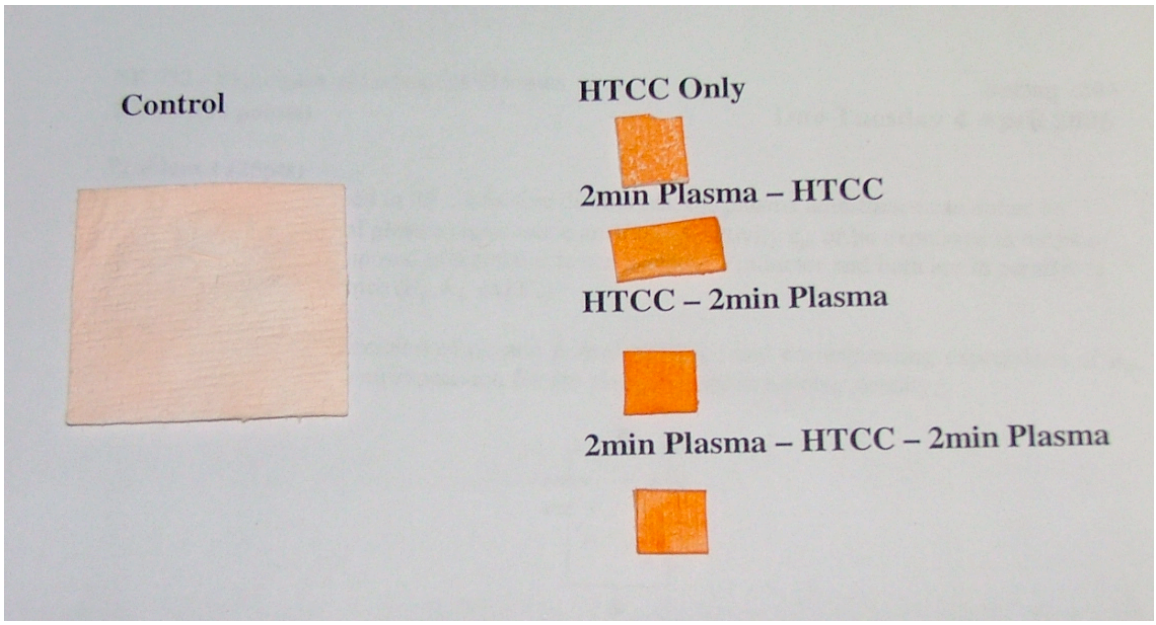

Figure 76: Colormetric testing of cellulosic paper samples grafted with HTCC

4.5.1.4 Fourier Transform Infrared Spectroscopy

A Nexus® 470 Fourier Transform Infrared Spectroscopy device was used in conjunction with a Nicolet® Omnisampler to observe the functional groups in each sample. The areas of deviation were then enlarged and are shown below in Figures 77 and 78. The FTIR analysis revealed the formation of a new trough at 3016nm, 1795nm, 874nm, and the significant enlargement of a peak at 1425-1432nm for the samples exposed to plasma. For the control and the sample sprayed with HTCC, but not exposed to the plasma, these peaks are not apparent. The creation of peaks signifies that some surface chemical modification of the cellulosic paper has occurred. This chemical modification can be attributed either to the plasma exposure and the substrate-plasma modification mechanisms such as etching, functionalization, and chain scission, or to the presence of the permanently bonded HTCC on the surface of the fabric. In addition to signifying chemical changes, the peaks on the FTIR

can be attributed to specific functional groups. For the "new" troughs observed on the plasma treated cellulosic paper grafted to HTCC, Table 9 displays the possible functional groups that can occur at these wavelengths. The strongest peak, at 3016, can be attributed to hydroxyl groups, double bonded carbons, and amine groups. The chemical structure of HTCC does not contain any double bonded carbons and although it is possible that plasma substrate interaction could cause these through reattachment processes, it is unlikely. The peak is very broad, suggesting that more than one functional group is present, and these are most likely due to the amine and hydroxyl groups. At 1432nm, the only functional group possible is the carboxylic acid group. This is not a group found on the chemical structure of the HTCC, but is a functional group that can be caused by the oxygen plasma interacting with the wool substrate[21,34]. The reason for the peak at 874nm is less clear, but is attributed to tri-substituted benzene and to double bonded carbons. Either the plasma has caused the formation of carbon-carbon double bonds as suggested by the appearance of the 874nm and 3016nm trough, which is not an expected modification; or the HTCC rings, which are not benzene but are tri-substituted, are causing the trough. Lastly, the peak at 1794nm can be attributed to a carbonyl group, the result of functionalization of the cellulose surface by the oxygen plasma or the result of a Fisher esterification, a possible chemical graft between the cellulose and the HTCC.

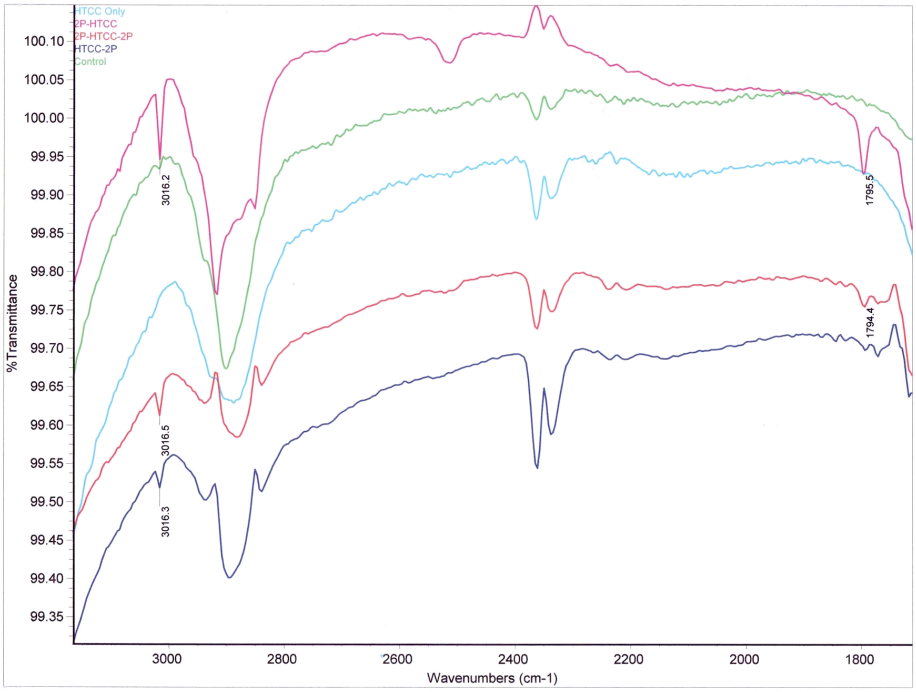

Figure 77: FTIR of HTCC grafted cellulosic paper from 3000-1800nm

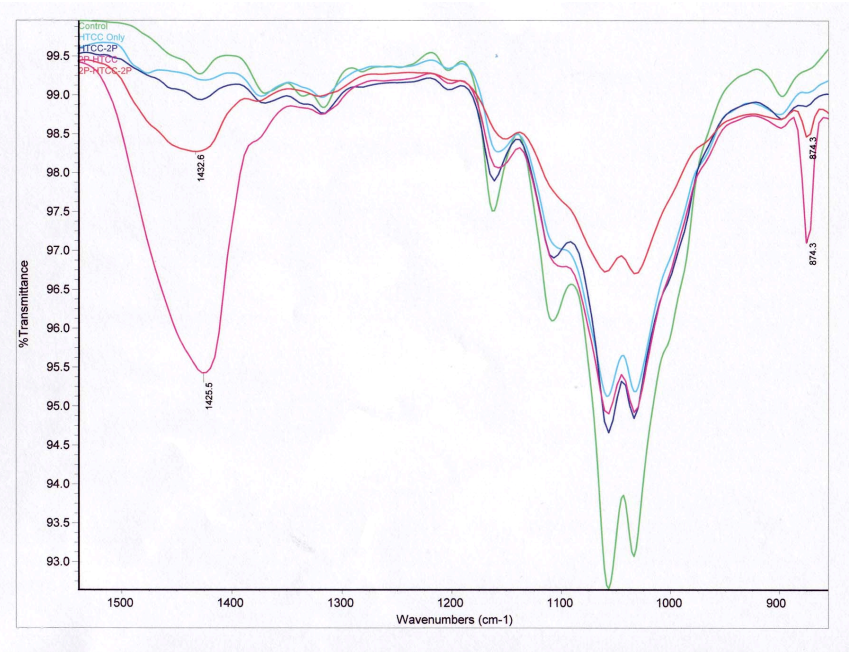

Figure 78: FTIR of HTCC grafted cellulosic paper from 1500-900nm

Table 9: Wavenumber and associated functional groups

New HTTC Peak	Possible Functional Groups	Functional Groups Range (nm)
874 nm	1,2,4-trisubstituted benzenes CH_2=C-R,R'	805-890 865-900
1432 nm	-OH in carboxylic acids	1400-1440
3016nm	=CH in hydrocarbons -OH in carboxylic acid $-NH_3$ amino acids	3000-3100 2400-3100 3000-3200
1794nm	-C=O in carbonyl	1820-1750

A comparison between the FTIR of the cellulosic paper and an FTIR of the HTCC compound can also be made to see if there are similarities between the troughs. The FTIR of HTCC, Figure 79, has been labeled for all the troughs at approximately the same wavelength as those found on the HTCC grafted cellulosic paper. For the 874 nm trough found on the HTCC grafted cellulose there is a corresponding 873.1 nm trough on the HTCC, for the 1432 nm trough on the former there is a 1419.0 nm trough on the later, and for the 3016 nm trough, a corresponding trough of 3028.5 on the HTCC. There is not a peak at all found on the HTCC for the 1794 nm peak of the cellulosic paper. This cannot therefore be attributed to the HTCC compound itself, but must be either a result of the plasma substrate interactions, or a result of the linkage between HTCC and the cellulose. Though the presence of the troughs

on the HTCC compound and on the HTCC grafted compound suggests a bond, it is curious that these peaks represent only the minor peaks found on the HTCC compound. Larger, more massive peaks for the HTCC do not appear on the HTCC grafted cellulosic paper.

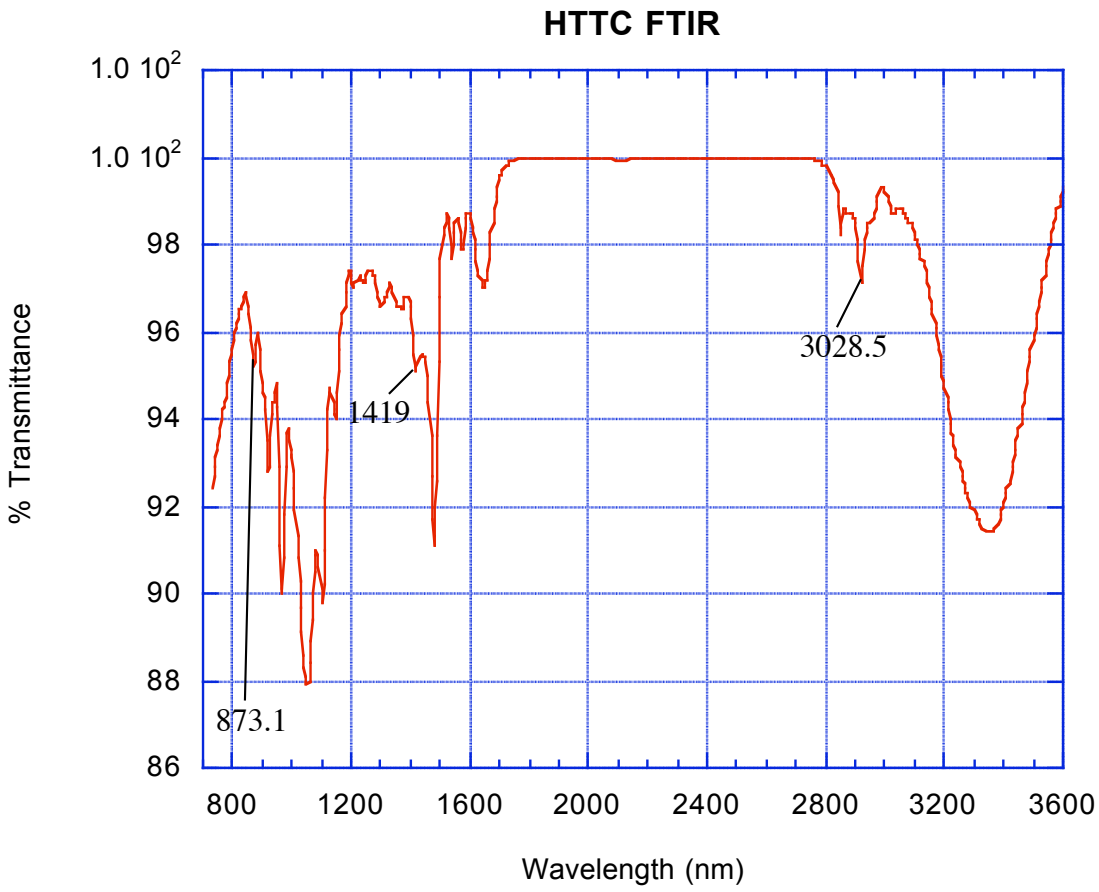

Figure 79: FTIR of HTCC from 3600nm to 800nm

4.5.1.5 Proposed Chemical Grafting Reaction

Data from the FTIR, colormetric testing, SEM, and change in weight indicate that a permanent bond between the cellulose and the HTCC has occurred. In order to explain the chemistry behind this bond, a possible mechanism of chemical reaction for permanent bonding is proposed herein. This chemical grafting reaction, shown in Figure 80 assumes the creation of a carboxylic acid group by the oxygen plasma as it interacts with the cellulose. This carboxylic acid functionalization is supported by the FTIR images, which suggest the formation of this functional group at 1432nm. Creation of carboxylic acid groups have been observed by other researchers on kraft paper with oxygen plasma treatment [36, 37]. After the formation of the carboxylic acid group, the modified cellulose reacts with the HTCC in a simple Fisher esterification reaction. Fisher esterification does not require high temperatures or catalysts, and thus can occur easily when HTCC contacts the carboxylic acid group. The only additional product is water and this is indistinguishable from the water of the surrounding solution, therefore unobservable. The esterification process creates carbonyl groups and these were detected by the FTIR, suggesting the validity of this proposed chemical reaction. More tests are needed to confirm this reaction mechanism and thus if Fisher esterification is occurring.

Also, Fisher esterification is an equilibrium reaction and can revert back to its products, particularly in the presence of acids, so further testing is needed to verify the permanence of this bond under non-neutral conditions.

This proposed chemical reaction is not the only possibility for formation of a covalent bond between cellulose and HTCC. Other reactions schemes exist as well, such as reactions

between the long-lived free radicals that have been observed on the surface of cellulose [38] and the HTCC. Additionally, if the HTCC is sprayed onto the cellulose before treatment by the plasma, it may undergo chain scission, surface functionalization, and radical formation. All of these processes represent possible chemical reactions that could bond the cellulose to the antimicrobial HTCC.

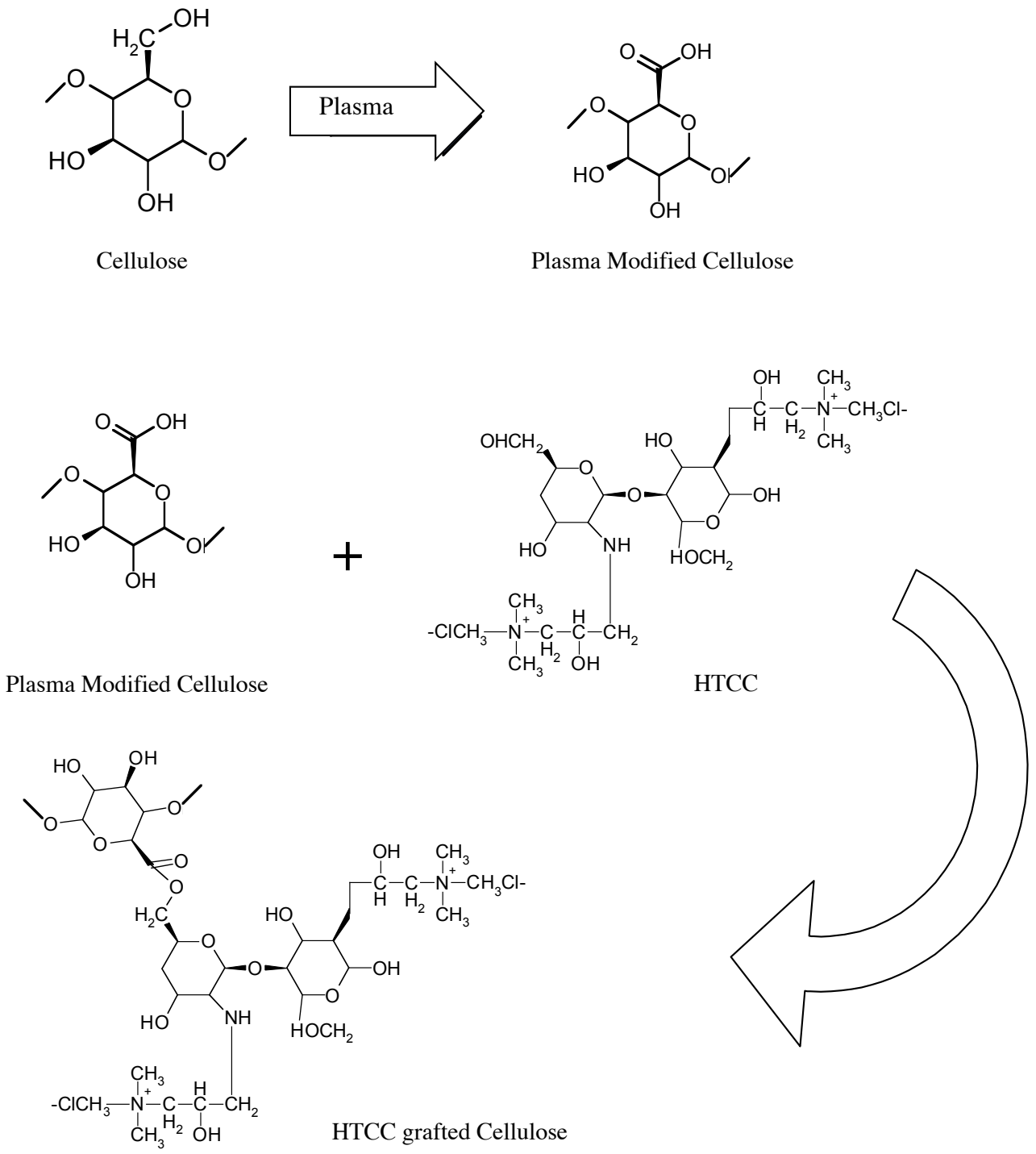

Figure 80: Proposed chemical grafting reaction for HTCC and cellulosic paper

5. Conclusions and Future Work

5.1 Conclusions

The Atmospheric Pressure Plasma System has been characterized for plasma parameters including gas ambient temperature and electron number density for six different gas mixtures containing helium, oxygen, and carbontetrafluoride in varying quantities. Ambient temperature profiles were obtained for all gases for the portion of a 26.5 cm square cell farthest from gas entry point. The profile for all gases shows lower temperatures along a horizontal line down the middle of the cell and increasing temperatures from the center of the cell towards the walls. This phenomenon is explained in view of the closed geometry of the cell. Room temperature gas enters from only one point located directly in the middle of one side of the square cell, and thus the gas along this central line is lower in temperature. The plasma gas resides for a significant period of time within the cell, heating up through collisions and causing an increase in temperature with proximity to the wall. Gases also show differences in overall temperatures, with the 2% CF_4 reaching the highest temperatures.

Electron number density was characterized using a plasma model for the dielectric constant of the plasma. The model described the plasma as three capacitors, two due to the dielectrics surrounding both electrodes, and one due the plasma itself. The plasma electron number density is in the range 10^{12} - $10^{13}/m^3$, which is consistent with reported density for similar devices. The model solves for electron number density as a function of peak voltage, current, and ambient temperature. Profiles for two gases were obtained, showing that after a

brief plasma duration, electron number density remained relatively constant throughout the entire test cell.

Emission spectroscopy was used to determine the elemental content of each gas mixture. It was observed that even for a pure helium plasma, there is always a fraction of oxygen from the fractional air residing in the cell. The helium and carbontetrafluoride mixtures showed molecular peaks not found on the helium/oxygen and helium/oxygen/carbontetrafluoride gas mixtures. For carbontetrafluoride/helium mixtures, fluorine peaks were observed confirming the formation of elemental fluorine due to dissociation of CF_4.

Wool fabrics were exposed to various plasmas formed by gas mixtures. This exposure caused an increase in ambient temperature and a decrease in the electron number density of the plasma for all gas mixtures, due to the introduction of a new dielectric material and the creation of new radicals from the etched wool. The wool fabric was also tested for observable changes in weight and hydrophilicity. Changes in weight showed significant etching by all gases, with the amount of etching increaseing over time, except for the case of the helium/oxygen/carbontetrafluoride gas mix. Data also shows that wool becomes more hydrophilic with increased exposure to plasma and that hydrophilicity rapidly increases with increased concentration of oxygen. Oxygen is known to cause the creation of hydrophilic groups and the other gases may be etching off the waxy coating of the wool fibers. The helium/oxygen/carbontetrafluoride gas mixture showed the greatest contact angles and the longest absorption times.

Additionally, tensile strength and % elongation tests were conducted. The tensile strength increases with increased oxygen concentration. Other gas mixtures, excluding helium/oxygen/carbontetrafluoride mixture, showed initial reduction with gradual improvement as exposure to plasma extended. However, deviation was not great from the control. Only helium/oxygen/carbontetrafluoride gas mixture showed a decrease that did not improve with extended exposure to plasma.

Finally, EDS showed an increase in fluorine with increased exposure to plasma. The existence of fluorine gas in the 1% and 2% carbontetrafluoride/helium mixtures was confirmed by optical emission spectroscopy. However, fluorine content was also found on the helium/oxygen/carbontetrfluoride gas mixture suggesting small amounts of fluorine undetectable by the spectroscopy.

Cellulosic paper was also exposed to plasma in order to graft the anti-microbial agent HTCC, a derivative of chitosan and chitin. Success of the graft was confirmed by a permanent gain in weight of the plasma-treated samples even after soxhlet extraction. In addition colorimetry test showed the grafting of HTCC on all samples including the control. However, the HTCC gain on the control was much smaller than the other samples as determined by % weight change, SEM and FTIR.

A possible reaction chemistry was proposed suggesting the creation of carboxylic acid groups on the cellulose by the oxygen plasma and an esterification reaction between the HTCC and the cellulose. Future testing will be needed to determine if this is the proper reaction or if radical formation may play a role.

5.2 Recommendations for Future Work

Extensive characterization of the Atmospheric Pressure Plasma System should be conducted to determine the plasma kinetic temperature, collision frequency and chemical reactions during sample treatment. The neutral bermesstrahlung technique should be used to determine the plasma parameters under non-equilibrium conditions, and a model should be developed to determine the time-dependent changes in the plasma kinetic temperature.

Further investigation of grafting HTCC onto cellulosic paper should continue, in order to optimize the criteria under which simultaneous spraying of HTCC and exposure to plasma gives maximum efficiency. Anti-microbial assay should also be performed on grafted samples to ascertain the anti-microbial effectiveness and an investigation into the reaction mechanism should be conducted to verify if esterification is a valid mechanism.

References

[1] Chen, F. (1984). *Plasma Physics and Controlled Fusion*. New York: Plenum Press

[2] Princeton Physics Laboratory: Science Education. Retrieved October 20th, 2006, from http://science-education.pppl.gov/SummerInst/SGershman/Structure_of_ Glow_Discharge.pdf

[3] Wikipedia. Retrieved October 8th, 2006 from http://en.wikipedia.org/wiki/Glow_discharge)

[4] Lieberman, M., Lichtenberg, A. (2005). *Principles of Plasma Discharges and Materials Processing*. New Jersey: John Wiley and Sons, Inc.

[5] Yokoyama, T., Kogoma, M., Moriwaki, T., Okazaki, S. (1990). The mechanism of the stabilization of glow plasma at atmospheric pressure. *Journal of Physics D: Applied Physics*, 23(8), 1125-1128.

[6] Shenton, S, (2001). Surface modification of polymer surfaces: atmospheric plasma verse vacuum plasma treatments. *Journal of Physcics D: Applied Physics*, 34, 2761-2768.

[7] Bures, B. (2001). *Diagnosis and application of atmospheric radio frequency glow discharge plasma*. College of Engineering, Department of Nuclear Engineering, North Carolina State University.

[8] Deichman, T. *Plasma substrate interaction*. College of Engineering. University of Aachen, Germany.

[9] Milligan, M. (1981). *Wool Science: the Chemical Reactivity of the Wool Fibre*. Australia: Science press.

[10] Onions, W. (1962). *Wool, An Introduction to its Properties Varieties Uses and Production*. London: Earnest Benn Limited.

[11] Sugawara M. (1998). *Plasma Etching Fundamentals and Applications*. Oxford University Press

[12] Griem, H. (1968). *Plasma Spectroscopy.* McGraw-Hill Press.

[13] Greim, H. (1974). *Spectral Line Broadening by Plasmas*. New York: Academic Press.

[14] Henins, P., Herrmann, H., Selwyn, G. (2000). Neutral bremsstrahlung measurement in an atmospheric-pressure radio frequency discharge. *Physics of Plasmas*, 7(8) 3141-3144.

[15] Bures, B., Donohue, K., Bourham, M., Roe, M. (2006). Non-chemical dielectric barrier discharge treatment as a method of insect control. *IEEE Trans. Plasma Sc.*, 34(1), 55-62.

[16]Rakowski, W. (1982). Plasma treatment of textiles-potential applications and future prospects. *Melliand Textilberichte,* 301

[17] Chapman, B. (1980). *Glow Discharge Processes: Sputtering and Plasma Etching*. New York: John Wiley and Sons, Inc.

[18] Manos, D., Flamm,D. (1989). *Plasma Etching an Introduction.* Academic Press, Inc.

[19] Kuzuya, M., Noguchi, A., Ishikawa, M. et all. (1991). Electron spin resonance study of free- radical formation and its decay of plasma-irradiated poly(methacrylic acid) and its esters. *J. Phys. Chem.,* 95 2398

[20] Inagaki, N. (1996). *Plasma Surface Modification and Plasma Polymerization.* Lancaster, Pennsylvania: Pub. Co., Inc.

[21] Clark, D., Wilson, R., (1983). Selective surface modification of polymers by means of hydrogen and oxygen plasmas. *Journal of Polymer Science-Polymer Chemistry Edition 21*.

[22] Kim, J., Liu, G., Kim, S. (2006). Deposition of stable hydrophobic coatings with in-line CH4 atmospheric rf plasma. *Journal of Material Chemistry*, 16, 977-981.

[23] Vermont Organic Fiber Co. Retrieved October 28, 2006 from www.vtorganicfiber.com/ wool_facts.html

[24] Biochemistry (2004). Prentice-Hall, Inc.

[25] Errera, J. Sack, H. (1943). Dielectric properties of animal fibers. *Industrial and Engineering Chemistry*. 712-716.

[26] Britannica. Retrieved October 12, 2006 from http://www.britannica.com/eb/article-82571/man-made-fibre

[27] Kocurek, Michael (1978). *Introduction to Pulp and Paper Technology*. Seminar Notes Tappi Annual Meeting Seminar March 8-10. The Mead Paper Corporation.

[28] Salmon, S. and Hudson, J. (1997) Crystal morphology, biosynthesis, and physical assembly of cellulose, chitin, and chitosan. *Makcromol. Chem. Phys.,*37 (2) 199-276.

[29] Dalwoo-Chitosan. Retrieved October 12, 2006 from http://members.tripod.com/~Dalwoo/preparation.htm

[30] Matthews, S., Hausesr, P. Colorimetric testing of quaternary ammonium finishes. Department of Textile Engineering, Chemistry & Science North Carolina State University, Raleigh, NC

[31]Molina, R. Erra, P., Free radical formation in wool fibers treated by low temperature plasma. *Textile research journal,* 73 (11) 955-959.

[32] Clark, D., Wilson, R., (1983). Selective Surface Modification of Polymers by Means of Hydrogen and Oxygen Plasmas. *Journal of Polymer Science-Polymer Chemistry Edition 21*

[33] Shao, J. Jones, D., Mitchell, R. Vickerman, J., Carr, C. (1997). Time of flight secondary ion mass spectrometric (ToF-SIMS) and X-ray photoelectron Spectroscopic (xps) analyses of the surface lipids of wool. *Journal of textiles institute,* 88 317-324

[34] Kan, C. , Chan, K., Yuen, W. (1999). Low Temperature Plasma on Wool Substrates: The effect of the Nature of the Gas. *Textile Research Journal,* 69(6) 407-416.
,
[35] Kan, C. Yuen,C. (2006). Low Temperature Plasma Treatment for Wool Fabric. *Textile Research Journal,* 76(4) 309-314.

[36] Wakida, T., Tokino S., Niu S., Kawamura H. (1993). *Textile Research Journal*, 63(8) 433-438.

[37] Wielen, L. Elder, T. Ragauskas, A. (2005). Analysis of the topochemical effects of dielectric-barrier discharge on cellulosic fibers". *Cellulose,* 12 185-196.

[38] Chen, J. (1996). Study on free radicals of cotton and wool fibers treated with low-temperature plasma. *Journal of applied Polymer Science,* 62 1325-1329.